*Chapter 2*

# SUBSIDENCE HISTORY OF THE EDIACARAN JOHNNIE FORMATION AND RELATED STRATA OF SOUTHWEST LAURENTIA: IMPLICATIONS FOR THE AGE AND DURATION OF THE SHURAM ISOTOPIC EXCURSION AND ANIMAL EVOLUTION

Witkosky, R., and Wernicke, B.P., 2018, Subsidence history of the Ediacaran Johnnie Formation and related strata of southwest Laurentia: Implications for the age and duration of the Shuram isotopic excursion and animal evolution: Geosphere, v. 14, n. 5, https://doi.org/10.1130/GES01678.1.

## ABSTRACT

The Johnnie Formation and associated Ediacaran strata in southwest Laurentia are ~3000 m thick, with a Marinoan cap carbonate sequence at the bottom, and a transition from Ediacaran to Cambrian fauna at the top. About halfway through the sequence, the Shuram negative carbon isotopic excursion occurs within the Rainstorm Member near the top of the Johnnie Formation, followed by a remarkable valley incision event. At its type locality in the northwest Spring Mountains, Nevada, the Johnnie lithostratigraphy consists of three distinctive sand-rich intervals alternating with four siltstone/carbonate-rich intervals, which appear correlative with other regional Johnnie Formation outcrops. Carbon isotope ratios in the sub-Rainstorm Member part of the Johnnie Formation are uniformly positive for at least 400 m below the Shuram excursion and compare well with sub-Shuram excursion profiles

from the Khufai Formation in Oman. There is historical consensus that the Johnnie and overlying formations were deposited on a thermally subsiding passive margin. Following previous authors, we used Paleozoic horizons of known biostratigraphic age to define a time-dependent exponential subsidence model, and extrapolated the model back in time to estimate the ages of the Shuram excursion and other prominent Ediacaran horizons. The model suggests that the Shuram excursion occurred from 585 to 579 Ma, and that incision of the Rainstorm Member shelf occurred during the 579 Ma Gaskiers glaciation. It further suggests that the base of the Johnnie is ca. 630 Ma, consistent with the underlying Noonday Formation representing a Marinoan cap carbonate sequence. Our results contrast with suggestions by previous workers that the Shuram excursion followed the Gaskiers event by some 20 - 30 m.y. We suggest instead that the Shuram and Gaskiers events were contemporaneous with the biostratigraphic transition from acanthomorphic to leiospherid acritarchs, and with the first appearance of widespread macroscopic animal life, 38 m.y. prior to the Ediacaran-Cambrian boundary.

## INTRODUCTION

Ediacaran strata record a critical period in Earth history (635-541 Ma), during which metazoan life first appeared (Knoll et al., 2004, 2006; Narbonne et al., 2012). They also record a significant rise in atmospheric and oceanic oxygen (Fike et al., 2006; Canfield et al., 2007; McFadden et al., 2008; Sahoo et al., 2012), which was a prerequisite to metabolic function in animals (Knoll and Carroll, 1999; Och and Shields-Zhou, 2012). Neoproterozoic oxygenation resulted in atmospheric levels generally interpreted as similar to those of the

present day (Holland, 2006; Kump, 2008). Today, atmospheric oxygen levels are maintained by photosynthesis from land plants and marine organisms in roughly equal proportions (e.g., Field et al., 1998). It has therefore long been enigmatic that land plants are not preserved in rocks older than ca. 400 Ma, or ~150 m.y. later than the first appearance of animals. For that reason, it is widely presumed that the rise of animal life required sufficient oxygen production, from either marine photosynthesis, or perhaps some sort of "bootstrap" mechanism from animals themselves, to survive (e.g., Butterfield, 2009; Lenton et al., 2014). In any event, progress toward understanding the fundamental question, "what is the origin of animals?," hinges in part on understanding how and when oxygen became sufficiently available to make animal metabolism possible (e.g., Nursall, 1959).

Among the most fruitful avenues of research along these lines to date has been exploration of proxies for the chemistry of seawater in which animal life first appeared, primarily the stable isotope geochemistry of shallow-marine carbonate strata. The best-preserved Ediacaran strata around the globe that contain carbonate all feature a singularly large (by about a factor of two) negative anomaly in the isotopic composition of carbon, which has been attributed primarily to the isotopic composition of ancient seawater itself (Fike et al., 2006; McFadden et al., 2008; but for an alternative view, see Swart and Kennedy, 2012). The anomaly is best preserved and documented in the Ediacaran Shuram Formation in Oman (Burns and Matter, 1993; Le Guerroué et al., 2006a, 2006b; Osburn et al., 2015), and is generally referred to as the "Shuram excursion," taking its name from the discovery formation. A similar excursion has been documented in Neoproterozoic sections on five of Earth's seven modern continents, and it occurs only once in each section: Africa (Kaufman et al., 1991; Halverson et al., 2005), Asia (Burns and Matter, 1993; Condon et al., 2005;

Melezhik et al., 2005; Fike et al., 2006; McFadden et al., 2008; Macdonald et al., 2009; Osburn et al., 2015), Australia (Calver, 2000; Husson et al., 2015), Europe (Melezhik et al., 2005; Prave et al., 2009), and North America (Myrow and Kaufman, 1999; Corsetti et al., 2000; Corsetti and Kaufman, 2003; Kaufman et al., 2007; Bergmann et al., 2011; Petterson et al., 2011; Verdel et al., 2011; Macdonald et al., 2013). The Shuram excursion is the largest known Neoproterozoic or younger carbon isotope anomaly (Grotzinger et al., 2011), and its magnitude is among the largest recorded in Earth history (see, for example, the Paleoproterozoic Lomagundi-Jatuli excursion; Bekker and Holland, 2012).

Global chemostratigraphic expression of the Shuram excursion is a remarkable discovery from at least three perspectives. First, it represents a presumably isochronous fingerprint of a specific interval of time from sections with notoriously sparse age constraints. Second, it implies that a geologically extreme event of uncertain origin occurred at the same time as the rise of animals. Last, the singular magnitude of the excursion contributes to the goal of creating a global composite time series of secular variations in marine carbon isotope ratios. In regard to the third point, the duration of the anomaly raises the potential for using the shapes of the curves, rather than simply the magnitudes of the excursions, as a correlation tool from section to section; this of course presumes a relatively constant sedimentation rate at the hundred-meter scale (Halverson et al., 2005; Saltzman and Thomas, 2012). For the Shuram excursion, $\delta^{13}C$ values rapidly descend with stratigraphic position to < -11‰ followed by a recovery that is at first gradual and then moderate in slope, with the change occurring near -4 ‰ (Figure 2 in Condon et al., 2005; Figure 3 in Prave et al., 2009; Figure 16 in Verdel et al., 2011; Figure 3 in Grotzinger et al., 2011; Figure 13 in Macdonald et al., 2013; Figure 1A in Husson et al., 2015).

At present, the most significant impediment to understanding Ediacaran biostratigraphy is the lack of internal age control in most sections around the globe. The ages of the boundaries of the Ediacaran Period are well defined radiometrically in multiple sections. The base is defined by the lithologically distinctive post-Marinoan cap carbonate sequence, which is associated with a -6 ‰ $\delta^{13}C$ excursion in carbonate and is precisely dated at 635 Ma in Namibia and China (Hoffmann et al., 2004; Condon et al., 2005). The top is defined by the first appearance of the trace fossil *Treptichnus pedum* (541 Ma), which is also associated with a -6 ‰ $\delta^{13}C$ excursion in carbonate. Other than the first appearance of large Ediacaran body fossils, which usually occurs rather high in most sections relative to the Ediacaran-Cambrian boundary, the Shuram excursion has emerged as the single most distinctive stratigraphic datum that is globally recognized. However, its precise age is poorly constrained, precluding any attempt to meaningfully subdivide some 94 m.y. of Ediacaran time, and creating first-order uncertainties in the relative timing of major environmental and biostratigraphic events (Xiao et al., 2016). A second major stratigraphic feature, largely restricted to sections in the North Atlantic region, is the Gaskiers glaciation (Myrow and Kaufman, 1999), which, in contrast to the Shuram event, is precisely dated at 579 Ma (Bowring et al., 2003a, 2003b; Pu et al., 2016). The mismatch between sections with glaciogenic rocks and precise radiometric ages on one hand, and the Shuram excursion in carbonate strata on the other, has left it uncertain whether or not these two events are correlative (Xiao et al., 2016). A 580 Ma age for the Shuram excursion provides an obvious correlation between the two most conspicuous events in the Ediacaran record (e.g., Xiao et al., 2004; Fike et al., 2006; Zhou et al., 2007; Halverson et al., 2005, 2010; Loyd et al., 2012; Schiffbauer et al., 2016). Alternatively, the stratigraphic proximity of the Shuram excursion

to the Precambrian-Cambrian boundary, and a 551 Ma ash bed near the apparent upper zero crossing of the excursion in the Doushantuo Formation of China, suggests that it may be as much as 20-30 m.y. younger than the Gaskiers glaciation (Condon et al., 2005; Bowring et al., 2007; Cohen et al., 2009; Sawaki et al., 2010; Narbonne et al., 2012; Macdonald et al., 2013; Tahata et al., 2013; Xiao et al., 2016).

One chronological tool that has heretofore only been sparingly applied to Ediacaran strata is thermal subsidence analysis (e.g., Le Guerroué et al., 2006b). It is well known that thermal subsidence associated with seafloor spreading is a useful chronometer that can predict the age of the ocean floor based on the exponential decay of its elevation with respect to the abyssal plains for lithosphere older than 20 m.y. (e.g., Equation 22 in Parsons and Sclater, 1977). The same principle also applies to models of the subsidence history of passive-margin basins, which include an initial thickness of newly stretched continental crust and substantial sediment loading (McKenzie, 1978). The decay is predicted by laws of diffusive heat transport of physical rigor that are on par with laws of closed-system radioactive decay used to date the timing of crystallization of minerals. The principal limitations in using thermal conduction as a chronometer are (1) the requirement that subsidence records thermal relaxation without significant mechanical modification of the lithosphere, such as extension, flexural loading, instability of a thermal boundary layer, or unmodeled sources of dynamic topography; and (2) correction of the observed stratigraphic subsidence for the compaction and lithification of sediment after deposition, and for water depth and changes in sea level (e.g., Steckler and Watts, 1978; Allen and Allen, 2005).

In comparison with Phanerozoic sedimentary basins, published subsidence analyses of Ediacaran strata have been limited, with most of the effort thus far concentrated on the

western Laurentian continental margin (Stewart and Suczek, 1977; Bond et al., 1983; Armin and Mayer, 1983; Levy and Christie-Blick, 1991; Yonkee et al., 2014). The focus on this region as a testing ground for thermal subsidence modeling was due to the fact that it is perhaps the best-preserved example of an ancient passive margin, analogous to present-day Atlantic-type margins, but with virtually complete surface exposure of apparent synrift and postrift sedimentary archives spanning several hundred million years (Stewart, 1972; Gabrielse, 1972; Burchfiel and Davis, 1972, 1975; Stewart and Poole, 1974; Dickinson, 1977; Monger and Price, 1979). Because these sequences span the Ediacaran-Cambrian boundary, such that roughly half their thickness is Proterozoic in age, temporal control on subsidence has been restricted mainly to the Phanerozoic portion of subsidence curves. The lack of age control on the lower part of the section precludes precise definition of the transition from mechanical extension to pure thermal subsidence. Fortunately, the accurate definition of an exponentially decaying system, in particular, extrapolating stratigraphic age backward in time from a curve with known ages, is independent of the timing of onset and total amount of purely thermal subsidence.

Here, we address the problem of the correlation and age of the Shuram isotopic excursion through lithostratigraphic and chemostratigraphic study of the type locality of the Ediacaran Johnnie Formation in the Spring Mountains of southern Nevada. The Johnnie Formation is at least 1800 m thick at the type locality, and it makes up more than half of the maximum known thickness of ~3000 m of total Ediacaran strata exposed in this region. The underlying Noonday Formation provided the first isotopic match between the Marinoan cap carbonate sequence in Namibia (Hoffman et al., 1998) and a section from another continent (Petterson et al., 2011). The overlying Stirling and Wood Canyon Formations contain

Ediacaran and Lower Cambrian fossil assemblages that define the Cambrian-Precambrian boundary within the lower part of the Wood Canyon Formation (Corsetti and Hagadorn, 2000; Hagadorn and Waggoner, 2000), 1200 m above the top of the Johnnie Formation in the Spring Mountains. The uppermost 300 m of section of the Johnnie Formation contains the best expression of the Shuram excursion in Laurentia (Corsetti and Kaufman, 2003; Kaufman et al., 2007; Bergmann et al., 2011; Verdel et al., 2011). Therefore, to the extent that the section was deposited at or very near sea level on a thermally subsiding continental shelf, subsidence analysis may be used to estimate the age of the Shuram excursion and perhaps even broadly constrain the overall age of the Johnnie Formation.

## GEOLOGIC SETTING

Neoproterozoic-Cambrian strata in western Laurentia are divisible into two principal components, including a lower diamictite and volcanic sequence, and an upper terrigenous detrital sequence (Stewart and Suczek, 1977; Poole et al., 1992). The Johnnie Formation is the lowest siliciclastic formation in the upper terrigenous detrital sequence, forming the basal deposits of a westward-thickening continental margin terrace wedge, widely regarded to have developed in the wake of late Neoproterozoic rifting of the Rodinian supercontinent (Li et al., 2008, 2013). The formation is a few hundred meters thick near its eastern pinchout beneath Lower Cambrian cratonic strata, systematically increasing to at least 1500 m thick in its westernmost exposures, where the base is not definitively exposed (Stewart, 1970; this report). Lithologically, it is primarily variegated siltstone and very fine-grained sandstone that contains varying amounts (10-40%) of carbonate and orthoquartzite, distinguishing it

from the carbonate-dominated Noonday Formation below and coarse siliciclastic rocks of the Stirling Formation above (Figure 1).

The Johnnie Formation was first defined and described in the northwest Spring Mountains in the Johnnie Wash area (Figure 2; Nolan, 1924, 1929), where its contact with the underlying Noonday Formation is apparently not exposed, and hence its thickness is a minimum for this location. Nolan's (1924) thickness and description were included in the regional stratigraphic synthesis of Stewart (1970). The type locality was subsequently mapped and briefly described by Burchfiel (1964, 1965), and relatively complete lithostratigraphic sections were measured by Hamill (1966) and Benmore (1978). The type locality has since received little attention in comparison to the much thinner sections in the Nopah Range and environs 70 km to the south, or equivalents 100 km to the west in the Panamint Range, where its basal contact with the Noonday Formation is extensively exposed (e.g., Hazzard, 1937; Wright and Troxel, 1966; Labotka et al., 1980; Albee et al., 1981; Benmore, 1978; Summa, 1993; Fedo and Cooper, 2001; Corsetti and Kaufman, 2003; Kaufman et al., 2007; Verdel et al., 2011). With the exceptions of detailed studies of parts of the formation (Summa, 1993; Abolins, 1999; Bergmann et al., 2011), no systematic attempt has yet been made to describe and interpret the entire formation at its type locality in terms of key bed forms, depositional environments, sequence architecture, or chemostratigraphy, at the level of more southerly or westerly sections.

The uppermost part of the Johnnie Formation, the Rainstorm Member, is a lithostratigraphically distinctive unit that can be correlated with confidence over a broad region of southwestern North America, including eastern California and southern Nevada (Stewart, 1970), and it probably occurs as far south as northern Sonora, Mexico, where it

forms a part of the Clemente Formation (Stewart et al., 1984). The basal strata of the Rainstorm Member are its most distinctive part. They include a thin (~2 m), siltstone-enveloped, regionally extensive oolitic marker bed known as the "Johnnie oolite" (e.g., Bergmann et al., 2011). The oolite is underlain by greenish gray siltstone, and it is overlain by distinctive pale-red, fine-grained sandstone with or without associated sandy or silty micrites ("liver-colored limestones"). The overlying units characteristically contain groove marks, flute casts, intraformational conglomerate, and other indicators of shallow water, high-energy currents. These carbonates record the onset and most negative part of the Shuram excursion in eastern California and southern Nevada (Corsetti and Kaufman, 2003; Kaufman et al., 2007; Verdel et al., 2011), as well as in the Sonora sections (Loyd et al., 2012). Similar to formation-scale thickness variations in the terrigenous detrital sequence as a whole, the Rainstorm Member generally thickens westward from as little as 20 m in the thinnest measured section to more than 300 m in the thickest sections (Stewart, 1970; Verdel et al., 2011).

Lower and middle Johnnie Formation strata are sufficiently variable in their lithostratigraphy, that recognition of regionally mappable members is not as straightforward as in the case of the Rainstorm Member. As noted by Summa (1993), sub-Rainstorm Member depositional settings of the Johnnie Formation are interpreted as inner-shelf to tidally influenced nearshore environments that were highly susceptible to sea level fluctuation (Benmore, 1978; Fedo and Cooper, 2001; Schoenborn et al., 2012). As we describe herein, depositional environments tend to be more landward to the south and east in these units, as suggested by the abundance versus absence of dessication features, fluvial versus marine deposition, and medium- to coarse-grained sandstones versus fine- to medium-grained

sandstones. Although this variability complicates simple lithostratigraphic correlation, if interpreted correctly, it can be used as an effective indicator of sea-level rise and fall.

Reported age constraints from the Johnnie and correlative Clemente Formations include (1) a 640 Ma U-Pb age from a single detrital zircon grain in sub-Rainstorm Member siltstones in the Panamint Range of eastern California (Verdel et al., 2011), and (2) potential Ediacaran body and trace fossils (e.g., *Cyclomedusa plana* and *Palaeophycus tubularis*, respectively) ~75 m below the oolite in the Clemente Formation (McMenamin, 1996). The U-Pb age, because it is based on a single grain, is subject to the uncertainty of contamination during mineral processing and needs to be confirmed with duplicate analyses. The putative fossils have been questioned after examination by other paleontologists (e.g., J.W. Hagadorn, 2017, personal communication), and they have generally not been accepted in subsequent stratigraphic studies of the region (e.g. Loyd et al., 2012, 2015). Latest Ediacaran fossils have been recovered from the uppermost Stirling Formation and the Lower Member of the Wood Canyon Formation in the Spring Mountains and neighboring Montgomery Mountains to the south (e.g. *Cloudina* and *Swartpuntia*; Hagadorn and Waggoner, 2000; Smith et al., 2017), from sections in stratigraphic continuity with the type Johnnie Formation. These are succeeded immediately upward by Lower Cambrian trace fossils (*Treptichnus pedum*), which places the Ediacaran-Cambrian boundary in the Lower Member of the Wood Canyon Formation (Figure 1; Corsetti and Hagadorn, 2000).

The underlying Noonday Formation has been interpreted as the cap carbonate sequence of the Marinoan “snowball Earth” glaciation (Petterson et al., 2011), which by definition would place its base at the beginning of the Ediacaran period (635 Ma; Knoll et al., 2004, 2006; Narbonne et al., 2012). The Johnnie Formation’s basal contact with the

Noonday Formation is lithostratigraphically gradational, transitioning from sandy dolostones of the upper Noonday Formation (Mahogany Flats Member of Petterson et al., 2011), to interstratified dolomitic sandstone and orthoquartzite in the lower Johnnie Formation (Transitional Member of Stewart, 1970). Although traditionally regarded as a conformable contact on the basis of this gradation (Hazzard, 1937; Stewart, 1970; Wright and Troxel, 1984), the identification of local karstic surfaces along the contact raises the possibility that it is a disconformity with a substantial depositional hiatus (Summa, 1993).

In terms of chemostratigraphic constraints on age, the conspicuous excursions to -6 ‰ at the base and top of the Ediacaran section are well expressed in the south Laurentian sections (e.g., Petterson et al., 2011; Smith et al., 2016). The presence of the Shuram excursion in the Rainstorm Member, despite its value as a correlation tool, does little to constrain the depositional age, because unlike the tightly constrained boundary excursions, hard chronological constraints are lacking, as noted already.

For almost a century, the terrigenous detrital sequence has been studied extensively on many different levels. Much of the early work focused on stratigraphic group-level packages that record the transition from Precambrian to Cambrian time (Nolan, 1929; Burchfiel, 1964; Stewart, 1970). More recent work on the Johnnie Formation has focused largely on outcrops in eastern California (Summa, 1993; Fedo and Cooper, 2001; Verdel et al., 2011; Schoenborn and Fedo, 2011; Schoenborn et al., 2012), or on specific features related to the Rainstorm Member, such as an incision-related conglomeratic member (Summa, 1993; Abolins, 1999; Abolins et al., 2000; Clapham and Corsetti, 2005; Verdel et al., 2011), giant ooids (Trower and Grotzinger, 2010), or detailed chemostratigraphy of the Johnnie oolite (Bergmann et al., 2011). The lower and middle portions of the Johnnie

Formation have not been given as much detailed attention, except in areas close to the craton miogeoclinal hinge where the Johnnie Formation is only a few hundred meters thick. The 1600 m stratigraphic thickness of sub-Shuram excursion Johnnie Formation at the type locality exceeds the thickness of any globally correlative Ediacaran strata of which we are aware. Furthermore, total Ediacaran stratigraphic thickness in southwest Laurentia measures over 3000 m, greater than the approximate thicknesses of sections in Australia (2500 m), Oman (1500 m), and China (300 m). Strata of the lower and middle Johnnie Formation at its type locality therefore represent one of the best opportunities among sections globally to provide a relatively complete record of Ediacaran time prior to the Shuram excursion. An important gap in our understanding of Ediacaran chemostratigraphy is the paucity of carbonate strata below the Shuram anomaly in most sections. Of the major global sections that contain it, only the Oman example contains abundant carbonate in immediately underlying strata, the Khufai Formation. Discovery of correlative carbonate-bearing strata in one or more sections around the globe would thus represent a significant step in expanding the global inventory of chemostratigraphic time series for a critical interval in Neoproterozoic time.

## METHODS

### Lithostratigraphy

To identify a structurally intact section of the Johnnie Formation, we performed geologic mapping at 1:10,000 scale in the northwest Spring Mountains, Nevada, both of the type

locality at Johnnie Wash, and in an area ~4 km to the southwest near Nevada Highway 160, 3 km west-southwest of Mount Schader (Figure 2). We used the Mount Schader, Nevada 1:24,000 quadrangle map (U.S. Geological Survey, 1968) as a topographic base. Our field mapping spanned 9 days total between 21 April 2015 and 2 May 2015. The geologic maps were used to identify optimum transects for measuring stratigraphic section. The Mount Schader section was measured and sampled in detail using a Jacobs staff mounted with a Brunton® compass set to the dip of bedding. For each stratigraphic subunit, we recorded (1) fresh and weathered color of lithology using a Munsell color chart, (2) grain size, and (3) bedding thickness (supplemental text). Section was measured to the resolution of ~0.5 m (or finer in some instances, if warranted). The Johnnie Wash section was measured using geologic cross sections, and the general lithologic characteristics were recorded in the field during geologic mapping (see Appendix for unit names and descriptions).

**Chemostratigraphy**

For carbon and oxygen isotope chemostratigraphy, we collected samples at 0.3-1 m resolution in carbonate units. Samples from the upper ~400 m of sub-Rainstorm Member lithostratigraphic units were collected from the Mount Schader section during stratigraphic logging. Samples from two prominent carbonate horizons that occur below the deepest exposed strata of the Mount Schader section were collected in the Johnnie Wash locality of the Spring Mountains, and at a location ~3 km north of Johnnie Wash (Locality A in Figure 2A). In total, 107 centimeter-scale sample chips were collected for carbon and oxygen isotopic analysis, including 36 from the Johnnie Wash section and Locality A and 71 from

the Mount Schader section. In the laboratory, sample chips were sliced open using a diamond-bladed wet saw to expose fresh, unweathered surfaces. From the fresh surfaces, a high-speed rotary tool with a diamond-tipped drill bit was used to powder the sample. We carefully extracted ~0.1 mg of analyte from each sample chip, taking care to avoid any visible alteration or veining. Sample powder was loaded into vials and the air was purged and replaced with helium gas, and then the powder was digested in phosphoric acid at 72° C for at least one hour to evolve sufficient $CO_2$ gas for analysis. Carbon and oxygen isotope ratios were measured at Caltech using a Delta V Plus Isotope Ratio mass spectrometer ("gas bench"). Our values for $\delta^{13}C$ and $\delta^{18}O$ are reported relative to the Vienna Pee Dee Belemnite (VPDB) standard in per mil notation. We used Caltech's laboratory working standards, which were calibrated to NBS 18 and NBS 19 and have uncertainties of +/-0.1 ‰. Standards were measured once for every nine samples to assess systematic error.

**Subsidence Analysis**

Our tectonic subsidence analysis is based on stratigraphic thicknesses compiled from multiple sources for the northwest Spring Mountains, Nevada. The inner shelf to fluvial-deltaic facies of virtually all units within the terrigenous detrital sequence in this region suggest shallow water deposition, removing the need for paleobathymetric correction (Levy and Christie-Blick, 1991). We used thicknesses from this study combined with thicknesses for overlying formations principally based on Stewart (1970) and Burchfiel et al. (1974). Our analysis encompasses known time points ranging from the Ediacaran-Cambrian boundary in the Lower Member of the Wood Canyon Formation (Corsetti and Hagadorn, 2000; Hagadorn

and Waggoner, 2000; Smith et al., 2016, 2017) at 541 Ma, up through the Devonian-Mississippian boundary at the top of the Devils Gate Formation (Burchfiel et al., 1974) at 359 Ma (Ogg et al., 2016). The only previous attempt at a geohistory analysis of the Spring Mountains (Levy and Christie-Blick, 1991) was temporally constrained mainly by the Lower-Middle and Middle-Upper Cambrian boundaries, which were then deemed to be ~30 m.y. older than their currently accepted ages. We followed methods described in Allen and Allen (2005) to delithify and progressively unload (backstrip) the stratigraphic column in order to obtain the tectonic component of subsidence. Delithification parameters for siliciclastic rocks were taken from Table 9.1 in Allen and Allen (2005), and parameters for carbonate rocks were taken from Equation 3 in Halley and Schmoker (1983). Tectonic subsidence curves were calculated using *Backstrip*, an open-source software for decompaction and tectonic subsidence calculations (Cardozo, 2009). Results for our earliest model runs were verified by hand using a spreadsheet program (e.g., Larrieu, 1995).

## RESULTS

### Lithostratigraphy

The most salient feature of the Johnnie Formation in the Johnnie Wash type locality (Figure 3) is that, although very fine-grained sandstone and siltstone is present in all mappable units (distinguishing it from the overlying Stirling and underlying Noonday formations), three intervals are characterized by an abundance of fine- to medium-grained sandstone (identified with Roman numerals I, II, and III on Figure 4). The sand-rich intervals

range from 160-430 m thick, form distinct, resistant ridges within the otherwise recessive Johnnie Formation, and establish a basis for subdividing it into mappable units. Each sand-rich interval exhibits characteristics that readily distinguish it from the other two, in terms of either bedforms (intervals I and II) or parasequence architecture (interval III). Further subdivision of the formation is afforded by a conspicuous, 30 to 40 m-thick cherty carbonate unit near the middle of the section, and by lithological variation within sand-rich interval III. Our subdivision into map units includes the Rainstorm Member at the top, underlain by twelve informal units designated A through L (Figures 4 and S1). Sand-rich intervals I and II define units B and D, and their enveloping sand-poor strata define units A, C, and E. The cherty carbonate marker and overlying sand-poor strata define units F and G. The upper sand-rich interval exhibits rhythmic variations of sandstone, siltstone, and carbonate that are divided into five units, H through L, each of which is defined at the base of a 30 to 100 m-thick sand-rich subinterval (Figures 3, 4, and S1).

At the Johnnie Wash type section, bedding strikes approximately north-south and dips moderately to steeply eastward (Figure 3). The total thickness of sub-Rainstorm strata is 1595 m. The lowest stratigraphic unit (unit A) encountered is a recessive, slope-forming phyllitic siltstone which contains a continuous cleavage at high angle to bedding. The base of unit B is defined by the lowest occurrence of meter-scale orthoquartzite beds, which are abundant in the unit. Unit B is readily distinguished from higher sand-rich intervals by pervasive penecontemporaneous deformation. Nearly every sandstone horizon is affected, principally by ball-and-pillow structure, so much so that individual orthoquartzite beds are difficult to trace along strike for more than a few tens of meters. Individual ball-and-pillow structures are up to meter-scale in size (roughly equal to orthoquartzite bed thickness) and

occur where fine-grained sandstone and siltstone underlie coarser sandstone. The ball-and-pillow structure is in places manifested as simple load casts with folded lamination (Figure 5A), and in others as completely detached sand bodies that have slumped downward into the underlying siltstone, surrounded by flame structure developed within the siltstone (Figure 5B). At the type locality, the occurrence of ball-and-pillow structure in the Johnnie Formation is restricted to unit B, but was also observed along one horizon at the top of the Rainstorm Member in the Mt. Schader section (Figures 6 and 7).

Unit C marks a return to generally inconspicuous, slope-forming siltstone with a prominent orthoquartzite marker horizon near the middle of the unit. The uppermost beds include a brown, resistant, 2-m-thick dolostone bed, which marks the lowest occurrence of carbonate in the type section.

Unit D includes orthoquartzite and less abundant siltstone. The sedimentary characteristic that distinguishes unit D from the other two sand-rich intervals is abundant high-angle cross-stratification, preserved in medium- to thick-bedded orthoquartzite (Figure 8A). Millimeter- to centimeter-scale laminae or thin beds are preserved in foresets within decimeter- to meter-scale beds that can be followed for tens of meters along strike. Foreset lamination is consistently truncated at high angles, ranging from 20-30°, by overlying beds (Figure 8B). In stratigraphic coordinates (corrected by tilting to horizontal about the line of strike), poles to foreset lamination are strongly unimodal, dispersed in trend by more than 90° around a mean vector of ~N30°E 65° (Figure 8B). We measured grain-size variation with stratigraphic height across a sequence of about ten foreset layers (Figure 8C and 8D), to test for the presence of reverse grading, which is characteristic of dry grain flows on the lee side of dunes (e.g., Hunter, 1977; Boggs, 2012). The result indicated that the mean grain

size of ~200 microns varies little through the sample, if anything fining slightly upward. In general, the lamination is not defined by concentrations of detrital heavy minerals. Opaque phases in these quartzites are largely diagenetic and relatively uniformly distributed throughout the rock.

The boundary between Units D and E is among the most readily mappable in the area and is also associated with a color change on remote imagery from dark brown to light brown, which is the most conspicuous color contrast in the section (Figure 2A). Unit E is about 280 m thick, and is dominated by very fine-grained sandstone and siltstone, generally lacking the mature, fine- to medium-grained quartzitic sandstone characteristic of unit D. Near the top, unit E contains an interval of about 30 medium-bedded cycles that alternate between massive, immature fine-grained sandstone and laminated siltstone. Unit F is a conspicuous, 30 to 40 m-thick, gray cherty dolostone (Figure 5C) that can be followed for at least 5 km along strike, albeit with some minor faulting. Unit G, 135 m thick, returns to siltstone and very fine-grained sandstone similar to unit E, with a few inconspicuous orthoquartzite beds.

The overall lithostratigraphic character changes beginning at the base of unit H, from relatively thick, homogeneous sandstone-, siltstone-, or carbonate-dominated units below, to the far more compositionally heterogeneous units above. From the base of unit H up to the base of the Rainstorm Member, the section contains abundant orthoquartzite, defining the uppermost of the three sand-rich intervals in the Johnnie Formation (Figure 4). For mapping purposes, the most straight forward subdivision of sand-rich interval III in the Johnnie Wash area is defined by five quartzite-dominated subunits ranging from 10 to 100 m thick, which define the lower parts of units H, I, J, K, and L (Figures 4 and S1). Each of these subunits is overlain by variable thicknesses of recessive, variegated siltstone (Figure 5E). The

occurrence of carbonate is sporadic. In the section in Johnnie Wash units I, J, and K are each capped by a resistant, 1 to 3 m-thick subunit of brown-weathering, laminated dolostone (Figure 5D), and units H and L do not contain carbonate (Figure 4). The Mt. Schader section contains a lesser proportion of quartzitic sandstone and a greater proportion of carbonate and siltstone (Figures 6 and 7), which is the basis for selecting it, instead of the type locality, for detailed measurement and chemostratigraphic sampling. Even within the Johnnie Wash area, the distribution of quartzite, siltstone, and carbonate changes along strike, on a scale of a few kilometers (Abolins, 1999). Although orthoquartzite beds in units H through L locally exhibit some high-angle cross-stratification in the Johnnie Wash section, they contrast with unit D (sand-rich interval II) in mainly being parallel-bedded or, in the case of the Mt. Schader section, hummocky cross-stratified. Orthoquartzite in units H-L is generally fine- to medium-grained, and appears to contrast with lower sand-rich intervals in containing a greater proportion of medium-grained and locally coarse-grained sand.

Our informal unit nomenclature ends at the base of the formally defined Rainstorm Member which, as noted earlier, is readily identified throughout the region on the basis of lithologic characteristics. In the northern Spring Mountains, the Rainstorm Member contrasts with the underlying units H through L in lacking fine- to medium-grained orthoquartzite beds. At the base of the Rainstorm Member, a fissile, phyllitic siltstone is overlain by the ochre-colored, 2 m-thick Johnnie oolite. The ooids are up to about 2 mm in diameter (Figure 5F) and exhibit local cross-stratification. The oolite horizon has erosional basal and upper contacts, locally including intraformational breccia and conglomerate, containing cobbles and small boulders of the oolite. Above the Johnnie oolite, pale-red limestones locally contain dispersed, coarse quartz grains interstratified with carbonate-cemented, fine-grained

sandstone. These carbonate-rich rocks are overlain by argillaceous mudstone with interbedded limestones, with scattered horizons of intraformational conglomerate. The uppermost part of the Rainstorm Member in the Mt. Schader section contains a 4 m-thick triad of quartzite, siltstone, and dolostone, in which the quartzite is disrupted by locally intense ball-and-pillow structure (Figure 5G and 5H). The base of the overlying A Member of the Stirling Formation is marked by highly resistant, massively textured to cross-stratified, medium- to thick-bedded, medium- to coarse-grained orthoquartzite. The principal contrast between the Stirling Formation's A Member and any of the orthoquartzites in the Johnnie Formation is the coarse grain size, including the common occurrence of granules and small pebbles of vein quartz and jasper in the Stirling Formation A Member. Neither the Johnnie Wash nor the Mt. Schader sections appear to preserve incised valley fill characteristic of the conglomeratic member of the Johnnie Formation (Abolins, 1999; Verdel et al., 2011).

**Chemostratigraphy**

Carbon isotope ratios range from a low of -4.4 ‰ (VPDB) to a high of 4.9 ‰ (Table S1). The data are mainly concentrated in carbonate beds in units H through L, which constitute the uppermost 400 m of pre-Rainstorm Member strata (Figure 7). Within the underlying c. 1100 m of exposed Johnnie Formation strata, carbonate intervals are present only in units C and F, approximately 1440 m and 860 m below the base of the Rainstorm Member, respectively (Figures 4 and 9). The lowest and highest values of $\delta^{13}C$ occur in the stratigraphically highest samples, and define a strong negative trend, beginning near the top of unit K and ending at the top of the Johnnie oolite bed. Below this marked trend in the data,

there is otherwise no general trend. More than 90% of the values recorded from the bottom of unit K to the unit C carbonate are positive, averaging 1.5 ‰ with a standard deviation of 1.2 ‰. The scatter in values within individual carbonate intervals is approximately the same as variations in the average values between carbonate intervals (Figure 7). However, variation in $\delta^{13}C$ values with stratigraphic position within each relatively thin carbonate interval does not appear to be entirely random (Figure 10). For example, carbonates from units C and the lower part of unit K show decreasing $\delta^{13}C$ values stratigraphically upward ($R^2$ = 0.74, 0.88 respectively), whereas values from the lower two carbonates in unit H and the upper carbonate interval in unit J suggest increasing $\delta^{13}C$ values stratigraphically upward ($R^2$ = 0.26 - 0.83).

Oxygen isotope ratios range from a low of -16.0 ‰ (VPDB) to a high of -5.0 ‰, with an average value of -9.4 ‰ (Table S1). There is no general trend in the mean values for each individual carbonate interval with stratigraphic position (Figure 7C). The range of values within the carbonate intervals is as great as 6 ‰, i.e., greater than the variation of mean values for each interval. Correlation of $\delta^{18}O$ and $\delta^{13}C$ is poor for the dataset as a whole (Figure 11). Plots of $\delta^{18}O$ versus stratigraphic position with side-by-side comparison with $\delta^{13}C$ values are presented in the Supplemental Items (Figure S2). Correlation of $\delta^{18}O$ values with stratigraphic position within each interval is also generally poor. Of twelve beds with > 3 samples, $R^2 > 0.5$ only for beds Zjj1, Zji2, and Zjc (see Table 1 for nomenclature). In regard to correlation of $\delta^{18}O$ with $\delta^{13}C$, only the carbonate in unit C shows good positive correlation ($R^2$ = 0.9), but this interval only has four data points. Intervals with 10 or more data points all show poor ($R^2 < 0.1$) intrabed correlation of $\delta^{18}O$ with $\delta^{13}C$ (Figure S2).

**Subsidence Analysis**

Our analyses focused on modeling the tectonic component of subsidence for strata in the Spring Mountains section: Johnnie unit A through the Devonian Devils Gate Formation (Table 1). The model results define the relationship between the stratigraphic thickness *S*, and the tectonic component of subsidence *Y* (Table 2), which yields a resulting curve for the function *Y*(*S*) (Figure 12). This curve depends on parameters that describe lithification and isostatic adjustment due to sediment loading (Tables 2 and 3), and is independent of time (Eqs. 1 and 2 in Steckler and Watts, 1978). We will model the time dependence of subsidence in the Discussion section below.

Our determinations of *Y*(*S*) include the effects of some 3000 m of Mississippian through Triassic overburden that lay above the Johnnie-Devils Gate interval during Jurassic and Early Cretaceous time (Giallorenzo et al., 2017). They also include two major sources of uncertainty. The first is the possible effect of a significant sedimentary substrate, pre-dating Johnnie unit A, on the calculated tectonic subsidence. The substrate may either have been (1) limited to the Noonday Formation or its equivalents, which are at most a few hundred meters thick and may be represented by the lowest units of the Johnnie Wash section (values $Y_{ns}$ indicate "no substrate"); or (2) a thick succession of Proterozoic Pahrump Group strata (Crystal Spring through Kingston Peak formations), which could be present at depth beneath the northwest Spring Mountains (values $Y_{ws}$ indicate "with substrate"; note that in Figure 12, $Y_{ws}$ values were plotted using the base of the Spring Mountains section as a datum for zero, for a direct comparison to $Y_{ns}$). The oldest Pahrump Group strata, the Crystal Spring Formation, were c. 500 m.y. old in Ediacaran time, and therefore these models may

somewhat overestimate its effect on late Cryogenian-Ediacaran subsidence. The second major source of uncertainty lies in the resulting density of the delithified sediment column (Bond and Kominz, 1984; Bond et al, 1988). We simulated this error by varying sediment grain density by ±5%, and note that the effect of sediment unloading is such that the lowest assumed density results in the highest tectonic component of subsidence and vice-versa. This density range yields variations in values of $Y$ for a given $S$ ($Y_{low}$ or $Y_{high}$; Table 4) that are similar to those obtained by Bond and Kominz (1984) and Levy and Christie-Blick (1991).

The resulting plots for $Y(S)$ (Figure 12) show a decreasing ratio of tectonic subsidence per meter of sediment thickness, with slopes ($\Delta Y/\Delta S$) ranging from values near 1.0 at the base of the section for the "no substrate" curves, to as little as 0.1 near the middle of the section for the "with substrate" curve. More typically, slopes range from 0.3 to 0.6. There is an abrupt change in slope at $S \approx 3500$ m, where the section transitions from predominantly siliciclastic to predominantly carbonate sedimentation. On the no-substrate curve, the slopes defined by the five values closest to $S = 3500$ m are 0.5 ($S < 3500$ m) and 0.2 ($S > 3500$ m), with each of the two arrays appearing quite linear. Corresponding values on the "with substrate" curve are 0.4 and 0.1. Thus, although there is a degree of gradual curvature above and below $S = 3500$ m, most of the flattening of $Y(S)$ is associated with the lithologic transition.

The effect of including a thick substrate of Pahrump Group strata is to greatly reduce our estimate of $Y$ for any given $S$. In other words, by not accounting for the substrate, we overestimate the tectonic component of subsidence by 50% or more, particularly in the early phases of subsidence. Physically, the reason for this is that the no-substrate model inadvertently places incompressible basement rocks where a compacting substrate exists; in

the event that there is substrate, the model incorrectly assigns the compaction of the substrate to tectonic subsidence, resulting in an overestimate.

The uncertainties in *Y* due to sediment grain density are generally in the ± 10 to 15% range. And, to the extent that a thick sedimentary substrate is present below the lowest exposures of the Johnnie Formation in Johnnie Wash, tectonic subsidence may be overestimated by several tens of percent. Despite the sensitivity of both the density and substrate effects on the absolute value of *Y*, as we will discuss in the next section, their effects on estimating the age of tectonic subsidence are not large, because these estimates depend mainly on relative, not absolute values of *Y*. Specifically, (1) errors arising from density and substrate are correlated, such that $Y(S)$ retains its shape even though *Y* may vary significantly, and (2) the exponential equation describing time dependence of *Y* is defined by ratios between values of *Y*, rather than their absolute magnitudes.

## DISCUSSION

Perhaps the most basic question in regard to the origin of the Johnnie Formation is whether the sub-oolite interval contains recognizable sub-units that can be correlated across its region of exposures, and the extent to which the section contains major unconformities. These issues are best addressed through lithostratigraphic characteristics and comparisons between the Spring Mountains section and the two other major sections in the region, the Desert Range to the north and the Nopah Range to the south. A second important question is whether or not the sub-oolite (sub-Shuram excursion) interval is a chemostratigraphic correlative with the sub-Shuram excursion Khufai Formation in Oman. A third significant

issue is whether continuous Johnnie Formation (and subsequent) deposition occurred through most or all of Ediacaran time, because this aspect is critical to dating the Johnnie using thermal subsidence modeling. A time-dependent exponential thermal subsidence model, applied to our decompacted and backstripped subsidence model, *Y*(*S*) (Figure 12), implies continuous sedimentation along the southwest Laurentian passive margin through the whole of Ediacaran time (i.e., from basal Noonday to early Wood Canyon time, or 635 - 541 Ma). If such a model is correct, it provides an independent estimate of the age and duration of the Shuram excursion, and whether or not it occurred near the time of the Gaskiers glaciation.

**Lithostratigraphy**

Although lithostratigraphic correlation of sub-Rainstorm Member Johnnie Formation units is not as straightforward as for the overlying intervals, neither is it particularly complex. The two thickest sections, which both lie in Nevada, the northern part of the Johnnie outcrop belt, include the northern Spring Mountains and Desert Range sections. Both sections are readily divisible into alternating sand-rich and siltstone/carbonate-rich intervals, each of order one hundred to a few hundred meters thick (I, II, III in Figure 13 on the northern Spring Mountains section). The three sand-rich intervals of the Johnnie Formation are succeeded by four additional sand-rich intervals that have long been recognized as regionally correlative units (IV-VII in Figure 13 on the northern Spring Mountains section), of which the top three have paleontological age constraints. The two sections each contain three sand-rich intervals below the Rainstorm Member that are of proportionate relative thickness. Further, the

siltstone/carbonate-rich interval between sand-rich intervals II and III contains a c. 40 m-thick cherty dolostone unit in both sections, strengthening correlation, as noted by Stewart (1970) and Benmore (1978). We correlate sand-rich interval I of the Spring Mountains (unit B) with the Carbonate member in the Desert Range section, on the basis of stratigraphic position. We note, however, that the pervasive soft sediment deformation in unit B has not been reported from orthoquartzites in the Carbonate member, and that unit B does not contain carbonate. Unit A, which is predominantly siltstone, would therefore correlate with siltstones and oolitic limestones underneath the Carbonate member. The oolitic limestone unit at the base of the Desert Range section has been considered to be correlative with the Noonday Formation (Longwell et al., 1965; Gillett and Van Alstine, 1982), implying that unit A in the Spring Mountains may also be a Noonday correlative (Figure 13).

The southern Nopah Range section is approximately half the thickness of the northern Spring Mountains and Desert Range sections, and contains a number of subaerial erosion surfaces that thus far have not been observed in the thicker Nevada sections (Summa, 1993). Like the Nevada sections, however, it does contain three sub-Rainstorm sand-rich intervals, suggesting lithostratigraphic correlation (Figure 13). Specifically, the lower part of the Transitional, Quartzite, and Upper carbonate-bearing members of Stewart (1970) would correspond to sand-rich intervals I, II, and III, respectively, in the Spring Mountains. The correlation is strengthened by: 1) the alternating orthoquartzite/carbonate cycles evident in sand-rich interval III in both the northern Spring Mountains and southern Nopah Range sections; 2) the lack of carbonate and abundance of high-angle cross stratification in interval II in all three sections (Quartzite member = upper part of Lower quartzite and siltstone member = unit D, Figure 13); 3) the consistency of unimodal, south-southwest directed

paleoflow directions in pre-Rainstorm orthoquartzites in the Spring Mountains and Desert Range sections (Figure 14); and 4) the lithological similarity between the lowest sand-rich intervals in the southern Nopah Range and Desert Range sections, both of which contain a mixed carbonate-siliciclastic assemblage. Militating against these lithostratigraphic correlations are the observations that: (1) the interval III correlative in the Desert Range lacks carbonate; (2) interval I in the Spring Mountains (unit B) also lacks carbonate; and (3) the proposed Noonday substrate of interval I is lithostratigraphically dissimilar in the three sections, ranging from pale-gray quartz-rich dolomite boundstone in the Nopah Range, to phyllitic siltstone in the Spring Mountains to medium-gray oolitic limestone in the Desert Range. Regardless of the details of these correlations, the most important facets of the two sections in Nevada are (1) the sub-Rainstorm sections are at least twice as thick as the Nopah Range section, and (2) evidence for subaerial erosion, such as grikes, paleosols, channel scour, and dessication cracks, which is conspicuous in the Nopah Range section, appears to be lacking. Although significant depositional hiatuses within the Nevada sections cannot be ruled out, the overall lithostratigraphic uniformity or "monotony" of these sections (siltstone and fine- to medium-grained sandstone and orthoquartzite, with sporadic thin carbonate beds) is consistent with conformable sedimentation on a stably subsiding continental shelf (Stewart, 1970; Fedo and Cooper, 2001; Schoenborn et al., 2012).

The pervasive ball-and-pillow and other paleoliquefaction structures in sand-rich interval I (unit B) are most simply interpreted as reflecting a period of high sediment flux in early Johnnie Formation deposition. These structures may have significance for the timing of transition from mechanical stretching of the lithosphere to purely thermal subsidence, because 1) rapid subsidence is characteristic of both the rift phase and early thermal

subsidence phase of passive margin formation (e.g. Sawyer et al., 1982), and 2) such structures could be evidence for seismic shaking (e.g. Sims, 2012). The observation that essentially the entire 160 m thickness of unit B is affected implies that, whatever its cause, it was persistent over a sustained period of time. The other significant observation is that with only one exception, paleoliquefaction structures do not appear anywhere else higher in the section, despite the ubiquity of meter-scale interbeds of fine- to medium-grained sandstone overlying fine-grained sandstone or siltstone throughout the section. Thus, the cause, or causes, of soft-sediment deformation appears to be temporally restricted to, at most, sand-rich interval I and enveloping siltstone units A and C, and presumably ended by the time of deposition of sand-rich interval II (unit D). If it is assumed that the cause is earthquakes, then sand-rich intervals I and II record a transition from frequent seismic shaking to apparent seismic quiescence. Such an interpretation is consistent with previous suggestions that the end of mechanical stretching may have occurred near the base of the Johnnie Formation (Summa, 1993; Fedo and Cooper, 2001; Schoenborn et al., 2012). A ready alternative to a seismic trigger, however, is the effect of pressure contrasts from storm waves, which have also been shown to induce liquefaction and soft sediment deformation, including ball-and-pillow structure (Alfaro et al., 2002).

**Chemostratigraphy**

A composite plot of $\delta^{13}C$ values of carbonate from the Johnnie Formation in southwest Laurentia (Verdel et al., 2011; this study) yields an overall pattern that is similar to profiles in Oman that contain the Shuram excursion, including a period of positive values

as high as 4 - 6 ‰, rapid descent to values as low as -11 to -12 ‰, and a more gradual rise back to positive values (Figure 15). The uniformly positive $\delta^{13}C$ values below the excursion in southwest Laurentia, generally of 1 - 3 ‰, invite detailed comparison with chemostratigraphic profiles in the carbonate-rich Khufai Formation in Oman, which lies immediately below the type Shuram excursion. The stratigraphic thickness of units between the zero crossings of the Shuram excursion in Oman and southwest Laurentia are similar, approximately 500 - 700 m (Verdel et al., 2011). We therefore compared our profile to those from Oman without any modification to the vertical scaling (stratigraphic height), fixing the zero crossings at the base of the Shuram excursion at the same height. The Khufai sections in general are positive in $\delta^{13}C$ and show considerable variation, depending on the degree of diagenetic alteration. In least altered sections (Mukhaibah Dome area), maximum values range up to 6 ‰, averaging 4 - 5 ‰ (Figure 16A), considerably more positive than the Johnnie profile. In more-altered sections (Buah Dome area, Figure 16B), the profiles are quite similar to that of the Johnnie Formation. Given the close correspondence between the Johnnie profile and most of the Oman profiles (Figure S3), we conclude that the data are consistent with, but do not absolutely demonstrate, temporal correlation of the upper part of the sub-Rainstorm Johnnie Formation (units H through L in the Spring Mountains) and the Khufai Formation.

The least altered Khufai sections are generally considered to be representative of sea water carbon isotopic composition, defining a prolonged interval of $\delta^{13}C$ values in sea water near 6 ‰. Therefore, it seems clear that subsequent diagenesis is primarily responsible for reducing $\delta^{13}C$ values, in both Oman and the sub-Rainstorm Mt. Schader section by as much as 4 - 5 ‰. In the Pleistocene environment, such reduction has been shown to result from

carbon isotopic exchange between carbonate beds and meteoric water, often resulting in $\delta^{13}C$ values decreasing stratigraphically upward at the scale of a few meters in beds exposed to erosion (Allan and Matthews, 1977; 1982; Quinn, 1991; Melim et al., 1995; Melim et al., 2001). The strong intrabed variations in $\delta^{13}C$ values in 1 - 2 m-thick carbonate intervals in the Johnnie Formation (Figure 10) could potentially be explained by this mechanism, although $\delta^{13}C$ values of meteoric water at that time are poorly constrained and may not have been as strongly negative as modern values. Further, the intrabed trends in $\delta^{13}C$ values both increase and decrease downward, and there is no evidence of subaerial exposure on the tops of any of the beds. As with most Neoproterozoic carbonates, determining the mechanisms of depletion of $\delta^{13}C$ values and their relationship to diagenetic textures and the biosphere is a difficult and controversial issue (Knauth and Kennedy, 2009; Derry, 2010a; 2010b; Grotzinger et al., 2011), beyond the scope of this paper to resolve. One thing we can say, however, about the Mt. Schader data set is that it displays no clear correlations between $\delta^{18}O$ and $\delta^{13}C$ (Figure 11), as predicted by various isotopic exchange models (Figure 4 in Osburn et al., 2015). Despite this controversy, the good match between the type Johnnie sub-Rainstorm Member section and the Khufai Formation supports the hypothesis that regardless of the origin of the anomalies, they nonetheless appear to be a useful correlation tool (Grotzinger et al., 2011). Tectonic reconstructions of the Neoproterozoic continent Rodinia put both the Shuram and Johnnie formations roughly at the equator in Ediacaran time, but the two formations were located anywhere from 10,000 - 15,000 km away from each other (Li et al., 2008; Li et al., 2013), making the isotopic correlation of the Shuram and sub-Shuram intervals all the more impressive.

One of the hallmarks of Neoproterozoic glacial cap carbonates is their frequent

occurrence as thin, isolated intervals amid large thicknesses of enveloping strata that are entirely siliciclastic. Below unit H, there are two such isolated carbonate intervals, one in unit C and the other composing the entirety of unit F. Given their stratigraphic position between the Marinoan cap carbonate sequence (Noonday Formation, Figure 1) and the base of the Cambrian, it is possible that either one of these units represents post-glacial carbonate "rainout," for example, as might be expected in the more southerly latitudes in the wake of the Gaskiers glaciation at 579 Ma (e.g. Pu et al., 2016). The generally positive $\delta^{13}C$ values in the unit C and unit F carbonates, averaging between 1 - 2 ‰, argue strongly against either of these intervals representing a Gaskiers cap carbonate, which in Newfoundland yielded $\delta^{13}C$ values of -8 to -2 ‰ (Myrow and Kaufman, 1999). Further, textural features widely described from cap carbonates (e.g. sheet cracks, tubes, teepee structures, etc.) are not observed in either of these intervals.

**Subsidence Analysis**

The substantial thickness of the Johnnie Formation, lack of evidence for unconformities in the Nevada sections, and the strengthened isotopic tie to the type Shuram excursion, motivate the hypothesis that the Noonday through Lower Wood Canyon interval records continuous deposition through most or all of Ediacaran time. In the last section, backstripping and decompaction defined tectonic subsidence *Y* as a function of stratigraphic position *S*, independent of time. In this section, we model the element of time as exponential subsidence, assuming that Johnnie and subsequent deposition of the passive-margin wedge occurred as a result of conductive cooling of rifted lithosphere. Subsidence analysis with

well-defined ages at the Cambrian-Precambrian boundary (541 Ma) and at the base of Cambrian Age 5 (509 Ma) creates a considerably improved basis over previous studies for estimating stratigraphic age in Ediacaran strata by extrapolating the subsidence history back in time.

Regardless of the absolute elevation following mechanical extension of the lithosphere, once thermal subsidence begins, the elevation *e* of the surface, above its equilibrium value at $t = \infty$, is closely approximated by:

$$e(t) \cong E_0 r \mathrm{e}^{-\frac{t}{\tau}}, (1)$$

where $E_0 r$ is the elevation of stretched lithosphere above its equilibrium depth at infinite time (or in the case of infinite stretching, the height of the ocean floor above the abyssal plains), *t* is time, $\tau$ is the characteristic time (time at which $\frac{e}{E_0 r} = \frac{1}{\mathrm{e}}$), and:

$$r = \frac{\beta}{\pi} \sin \frac{\pi}{\beta}, (2)$$

where $\beta$ is the stretching factor (Figure 17; eqns. 10 and 11 in McKenzie, 1978). $E_0$ and *r* are not parameters of interest when using subsidence as a chronometer, because we are attempting to use the late history of post-rift subsidence, which is well dated, to constrain the earlier history of post-rift subsidence, which is not. The simple exponential formula for elevation versus time $e(t)$ of Equation 1 is converted to subsidence depth *Y* versus time by substituting ($E_0 r$ - *Y*) for *e*, yielding:

$$Y(t) \cong E_0 r \left(1 - \mathrm{e}^{-\frac{t}{\tau}}\right). (3)$$

In the case of mid-ocean ridges, where $\beta = \infty$ and $r = 1$, $E_0 r$ is empirically shown to be within a few percent of 3.2 km (Parsons and Sclater, 1977). We note that this value does not correspond to the actual ridge elevation above the abyssal plain, which is much higher for oceanic crust less than 20 m.y. old. The characteristic time $\tau$, which depends on the thermal diffusivity and thickness of equilibrium lithosphere, shows somewhat greater variation depending on the ridge (±10% for the best-constrained ridges; Table 1 in Parsons and Sclater, 1977), but a generally accepted value in subsidence analyses of passive margins is 50 - 65 m.y. (McKenzie, 1978; Allen and Allen, 2005). This corresponds to a "half-life" of thermal subsidence of 35 - 45 m.y.. Even though this key parameter may vary significantly, we can estimate $\tau$ directly from our subsidence model, as an independent test of the hypothesis that the margin is in a state of exponential thermal subsidence, comparable to well-studied Mesozoic and Cenozoic examples. If our estimate of $\tau$ lies significantly outside the range of 50 - 65 m.y., it would falsify the thermal subsidence hypothesis.

Even though we do not know $E_0 r$, estimation of $\tau$ and extrapolation of the curve back in time requires as few as two known elevation-time pairs, ($e_1$, $t_1$) and ($e_2$, $t_2$) (Figure 17). Substituting these pairs into Equation 1, differencing the equations and solving for $\tau$ yields:

$$\tau = \frac{(t_2 - t_1)}{\ln(\frac{e_1}{e_2})}. (4)$$

The differencing of the two equations eliminates $E_0 r$, and hence the most important parameters in estimating both $\tau$ and the thermal subsidence curve itself are the elevation of two points relatively well separated in time from each other, and an estimate of zero elevation, i.e., where $e(\infty) = 0$ or the slope of $Y(t)$ is negligible. The thermal subsidence curve is then presumably applicable back in time to whatever point in the section we are still confident that the margin is in a state of pure thermal subsidence. As noted above, this level is probably no higher in the section than the lower part of the Johnnie Formation, and it may be much deeper, perhaps within the upper part of the underlying Pahrump Group.

Temporal constraints on the younger part of the subsidence curve are fairly similar to those used by Levy and Christie-Blick (1991) with the exception of their two oldest points, the base of the Cambrian Age 5 (~Middle Cambrian, 509 Ma, Walker et al., 2013) and the base of the Paibian (~Upper Cambrian, 497 Ma, Walker et al., 2013), which at the time were estimated to be 540 Ma and 523 Ma, respectively. Critically for this study, both the position and age of the Ediacaran/Cambrian boundary are well defined, lying within the Lower Member of the Wood Canyon Formation with an age of 541 Ma (Corsetti and Hagadorn, 2000). The 541 and 509 Ma constraints thus function as points ($e_1, t_1$) and ($e_2, t_2$) respectively in our initial analysis, defining an exponential subsidence curve. As the oldest reliable temporally constrained points on the curve, they are the strongest constraints on extrapolating the curve back in time.

Points younger than 509 Ma are also well-dated. These points clearly postdate the Sauk marine transgression, which marks a transition from predominantly siliciclastic to carbonate sedimentation due to flooding of the craton through middle and late Cambrian time. Associated with the transgression, the average deposition rate (the time derivative of

$S(t)$, $dS/dt$) increases markedly from c. 20 m/m.y. from 541 to 509 Ma to c. 80 m/m.y. from 509 to 497 Ma (Table 4). Clearly, a four-fold increase in accumulation rate appears incompatible with any form of exponential subsidence. As explained below, the remarkable increase in subsidence rate owes its origin to the combination of sea level rise and carbonate sedimentation, not renewed tectonism. The important point here is to note that the 541 and 509 Ma data points occur within the Lower Wood Canyon and Lower Carrara formations, respectively, both of which are shallow water, mixed carbonate-siliciclastic facies associations that were probably deposited at similar points in global sea level. Both were deposited during highstand intervals relative to their transgressive substrates (the Stirling E Member and Zabriskie Formation respectively). In the case of the Lower Wood Canyon Formation, the system evolved into a glacial drawdown of sea level (Smith et al., 2016). In the case of the Lower Carrara Formation, sea level kept rising to a level that generally exceeded those of Ediacaran-early Cambrian time (Palmer, 1981).

The late subsidence history is characterized by very slow accumulation in Silurian and Early Devonian time (<3 m/m.y., Table 4), and hence the difference between Silurian and Devonian values of $Y$ to those at 541 and 509 Ma provides firm estimates of $e_1$ and $e_2$. We note that with these constraints, the precise values of time and elevation for Paibian through Upper Ordovician strata provide little additional constraint on the form of the exponential subsidence curve.

### *Temporal Model*

We present a temporal model of both observed subsidence $S(t)$ (i.e., stratigraphic

thickness) and tectonic subsidence $Y(t)$ using a novel mode of presentation that orthogonally projects $Y(t)$ and $t(S)$ onto a graph of the numerically determined function $Y(S)$ (Figure 18). In this approach, $Y(S)$ is plotted in the upper left corner, $Y(t)$ in the upper right corner, $t(S)$ in the lower left corner, and $S(t)$ in the lower right corner. The plot shows a simultaneous projection of $Y$ and $S$ onto their respective temporal models, graphically showing the influence of the slope of $Y(S)$ on the observed subsidence rates. The graph shows that, between 509 and 485 Ma, the increase in compressibility of the carbonate sediment (lower slope on $Y(S)$), combined with the accelerated schedule of subsidence caused by the flooding of the craton (higher slope on $Y(t)$), resulted in a dramatic increase in sediment accumulation rate (lower slope on $t(S)$ and higher slope on $S(t)$), even though exponential subsidence was slowly decreasing. This result is critical because it obviates the primary reason that most previous workers have cited in favor of Cambrian rifting along western Laurentia (e.g., Bond and Kominz, 1984; Levy and Christie-Blick, 1991; Yonkee et al., 2014).

***Parameter Estimates and Sensitivities***

Estimates of the exponential time constant $\tau$ vary according to two main uncertainties, firstly the sediment grain density assumed in our delithification model, and secondly whether or not a thick substrate of Pahrump Group strata is present at depth beneath the exposed Spring Mountains section. We calculated values of $\tau$ for values of tectonic subsidence $Y$ in a series of models that encompass these parameter variations (Table 5). In addition, we defined $Y$ according to two different assumptions for the point at which mechanical stretching ends and purely thermal subsidence begins, where $Y = 0$ (i.e. $e = E_0 r$). One is at the lowest exposed

stratum (base of unit A), and the other is within unit C, above the youngest ball-and-pillow structure at the top of unit B, assuming seismic shaking ended near this point. In Table 5, models with no Pahrump Group substrate are designated $Y_{ns}$, and those that include the substrate are designated $Y_{ws}$; intermediate density models contain no additional subscript, and low and high density models are also subscripted "low" and "high" respectively. Models with superscript "4" define $Y = 0$ within unit C, and models with no superscript assume $Y = 0$ at the base of unit A. We defined the value of $Y$ for which $e = 0$ to be the average of $Y$(393 Ma) and $Y$(383 Ma), designated $Y$(c. 388) in Table 5. The results are insensitive to this choice because there is so little variation in $Y$ between 444 and 383 Ma. We cannot choose the next younger point in the subsidence profile (359 Ma) because it clearly reflects the onset of subsidence associated with Antler foredeep sedimentation.

The contrast in $\tau$ between models $Y_{ns}$ and $Y_{ws}$ is only 3 m.y., with $\tau = 55$ and 52 m.y. respectively. As expected from Equation 4, the definition point of $Y = 0$ has no effect, because we define $e_1$ and $e_2$ on the basis of differences in $Y$ values late in the subsidence history. For models with no substrate, varying the density between $Y_{ns,\,low}$ and $Y_{ns,\,high}$ (corresponding to the assumption of high and low sediment grain density respectively), has a substantial effect on $\tau$, which ranges from 42 to 65 m.y., respectively. For models $Y_{ws,\,low}$ to $Y_{ws,\,high}$, the sensitivity is even greater, with $\tau$ varying from 36 to 63 m.y., respectively. Clearly, the upper part of these ranges accords with subsidence patterns in Mesozoic and Cenozoic basins. Despite the nearly 30 m.y. variation in $\tau$ among these models, we note that there is relatively little variation in the modeled age and duration of the Shuram excursion (Table 5). Among this suite of models, the onset varies by 12 m.y. (from 569 to 581 Ma), the termination by 9 m.y. (from 566 to 575 Ma) and the duration varies by 3 m.y. (from 3 to 6 m.y.).

A further consideration in estimating $\tau$ is the fact that because the Sauk transgression was well underway by 509 Ma, relative sea level may have been slightly higher than at 541 Ma. To the extent that it was, a significant systematic error is introduced in our estimate of $\tau$. For example, for the model with no substrate and intermediate density, a correction in $Y(509)$ of just -50 m to account for the change in sea level (+50 m in $e_2$) changes the estimate of $\tau$ from 55 to 69 m.y. (Equation 1 in Steckler and Watts, 1978; Equation 4 herein). Thus, although the suite of models used for our sensitivity analysis may suggest an estimate of 50 ± ~15 m.y. for $\tau$, the systematic error introduced by the Sauk transgression, and the range of values indicated by models of Mesozoic and Cenozoic basins, both suggest a value toward the upper end of this range. We further note that the earliest empirical fits to long-term seafloor subsidence data suggested a value of 62.8 m.y. (Equation 22 in Parsons and Sclater, 1977; Table 1 in McKenzie, 1978).

Based on these considerations, we develop a second suite of models for estimating pre-541 Ma ages of various horizons within the Johnnie Formation. For this suite, we chose a "midrange" model using what are perhaps the simplest set of assumptions: 1) intermediate sediment grain density values; 2) negligible Pahrump Group substrate; and 3) a time constant of $\tau$ = 65 m.y. Using these assumptions, we tie the subsidence curve to the oldest dated time point at 541 Ma, minimizing both the amount of extrapolation back in time, and the degree to which the data reflect sea level rise due to the Sauk and subsequent cratonic flooding events. The resulting subsidence model for the Spring Mountains section is shown in Figure 18, and in Table 6 in the second column from the right hand side. The remaining columns in Table 6 and Table S2 demonstrate the sensitivity of our resulting age estimates for the Shuram excursion and other horizons in the Johnnie and Stirling formations to variations in

density, $\tau$, and the presence or absence of a substrate. Varying only sediment grain density, limits on the Shuram excursion (tops of units Zjr1 to Zjr2) are 581 - 575 Ma (low density case), 585 - 579 Ma (intermediate density), and 592 - 585 Ma (high density) (Figure S4). Thus, we see that the end of the excursion varies from 575 - 585 Ma, a range which is centered on the timing of the Gaskiers glaciation. We also note that the duration of the excursion is 6 - 7 m.y., and it is therefore insensitive to variations in sediment grain density. With regard to sensitivity to the time constant, the end of the Shuram excursion for intermediate density values is 579, 576, and 573 Ma for $\tau$ = 65, 60, and 55 m.y. respectively (Figure S5). In terms of the error introduced by the presence of a Pahrump Group substrate (Figure S6 and Table S2), for $\tau$ = 65 m.y. and intermediate values of density, the Shuram excursion occurs from 584 - 578 Ma, which is only 1 m.y. later than, and of the same duration as, the case of no substrate. The duration of the Shuram excursion, across all models in this suite ranges from 4 - 7 m.y. If we exclude with-substrate models (Table S2), the variation decreases to 5 - 7 m.y., and if we further restrict the time constant to 65 m.y., it decreases to 6 - 7 m.y. These estimates are consistent with recent estimates of 8 - 9 m.y. for the Johnnie, South Australia (Wonoka), and central China (Doushantuo) sections, based on rock magnetic chronostratigraphy (Minguez et al., 2015; Minguez and Kodama, 2017; Gong et al., 2017). These estimates are all considerably shorter than the subsidence-based estimate of 50 m.y. for the Shuram excursion in Oman (Le Guerroué et al., 2006b), which has been called into question on the basis that the Khufai/Shuram interval was probably not deposited on a thermally subsiding continental shelf (Bowring et al., 2007).

In sum, because the timing of the Shuram excursion is within c. 0.5$\tau$ of 541 Ma, varying parameters in the exponential subsidence model yields variations in our estimate of

age and duration of the Shuram excursion of just a few million years. The fact that a fairly broad range of parameters leads to estimates of the end of the Shuram excursion centered on 579 Ma, suggests that the valleys incised into the Rainstorm Member are indeed a manifestation of the Gaskiers glaciation at equatorial latitudes. To conclude otherwise strains credulity, because Johnnie/Stirling sequence architecture is relatively uneventful for 400 - 500 m both above and below the Rainstorm Member (Stirling Member A/B and Johnnie units H through L, respectively). If incision was unrelated to the Gaskiers glaciation, it requires (1) that the most dramatic stratigraphic event in the Johnnie/Stirling interval was close in time, but unrelated to, glaciation, and (2) that the Gaskiers glaciation itself had virtually no impact on the section. In essence, the subsidence analysis provides a relatively coarse estimate of age that "registers" the section with possible correlatives elsewhere. The detailed stratigraphy then fine tunes the age estimate based on a specific correlation with well-dated events elsewhere: in this case, shelf-incision and the Gaskiers glaciation.

The overall consistency of exponential subsidence models with the hypothesis that incision of the Rainstorm Member shelf is an expression of the Gaskiers glaciation suggests that modeled ages of other horizons in the Johnnie/Stirling interval may also be accurate to within a few million years. The overall accuracy of this model can be further tested by assessing how well it estimates the age of the lowermost Johnnie and Noonday interval. As noted above in our discussion of the possible correlation of unit A with the Noonday Formation, we would expect the age of this unit to be close to the age of the base of the Noonday Formation, or 635 Ma (Petterson et al., 2011). The range of modeled ages for the base of unit A are 639 - 608 Ma (Table 6), with the "mid-range" model shown in Figure 18B predicting an age of 628 Ma. As shown in Figure 18D, linear extrapolation below the deepest

exposed strata of unit A, assuming a linear deposition rate, would require only an additional 288 m of "sub-unit A" strata to bring the section to the base of the Noonday Formation and the Ediacaran Period. This thickness, plus the 125 m thickness of unit A yields a total thickness of 413 m, which is consistent with maximum known thicknesses of the Noonday Formation (Petterson et al., 2011). The apparent success of exponential subsidence models in predicting the age of both the Gaskiers event and the base of the Ediacaran Period at their most likely stratigraphic levels, supports the hypothesis that Ediacaran deposition on the southwest Laurentian margin was largely continuous, and that the Noonday through Wood Canyon interval in its thickest, most basinal exposures does not contain unconformities with significant depositional hiatuses.

## CONCLUSIONS

Lithostratigraphic and chemostratigraphic details of the Johnnie Formation at its type locality in the northwest Spring Mountains of southern Nevada provide a basis for regional lithostratigraphic correlation, global chemostratigraphic correlation, and subsidence analysis of the southwest Laurentian continental margin. The regional lithostratigraphy of Ediacaran through Cambrian Age 4 strata defines seven sand-rich intervals separated by siltstone- and carbonate-rich intervals, the upper two of which are the Sauk I and Sauk II sequences of Cambrian age (Palmer, 1981). The great overall thickness of the Johnnie Formation at its type locality (c. 1800 m), and the apparent absence of subaerial exposure surfaces or other evidence of erosion that are well expressed in more cratonic sections such as the Nopah Range section, support the hypothesis of continuous deposition. Nonetheless, the

lithostratigraphy is strongly cyclic at kilometer scale, suggesting that significant hiatuses, or at least greatly reduced rates of sediment flux, may be associated with the base of each of the seven sand-rich intervals, even in the more basinal sections. We therefore caution that the true slope of the observed sediment accumulation curve $S(t)$ is almost certainly more variable than shown in Figure 18D, especially for the segment between 635 Ma and 541 Ma. This concern is tempered by the fact that sediment flux was sufficient in Ediacaran and Paleozoic time to fill the accommodation space to within a few meters to a few tens of meters of sea level, implying that the tectonic component of subsidence is fully recorded.

Carbon isotopic data from sub-Rainstorm Member (sub-Shuram excursion) units in the Mt. Schader section are generally positive, and support correlation of Johnnie units H through L with the Khufai Formation in Oman, but they do not require it. If correlative, the Mt. Schader section would provide the first confirmation of an extended period (represented by 300 – 400 m of section) of positive $\delta^{13}C$ values prior to the Shuram excursion in both Oman and Nevada.

The Gaskiers glaciation marks the beginning of widespread preservation of macroscopic Ediacaran animals (Xiao et al., 2016), and the Shuram excursion is the largest known carbon isotopic excursion in the geological record. A central issue in animal evolution is thus whether or not the Shuram excursion was approximately synchronous with the Gaskiers event, because it suggests that the Shuram excursion, whatever its cause, was genetically related to creating a surface environment that could support the metabolic requirements of macroscopic animals. A second consequence of Shuram-Gaskiers correlation is that it places the transition from diverse, ornamented acritarchs to a lower diversity, unornamented assemblage in synchronism with the appearance of macroscopic

animals, rather than at some later time. The issue is addressable in southwest Laurentia, to the extent that deposition of Johnnie and related strata occurred more-or-less continuously on a thermally subsiding passive margin.

Based on this assumption, subsidence analysis strongly suggests that the end of Johnnie Formation deposition, at the time of valley incision and subsequent fill with the conglomeratic member, was correlative with the Gaskiers glaciation at 579 Ma. The analysis also suggests that the onset of the Shuram excursion near the base of the Rainstorm Member occurred at ~585 Ma. The implied 6 m.y. duration of the Shuram excursion is consistent with paleomagnetic and other proxies from sections in Laurentia and Australia. The subsidence analysis further indicates that if the assignment of the Gaskiers event to uppermost Johnnie time is correct, then the base of the Johnnie Formation is approximately 630 Ma. If so, then the Johnnie through lower Wood Canyon interval in the Spring Mountains represents a relatively complete, 3000 m-thick section that records most or all of Ediacaran time.

## ACKNOWLEDGEMENTS

We are grateful to Gillian Ferguson, Leah Sabbeth, Fenfang Wu, and the late Lindsey Hedges for assistance in the field and laboratory, and to Associate Editor Christopher J. Spencer and reviewer Tony Prave for insightful and constructive reviews. This material is based upon work supported by the National Science Foundation Graduate Research Fellowship Program under grant 1144469 awarded to R. Witkosky, and grant EAR 14-51055 awarded to B. Wernicke.

## APPENDIX. DESCRIPTION OF MAP UNITS

Descriptions apply to geologic maps and stratigraphic columns shown in Figures 3, 4, 6, and 7.

Qa: Alluvium and colluvium in active/ephemeral channels and piedmont-forming slopes.

QTl: In Johnnie Wash, a topographically prominent ridge of coarse, poorly-sorted debris, here interpreted as a landslide deposit.

Zsa: **Stirling Formation**. A Member (labeled "Zs" in map). Very pale orange, grayish-black weathering, medium-grained orthoquartzite, laminated to massive, medium- to thick-bedded, with trough cross-stratification. Contains some interbedded carbonate-cemented sandstone. In places, bedding is destroyed by secondary brecciation and recementation, forming irregular dark weathering masses. Unit forms resistant ridges relative to underlying Johnnie Formation.

Zjr: **Johnnie Formation**. Rainstorm Member. Includes four distinct subunits, from bottom to top: (1) green phyllitic siltstone, (2) highly-resistant, ochre-colored oolitic dolostone ("Johnnie oolite," indicated by red open-dotted line, c. 2 meters thick), (3) pale red, carbonate-cemented fine-grained sandstone and sandy limestone, and (4) a heterogeneous upper unit that includes siltstone, carbonate-rich sandstone, flaser-bedded sandy carbonate, and intraformational limestone breccia. In the Mt. Schader section, a c. 4 m-thick triad of orthoquartzite, siltstone, and dolostone immediately underlies the Stirling Formation. Orthoquartzite is affected by m-scale ball-and-pillow structure.

Zjl: Orthoquartzite and variegated siltstone. Generally a recessive/slope-forming unit. Red

dotted line in Mt. Schader map indicates a resistant, laminated, brown dolomitic marker bed, c. 2 meters thick.

Zjk: Orthoquartzite, variegated siltstone, and dolostone. Orthoquartzite is parallel bedded and forms erosionally resistant base; siltstone locally contains ripple laminations; resistant, brown, dolomitic marker bed, indicated by red dotted line in Mt. Schader map area, is hummocky cross-stratified, and contains chert in its lower portion.

Zjj: Orthoquartzite, variegated siltstone, and minor dolomitic sandstone. Orthoquartzite and siltstone occur in ~5 meter cycles. Orthoquartzite is white, resistant, locally granular and contains high-angle (c. 20°) cross-stratification; dolomitic sandstones are thick, brown, resistant, fine- to medium-grained beds. Red dotted line on both maps indicates a hummocky cross-stratified, brown dolomite marker bed.

Zji: Orthoquartzite, variegated siltstone, and dolomitic sandstone. Parallel bedded in the Johnnie Wash section, hummocky cross-stratified in the Mt. Schader section. Orthoquartzite is fine-grained and occurs as conspicuous thick bedded intervals in 5-10 meter cycles with siltstones. Red dotted line on Mt. Schader map indicates a hummocky cross-stratified, brown dolomitic sandstone marker bed.

Zjh: Orthoquartzite and variegated siltstone. Red dotted lines on Mt. Schader map indicate brown, hummocky cross-stratified dolomite marker beds that contain stromatolitic mounds.

Zjg: Variegated fine-grained sandstone and siltstone, weakly cemented. Also occasional interstratified orthoquartzite, fine to medium-grained, medium- to thick-bedded.

Zjf: Dolostone with centimeter- to decimeter-thick, centimeter- to meter-long chert nodules and lenses. The dolostone forms a conspicuous pale-weathering ridge. Finely laminated to massive texture. Microcrystalline varieties weather gray, coarser grained, secondary

dolomite weathers dark gray to brown.

Zje: Massive, fine-grained sandstone and laminated siltstone. Upper part contains several dozen rhythmic cycles, c. 2 m-thick, of sandstone and siltstone. Each cycle has a sharp, load-casted bottom and grades upward from sandstone to siltstone. Generally an olive hued, recessive/slope-forming unit, with occasional beds of cross-stratified sandstone, similar to unit D.

Zjd: Well-cemented, fine-grained orthoquartzite in meter-scale beds featuring cross-stratification with steep truncation angles (up to ~30°), interstratified with medium-grained, weakly hematite-cemented ferruginous sandstone and variegated siltstone. Unit forms resistant ridge that is conspicuously darker weathering than unit E.

Zjc: Siltstone (as Zja) with a calcareous, medium-grained orthoquartzite marker bed, similar to unit D, indicated on Figure 3 by green dotted line. The lowest carbonate in the Johnnie Wash section appears near the top of this unit as a brown, medium-grained, fabric-retentive dolostone.

Zjb: Interstratified fine-grained orthoquartzite and phyllitic siltstone. Orthoquartzite occurs in meter-scale beds with parallel lamination, pervasively disrupted by soft sediment deformation, primarily ball-and-pillow structure, such that individual beds are difficult to trace along strike.

Zja: Phyllitic siltstone, with a distinct crenulation cleavage at high angle to bedding. Generally a recessive unit.

**REFERENCES CITED**

Abolins, M.J., 1999, I. Stratigraphic constraints on the number of discrete Neoproterozoic glaciations and the relationship between glaciation and Ediacaran evolution; II. The Kwichup Spring thrust in the northwest Spring Mountains, Nevada: Implications for large-magnitude extension and the structure of the Cordilleran thrust belt [Ph.D. thesis]: Pasadena, California Institute of Technology, 341 p.

Abolins, M., Oskin, R., Prave, T., Summa, C., and Corsetti, F., 2000, Neoproterozoic glacial record in the Death Valley region, California and Nevada, *in* Lageson, D.R., Peters, S.G., and Lahren, M.M., eds., Great Basin and Sierra Nevada: Boulder, Colorado, Geological Society of America Field Guide 2, p. 319–336.

Albee, A.L., Labotka, T.C., Lanphere, M.A., and McDowell, S.D., 1981, Geologic map of the Telescope Peak Quadrangle, California: U.S. Geological Survey Geological Quadrangle Map GQ-1532, scale 1:62500, 1 sheet.

Alfaro, P., Delgado, J., Estévez, A., Molina, J.M., Moretti, M., and Soria, J.M., 2002, Liquefaction and fluidization structures in Messinian storm deposits (Bajo Segura Basin, Beltic Cordillera, southern Spain): International Journal of Earth Sciences, v. 91, p. 505- 513, doi: 10.1007/s00531-001-0241-z.

Allan, J.R., and Matthews, R.K., 1977, Carbon and oxygen isotopes as diagenetic and stratigraphic tools: Surface and subsurface data, Barbados, West Indies: Geology, v. 5, p. 16-20.

Allan, J.R., and Matthews, R.K., 1982, Isotope signatures associated with early meteoric diagenesis: Sedimentology, v. 29, p. 797-817.

Allen, P.A., and Allen, J.R., 2005, Basin analysis: principles and applications, second edition: Blackwell Publishing, Malden Massachusetts, 549 p.

Allmendinger, R.W., Cardozo, N., and Fisher, D., 2012, Structural geology algorithms: Vectors and tensors in structural geology: Cambridge University Press, 302 p.

Armin, R.A., and Mayer, L., 1983, Subsidence analysis of the Cordilleran miogeocline: Implications for timing of late Proterozoic rifting and amount of extension: Geology, v. 11, p. 702-705.

Bekker, A., and Holland, H.D., 2012, Oxygen overshoot and recovery during the early Paleoproterozoic: Earth and Planetary Science Letters, v. 317-318, p. 295-304, doi: 10.1016/j.epsl.2011.12.012.

Benmore, W.C., 1978, Stratigraphy, sedimentology, and paleoecology of the late Paleophytic or earliest Phanerozoic Johnnie Formation, eastern California and southwestern Nevada [Ph.D. thesis]: Santa Barbara, University of California, 243 p.

Bergmann, K.D., Zentmyer, R.A., and Fischer, W.W., 2011, The stratigraphic expression of

a large negative carbon isotope excursion from the Ediacaran Johnnie Formation, Death Valley: Precambrian Research, v. 188, p. 45-56, doi: 10.1016/j.precamres.2011.03.014.

Boggs, S. Jr., 2012, Principles of sedimentology and stratigraphy, 5th edition: New Jersey, Pearson Prentice Hall, 585 p.

Bond, G.C., Kominz, M.A., and Devlin, W.J., 1983, Thermal subsidence and eustacy in the Lower Palaezoic miogeocline of western North America: Nature, v. 306, n. 5945, p. 775-779, doi:10.1038/306775a0.

Bond, G.C., and Kominz, M.A., 1984, Construction of tectonic subsidence curves for the early Paleozoic miogeocline, southern Canadian Rocky Mountains: Implications for subsidence mechanisms, age of breakup, and crustal thinning: Geological Society of America Bulletin, v. 95, n. 2, p. 155-173.

Bond, G.C., Kominz, M.A., and Grotzinger, J.P., 1988, Cambro-Ordovician eustasy: Evidence from geophysical modelling of subsidence in Cordilleran and Appalachian passive margins, *in* Kleinspehn, K.L., and Paola, C., eds., New Perspectives in Basin Analysis: Springer, New York, p. 129-160.

Bowring, S., Myrow, P., Landing, E., Ramezani, J., Condon, D. and Hoffmann, K.H., 2003a: Geochronological constraints on Neoproterozoic glaciations and the rise of metazoans: Geological Society of America Abstracts with Programs, v. 35, n. 6, p. 516.

Bowring, S.A., Myrow, P.M., Landing, E., and Ramezani, J., 2003b, Geochronological constraints on terminal Neoproterozoic events and the rise of metazoans: Geophysical Research Abstracts, v. 5, 13219, p. 219.

Bowring, S.A., Grotzinger, J.P., Condon, D.J., Ramezani, J., Newall, M.J., and Allen, P.A., 2007, Geochronologic constraints on the chronostratigraphic framework of the Neoproterozoic Huqf Supergroup, Sultanate of Oman: American Journal of Science, v. 307, p. 1097-1145, doi: 10.2475/10.2007.01.

Burchfiel, B.C., 1964, Precambrian and Paleozoic stratigraphy of Specter Range quadrangle, Nye County, Nevada: American Association of Petroleum Geologists Bulletin, v. 48, n. 1, p. 40-56.

Burchfiel, B.C., 1965, Structural geology of the Specter Range quadrangle, Nevada, and its regional significance: Geological Society of America Bulletin, v. 76, n. 2, p. 175-192.

Burchfiel, B.C., and Davis, G.A., 1972, Structural framework and evolution of the southern part of the Cordilleran orogeny, western United States: American Journal of Science, v. 272, n. 2, p. 97-118.

Burchfiel, B.C., and Davis, G.A., 1975, Nature and controls of Cordilleran orogenesis, western United States: Extensions of an earlier synthesis: American Journal of Science, v.

275-A, p. 363-396.

Burchfiel, B.C., Fleck, R.J., Secor, D.T., Vincelette, R.R., and Davis, G.A., 1974, Geology of the Spring Mountains, Nevada: Geological Society of America Bulletin, v. 85, p. 1013-1022.

Burchfiel, B.C., Hamill, G.S. IV, and Wilhelms, D.E., 1983, Structural geology of the Montgomery Mountains and the northern half of the Nopah and Resting Spring Ranges, Nevada and California: Geological Society of America Bulletin, v. 94, p. 1359-1376.

Burns, S.J., and Matter, A., 1993, Carbon isotopic record of the latest Proterozoic from Oman: Eclogae Geologicae Helvetiae, v. 86, no. 2, p. 595-607.

Butterfield, N.J., 2009, Oxygen, animals, and oceanic ventilation: an alternative view: Geobiology, v. 7, p. 1-7, doi: 10.1111/j.1472-4669.2009.00188.x.

Calver, C.R., 2000, Isotope stratigraphy of the Ediacaran (Neoproterozoic III) of the Adelaide Rift Complex, Australia, and the overprint of water column stratification: Precambrian Research, v. 100, p. 121-150.

Canfield, D.E., Poulton, S.W., and Narbonne, G.M., 2007, Late-Neoproterozoic deep- ocean oxygenation and the rise of animal life: Science, v. 315 (5808), p. 92-95, doi: 10.1126/science.1135013.

Cardozo, N., 2009, Backstrip: http://www.ux.uis.no/~nestor/work/programs.html (accessed August 2017).

Cardozo, N., and Allmendinger, R.W., 2013, Spherical projections with OSXStereonet: Computers & Geosciences, v. 51, p. 193-205, doi: 10.1016/j.cageo.2012.07.021.

Clapham, M.E., and Corsetti, F.A., 2005, Deep valley incision in the terminal Neoproterozoic (Ediacaran) Johnnie Formation, eastern California, USA: Tectonically or glacially driven?: Precambrian Research, v. 141, p. 154-164, doi: 10.1016/j.precamres.2005.09.002.

Cohen, P.A., Bradley, A., Knoll, A.H., Grotzinger, J.P., Jensen, S., Abelson, J., Hand, K., Love, G., Metz, J., McLoughlin, N., Meister, P., Shepard, R., Tice, M., and Wilson, J.P., 2009, Tubular compression fossils from the Ediacaran Nama Group, Namibia: Journal of Paleontology, v. 83, p. 110-122.

Condon, D., Zhu, M., Bowring, S., Wang, W., Yang, A., and Jin, Y., 2005, U-Pb ages from the Neoproterozoic Doushantuo Formation, China: Science, v. 308, p. 95- 98, doi: 10.1126/science.1107765.

Corsetti, F.A., Awramik, S.M., Pierce, D., and Kaufman, A.J., 2000, Using chemostratigraphy to correlate and calibrate unconformities in Neoproterozoic strata from

the southern Great Basin of the United States: International Geology Review, v. 42, p. 516-533, doi: 10.1080/00206810009465096.

Corsetti, F.A., and Hagadorn, J.W., 2000, Precambrian-Cambrian transition: Death Valley, United States: Geology, v. 28, no. 4, p. 299-302.

Corsetti, F.A., and Kaufman, A.J., 2003, Stratigraphic investigations of carbon isotope anomalies and Neoproterozoic ice ages in Death Valley, California: Geological Society of America Bulletin, v. 115, no. 8, p. 916-932, doi: 10.1130/B25066.1.

Deer, W.A., Howie, R.A., and Zussman, J., 1992, An introduction to the rock-forming minerals, second edition: England, Pearson Education Limited, 696 p.

Derry, L.A., 2010a, A burial diagenesis origin for the Ediacaran Shuram-Wonoka carbon isotope anomaly: Earth and Planetary Science Letters, v. 294, no. 1-2, p. 152- 162, doi: 10.1016/j.epsl.2010.03.022.

Derry, L.A., 2010b, On the significance of $\delta^{13}C$ correlations in ancient sediments: Earth and Planetary Science Letters, v. 296, p. 497-501, doi:10.1016/j.epsl.2010.05.035.

Dickinson, W.R., 1977, Paleozoic plate tectonics and the evolution of the Cordilleran continental margin, *in* Stewart, J. H., Stevens, C. H., and Fritsche, A. E., eds., Paleozoic paleogeography of the western United States: Society of Economic Paleontologists and

Mineralogists, Pacific Section, Pacific Coast Paleogeography Symposium 1, p. 137-156.

Fedo, C.M., and Cooper, J.D., 2001, Sedimentology and sequence stratigraphy of Neoproterozoic and Cambrian units across a craton-margin hinge zone, southeastern California, and implications for the early evolution of the Cordilleran margin: Sedimentary Geology, v. 141-142, p. 501-522.

Field, C.B., Behrenfeld, M.J., Randerson, J.T., and Falkowski, P., 1998, Primary production of the biosphere: Integrating terrestrial and oceanic components: Science, v. 281, p. 237-240, doi: 10.1126/science.281.5374.237.

Fike, D.A., Grotzinger, J.P., Pratt, L.M., and Summons, R.E., 2006, Oxidation of the Ediacaran ocean: Nature, v. 444, p. 744-747, doi: 10.1038/nature05345.

Gabrielse, H., 1972, Younger Precambrian of the Canadian Cordillera: American Journal of Science, v. 272, n. 6, p. 521-536.

Giallorenzo, M.A., Wells, M.L, Yonkee, W.A., Stockli, D.F., and Wernicke, B.P., 2017, Timing of exhumation, Wheeler Pass thrust sheet, southern Nevada and California: Late Jurassic to middle Cretaceous evolution of the southern Sevier fold-and-thrust belt: Geological Society of America Bulletin, doi: https://doi.org/10.1130/B31777.1.

Gillett, S.L., and Van Alstine, D.R., 1982, Remagnetization and tectonic rotation of Upper

Precambrian and Lower Paleozoic strata from the Desert Range, southern Nevada: Journal of Geophysical Research, v. 87, n. B13, p. 10929-10953.

Gong, Z., Kodama, K.P., and Li, Y.-X., 2017, Rock magnetic cyclostratigraphy of the Doushantuo Formation, South China and its implications for the duration of the Shuram carbon isotope excursion: Precambrian Research, v. 289, p. 62-74, doi: 10.1016/j.precamres.2016.12.002.

Grotzinger, J.P., Fike, D.A., and Fischer, W.W., 2011, Enigmatic origin of the largest-known carbon isotope excursion in Earth's history: Nature Geoscience, v. 4, no. 5, p. 285-292, doi: 10.1038/ngeo1138.

Hagadorn, J.W., and Waggoner, B., 2000, Ediacaran fossils from the southwestern Great Basin, United States: Journal of Paleontology, v. 74, no. 2, p. 349-359.

Halley, R.B., and Schmoker, J.W., 1983, High-porosity Cenozoic carbonate rocks of south Florida: Progressive loss of porosity with depth: American Association of Petroleum Geologists Bulletin, v. 67, n. 2, p. 191-200.

Halverson, G.P., Hoffman, P.F., Schrag, D.P., Maloof, A.C., and Rice, A.H.N., 2005, Toward a Neoproterozoic composite carbon-isotope record: Geological Society of America Bulletin, v. 117, p. 1181-1207, no. 9/10, doi: 10.1130/B25630.1.

Halverson, G.P., Wade, B.P., Hurtgen, M.T., and Barovich, K.M., 2010, Neoproterozoic chemostratigraphy: Precambrian Research, v. 182, p. 337–350.

Hamill, G.S. IV, 1966, Structure and stratigraphy of the Mt. Shader quadrangle, Nye County, Nevada - Inyo County, California [Ph.D. thesis]: Houston, Texas, Rice University, 83 p.

Hazzard, J.C., 1937, Paleozoic section in the Nopah and Resting Springs Mountains, lnyo County, California: California Journal of Mines and Geology, v. 33, no. 4, p. 273-339.

Heaman, L.M., and Grotzinger, J.P., 1992, 1.08 Ga diabase sills in the Pahrump Group, California: Implications for development of the Cordilleran miogeocline: Geology, v. 20, p. 637-640.

Hoffman, P.F., Kaufman, A.J., Halverson, G.P., and Schrag, D.P., 1998, A Neoproterozoic Snowball Earth: Science, v. 281, p. 1342-1346, doi: 10.1126/science.281.5381.1342.

Hoffmann, K.-H., Condon, D.J., Bowring, S.A., and Crowley, J.L., 2004, U-Pb zircon date from the Neoproterozoic Ghaub Formation, Namibia: Constraints on Marinoan glaciation: Geology, v. 32, p. 817-820, doi: 10.1130/G20519.1.

Holland, H.D., 2006, The oxygenation of the atmosphere and oceans: Philosophical Transactions of the Royal Society B, v. 361, p. 903-915, doi: 10.1098/rstb.2006.1838.

Hollingsworth, J.S., 2005, The earliest occurrence of trilobites and brachiopods in the Cambrian of Laurentia: Palaeogeography, Palaeoclimatology, Palaeoecology, v. 220, p. 153-165, doi: 10.1016/j.palaeo.2004.08.008.

Hunt, D.L., 1990, Trilobite faunas and biostratigraphy of the Lower Cambrian Wood Canyon Formation, Death Valley region, California [Master's thesis]: Davis, University of California, 140 p.

Hunter, R.E., 1977, Basic types of stratification in small eolian dunes: Sedimentology, v. 24, n. 3, p. 361-387.

Husson, J.M., Maloof, A.C., Schoene, B., Chen, C.Y., and Higgins, J.A., 2015, Stratigraphic expression of Earth's deepest $\delta^{13}C$ excursion in the Wonoka Formation of South Australia: American Journal of Science, v. 315, p. 1-45, doi: 10.2475/01.2015.01.

Kamb, W.B., 1959, Ice petrofabric observations from Blue Glacier, Washington, in relation to theory and experiment: Journal of Geophysical Research, v. 64, no. 11, p. 1891-1909.

Kaufman, A.J., Hayes, J.M., Knoll, A.H., and Germs, G.J.B., 1991, Isotopic compositions of carbonates and organic carbon from upper Proterozoic succesions in Namibia: stratigraphic variation and the effects of diagenesis and metamorphism: Precambrian Research, v. 49, p. 301-327.

Kaufman, A.J., Corsetti, F.A., and Varni, M.A., 2007, The effect of rising atmospheric oxygen on carbon and sulfur isotope anomalies in the Neoproterozoic Johnnie Formation, Death Valley, USA: Chemical Geology, v. 237, p. 47-63, doi: 10.1016/j.chemgeo.2006.06.023.

Knauth, L.P., and Kennedy, M.J., 2009, The late Precambrian greening of the Earth: Nature, v. 460, no. 7256, p. 728-732, doi: 10.1038/nature08213.

Knoll, A.H., and Carroll, S.B., 1999, Early animal evolution: emerging views from comparative biology and geology: Science, v. 284 (5423), p. 2129-2137, doi: 10.1126/science.284.5423.2129.

Knoll, A.H., Walter, M.R., Narbonne, G.M, and Christie-Blick, N., 2004, A new period for the geologic time scale: Science, v. 305, p. 621-622.

Knoll, A.H., Walter, M.R., Narbonne, G.M., and Christie-Blick, N., 2006, The Ediacaran Period: a new addition to the geologic time scale: Lethaia, v. 39, p. 13-30, doi: 10.1080/00241160500409223.

Kump, L.R., 2008, The rise of atmospheric oxygen: Nature, v. 45, p. 277-278, doi: 10.1038/nature06587.

Labotka, T.C., Albee, A.L., Lanphere, M.A., and McDowell, S.D., 1980, Stratigraphy,

structure, and metamorphism in the central Panamint Mountains (Telescope Peak quadrangle), Death Valley area, California: Summary: Geological Society of America Bulletin, v. 91, p. 125-129.

Larrieu, T.L., 1995, Basin analysis with a spreadsheet: Journal of Geological Education, v. 43, p. 107-113.

Le Guerroué, E., Allen, P.A., Cozzi, 2006a, Chemostratigraphic and sedimentological framework of the largest negative carbon isotope excursion in Earth history: The Neoproterozoic Shuram Formation (Nafun Group, Oman): Precambrian Research, v. 146, p. 68-92, doi: 10.1016/j.precamres.2006.01.007.

Le Guerroué, E., Allen, P.A., Cozzi, A., Etienne, J.L., and Fanning, M., 2006b, 50 Myr recovery from the largest negative $\delta^{13}C$ excursion in the Ediacaran ocean: Terra Nova, v. 18, p. 147-153, doi: 10.1111/j.1365-3121.2006.00674.x.

Lenton, T.M, Boyle, R.A., Poulton, S.W., Shields-Zhou, G.A., and Butterfield, N.J., 2014, Co- evolution of eukaryotes and ocean oxygenation in the Neoproterozoic era: Nature Geoscience, v. 7, p. 257-265, doi: 10.1038/NGEO2108.

Levy, M., and Christie-Blick, N., 1991, Tectonic subsidence of the early Paleozoic passive continental margin in eastern California and southern Nevada: Geological Society of America Bulletin, v. 103, p. 1590-1606.

Li, Z.X., et al., 2008, Assembly, configuration, and break-up of Rodinia: A synthesis: Precambrian Research, v. 160, p. 179-2010, doi: 10.1016/j.precamres.2007.04.021.

Li, Z.X., Evans, D.A.D., and Halverson, G.P., 2013, Neoproterozoic glaciations in a revised global palaeogeography from the breakup of Rodinia to the assembly of Gondwanaland: Sedimentary Geology, v. 294, p. 219-232, doi: 10.1016/j.sedgeo.2013.05.016.

Longwell, C.R., Pampeyan, E.H., Bowyer, B., and Roberts, R.J., 1965, Geology and mineral deposits of Clark County, Nevada: Nevada Bureau of Mines, Bulletin 62, 218 p.

Loyd, S.J., Marenco, P.J., Hagadorn, J.W., Lyons, T.W., Kaufman, A.J., Sour-Tovar, F., and Corsetti, F.A., 2012, Sustained low marine sulfate concentrations from the Neoproterozoic to the Cambrian: Insights from carbonates of northwestern Mexico and eastern California: Earth and Planetary Science Letters, v. 339-340, p. 79-94, doi: 10.1016/j.epsl.2012.05.032.

Loyd, S.J., Corsetti, F.A., Eagle, R.A., Hagadorn, J.W., Shen, Y., Zhang, X., Bonifacie, M., and Tripati, A.K., 2015, Evolution of Neoproterozoic Wonoka-Shuram Anomaly-aged carbonates: Evidence from clumped isotope paleothermometry: Precambrian Research, v. 264, p. 179-191, doi: 10.1016/j.precamres.2015.04.010.

Macdonald, F.A., Jones, D.S., and Schrag, D.P., 2009, Stratigraphic and tectonic implications of a newly discovered glacial diamictite-cap carbonate couplet in southwestern

Mongolia: Geology, v. 37, no. 2, p. 123-126, doi: 10.1130/G24797A.1.

Macdonald, F.A., Strauss, J.V., Sperling, E.A., Halverson, G.P., Narbonne, G.M., Johnston, D.T., Kunzmann, M., Schrag, D.P., and Higgins, J.A., 2013, The stratigraphic relationship between the Shuram carbon isotope excursion, the oxygenation of Neoproterozoic oceans, and the first appearance of the Ediacaran biota and bilaterian trace fossils in northwestern Canada: Chemical Geology, v. 362, p. 250-272.

Mahon, R.C., Dehler, C.M., Link, P.K., Karlstrom, K.E., and Gehrels, G.E., 2014, Geochronologic and stratigraphic constraints on the Mesoproterozoic and Neoproterozoic Pahrump Group, Death Valley, California: A record of the assembly, stability, and breakup of Rodinia: Geological Society of America Bulletin, v. 126, n. 5/6, p. 652-664, doi: 10.1130/B30956.1.

McFadden, K.A., Huang, J., Chu, X., Jiang, G., Kaufman, A.J., Zhou, C., Yuan, X., and Xiao, S., 2008, Pulsed oxidation and biological evolution in the Ediacaran Doushantuo Formation: Proceedings of the National Academy of Sciences, v. 105, no. 9, p. 3197-3202.

McKenzie, D., 1978, Some remarks on the development of sedimentary basins: Earth and Planetary Science Letters, v. 40, p. 25-32.

McMenamin, M.A.S., 1996, Ediacaran biota from Sonora, Mexico: Proceedings of the National Academy of Sciences, v. 93, p. 4990-4993.

Melezhik, V.A., Fallick, A.E., and Pokrovsky, B.G., 2005, Enigmatic nature of thick sedimentary carbonates depleted in $^{13}C$ beyond the canonical mantle value: The challenges to our understanding of the terrestrial carbon cycle: Precambrian Research, v. 137, p. 131-165, doi: 10.1016/j.precamres.2005.03.010.

Melim, L.A., Swart, P.K., and Maliva, R.G., 1995, Meteoric-like fabrics forming in marine waters: Implications for the use of petrography to identify diagenetic environments: Geology, v. 23, no. 8, p. 755-758.

Melim, L.A., Swart, P.K., and Maliva, R.G., 2001, Meteoric and marine-burial diagenesis in the subsurface of the Great Bahama Bank, *in* Ginsburg, R.N., ed., Subsurface geology of a prograding carbonate platform margin, Great Bahama Bank: Results of the Bahamas Drilling Project: Society of Economic Paleontologists and Mineralogists (Society for Sedimentary Geology) Special Publication no. 70, p. 137-161.

Minguez, D., Kodama, K.P., and Hillhouse, J.W., 2015, Paleomagnetic and cyclostratigraphic constraints on the synchroneity and duration of the Shuram carbon isotope excursion, Johnnie Formation, Death Valley Region, CA: Precambrian Research, v. 266, p. 395-408, doi: 10.1016/j.precamres.2015.05.033.

Minguez, D., and Kodama, K.P., 2017, Rock magnetic chronostratigraphy of the Shuram carbon isotope excursion: Wonoka Formation, Australia: Geology, v. 45, n. 6, p. 567-570,

doi: 10.1130/G38572.1.

Monger, J.W.H., and Price, R.A., 1979, Geodynamic evolution of the Canadian cordillera—progress and problems: Canadian Journal of Earth Sciences, v. 16, n. 3, p. 770-791, doi: 10.1139/e79-069.

Myrow, P.M., and Kaufman, A.J., 1999, A newly discovered cap carbonate above Varanger-age glacial deposits in Newfoundland, Canada: Journal of Sedimentary Research, v. 69, no. 3, p. 784-793.

Narbonne, G.M., Xiao, S., Shields, G.A., and Gehling, J.G., 2012, The Ediacaran Period, *in* Gradstein, F.M., Ogg, J.G., Schmitz, M., and Ogg, G.M., eds., The Geologic Timescale 2012, Volume 1: Elsevier, p. 413-435, doi: 10.1016/B978-0-444-59425-9.00018-4.

Nolan, T. B., 1924, Geology of the northwest portion of the Spring Mountains, Nevada [Ph.D. thesis]: New Haven, Connecticut, Yale University, 125 p.

Nolan, 1929, Notes on the stratigraphy and structure of the northwest portion of Spring Mountain, Nevada: American Journal of Science, Series 5, v. 17, n. 101, p. 461-472.

Nursall, J.R., 1959, Oxygen as a prerequisite to the origin of the metazoa: Nature, v. 183, no. 4669, p. 1170-1172.

Och, L.M., and Shields-Zhou, G.A., 2012, The Neoproterozoic oxygenation event: Environmental perturbations and biogeochemical cycling: Earth-Science Reviews, v. 110, p. 26-57, doi: 10.1016/j.earscirev.2011.09.004.

Ogg, J.G., Ogg, G., and Gradstein, F.M., 2016, A concise geologic timescale: 2016: Amsterdam, Netherlands, Elsevier, 240 p.

Osburn, M.R., Owens, J., Bergmann, K.D., Lyons, T.W., and Grotzinger, J.P., 2015, Dynamic changes in sulfate sulfur isotopes preceding the Ediacaran Shuram Excursion: Geochimica et Cosmochimica Acta, v. 170, p. 204-224.

Palmer, A.R., 1981, Subdivision of the Sauk sequence, *in* Taylor, M.E., ed., Short papers for the Second International Symposium on the Cambrian System, U.S. Geological Survey Open File report 81-743, p. 160-163.

Palmer, A.R., and Halley, R.B., 1979, Physical stratigraphy and trilobite biostratigraphy of the Carrara Formation (Lower and Middle Cambrian) in the Southern Great Basin: U.S. Geological Survey Professional Paper 1407, 131 p.

Parsons, B. and Sclater, J.G., 1977, An analysis of the variation of ocean floor bathymetry and heat flow with age: Journal of Geophysical Research, v. 82, no. 5, p. 803-827.

Petterson, R., Prave, A.R., Wernicke, B.P., and Fallick, A.E., 2011, The Neoproterozoic

Noonday Formation, Death Valley region, California: Geological Society of America Bulletin, v. 123, no. 7/8, p. 1539-1559, doi: 10.1130/B30281.1.

Poole, F.G., Stewart, J.H., Palmer, A.R., Sandberg, C.A., Madrid, R.J., Ross, Jr., R.J., Hintze, L.F., Miller, M.M., and Wrucke, C.T., 1992, Latest Precambrian to latest Devonian time; Development of a continental margin, *in* Burchfiel, B.C., Lipman, P.W., and Zoback, M.L., eds., The Cordilleran Orogen: Conterminous U.S.: Boulder, Colorado, Geological Society of America, The Geology of North America, v. G-3.

Prave, A.R., Fallick, A.E., Thomas, C.W., and Graham, C.M., 2009, A composite C-isotope profile for the Neoproterozoic Dalradian Supergroup of Scotland and Ireland: Journal of the Geological Society, London, v. 166, p. 845-857, doi: 10.1144/0016-76492008-131.

Pu, J.P., Bowring, S.A., Ramezani, J., Myrow, P., Raub, T.D., Landing, E., Mills, A., Hodgin, E., and Macdonald, F.A., 2016, Dodging snowballs: Geochronology of the Gaskiers glaciation and the first appearance of Ediacaran biota: Geology, v. 44, n. 11, p. 955-958, doi:10.1130/G38284.1.

Quinn, T., 1991, Meteoric diagenesis of Plio-Pleistocene limestones at Enewetak Atoll: Journal of Sedimentary Petrology, v. 61, no. 5, p. 681-703.

Sahoo, S.K., Planavsky, N.J., Kendall, B., Wang, X., Shi, X., Scott, C., Anbar, A.D., Lyons, T.W., and Jiang, G., 2012, Ocean oxygenation in the wake of the Marinoan glaciation:

Nature, v. 489, p. 546-549, doi: 10.1038/nature11445.

Saltzman, M.R., and Thomas, E., 2012, Carbon isotope stratigraphy, *in* Gradstein, F.M., Ogg, J.G., Schmitz, M., and Ogg, G.M., eds., The Geologic Timescale 2012, Volume 1: Elsevier, p. 207-232, doi: 10.1016/B978-0-444-59425-9.00011-1.

Sawaki, Y., Ohno, T., Tahata, M., Komiya, T., Hirata, T., Maruyama, S., Windley, B.F., Han, J., Shu, D., and Li, Y., 2010, The Ediacaran radiogenic Sr isotope excursion in the Doushantuo Formation in the Three Gorges area, South China: Precambrian Research, v. 176, p. 46-64.

Sawyer, D.S., Swift, B.A., Sclater, J.G., and Toksöz, M.N., 1982, Extensional model for the subsidence of the northern United States Atlantic continental margin: Geology, v. 10, p. 134-140.

Schiffbauer, J.D., Huntley, J.W., O'Neil, G.R., Darroch, S.A.F., Laflamme, M., and Cai, Y., 2016, The latest Ediacaran wormworld fauna: Setting the ecological stage for the Cambrian explosion: GSA Today, v. 26, n. 11, doi: 10.1130/GSATG265A.1.

Schoenborn, W.A., and Fedo, C.M., 2011, Provenance and paleoweathering reconstruction of the Neoproterozoic Johnnie Formation, southeastern California: Chemical Geology, v. 285, p. 231-255, doi: 10.1016/j.chemgeo.2011.04.014.

Schoenborn, W.A., Fedo, C.M., and Farmer, G.L., 2012, Provenance of the Neoproterozoic Johnnie Formation and Stirling Quartzite, southeastern California, determined by detrital zircon geochronology and Nd isotope geochemistry: Precambrian Research, v. 206-207, p. 182-199, doi:10.1016/j.precamres.2012.02.017.

Sims, J.D., 2012, Earthquake-induced load casts, pseudonodules, ball-and-pillow structures, and convolute lamination: Additional deformation structures for paleoseismic studies, *in* Cox, R.T., Tuttle, M.P., Boyd, O.S., and Locat, J., eds., Recent Advances in North American Paleoseismology and Neotectonics East of the Rockies: Geological Society of America Special Paper 493, p. 191-201, doi:10.1130/2012.2493(09).

Smith, E.F., Nelson, L.L., Strange, M.A., Eyster, A.E., Rowland, S.M., Schrag, D.P., and Macdonald, F.A., 2016, The end of the Ediacaran: Two new exceptionally preserved body fossil assemblages from Mount Dunfee, Nevada, USA: Geology, v. 44, n. 11, p. 911-914, doi:10.1130/G38157.1.

Smith, E.F., Nelson, L.L., Tweedt, S.M., Zeng, H., and Workman, J.B., 2017, A cosmopolitan late Ediacaran biotic assemblage: new fossils from Nevada and Namibia support a global biostratigraphic link: Proceedings of the Royal Society of London B, v. 284, n. 1858, doi: 10.1098/rspb.2017.0934.

Steckler, M.S., and Watts, A.B., 1978, Subsidence of the Atlantic-type continental margin off New York: Earth and Planetary Science Letters, v. 41, p. 1-13.

Stewart, J.H., 1970, Upper Precambrian and lower Cambrian strata in the southern Great Basin, California and Nevada: U.S. Geological Survey Professional Paper 620, 206 p.

Stewart, J.H., 1972, Initial deposits in the Cordilleran geosyncline: Evidence of a Late Precambrian (<850 m.y.) continental separation: Geological Society of America Bulletin, v. 83, p. 1345-1360.

Stewart, J.H., and Poole, F.G., 1974, Lower Paleozoic and uppermost Precambrian Cordilleran miogeocline, Great Basin, western United States, *in* Dickinson, W.R., ed., Tectonics and Sedimentation: Society of Economic Paleontologists and Mineralogists Special Publication 22, p. 28-57.

Stewart, J.H., and Suczek, C.A., 1977, Cambrian and latest Precambrian paleogeography and tectonics in the western United States, *in* Stewart, J.H., Stevens, C.H., and Fritsche, A.E., eds., Paleozoic paleogeography of the western United States: Pacific Section Society of Economic Paleontologists and Mineralogists, p. 1-17.

Stewart, J.H., McMenamin, M.A.S., and Morales-Ramirez, J.M., 1984, Upper Proterozoic and Cambrian rocks in the Caborca region, Sonora, Mexico-Physical stratigraphy, biostratigraphy, paleocurrent studies, and regional relations: U.S. Geological Survey Professional Paper 1309, 36 p.

Summa, C.L., 1993, Sedimentologic, stratigraphic, and tectonic controls of a mixed carbonate-siliciclastic succession: Neoproterozoic Johnnie formation, southeast California [Ph.D. thesis]: Cambridge, Massachusetts, Massachusetts Institute of Technology, 331 p.

Swart, P.K., and Kennedy, M.J., 2012, Does the global stratigraphic reproducibility of $\delta^{13}C$ in Neoproterozoic carbonates require a marine origin? A Pliocene-Pleistocene comparison: Geology, v. 40, n. 1, p. 87-90, doi: 10.1130/G32538.1.

Tahata, M., Ueno, Y., Ishikawa, T., Sawaki, Y., Murakami, K., Han, J., Shu, D., Li, Y., Guo, J., Yoshida, N., and Komiya, T., 2013, Carbon and oxygen isotope chemostratigraphies of the Yangtze platform, South China: Decoding temperature and environmental changes through the Ediacaran: Gondwana Research, v. 23, p. 333-353.

Trower, E.J., and Grotzinger, J.P., 2010, Sedimentology, diagenesis, and stratigraphic occurrence of giant ooids in the Ediacaran Rainstorm Member, Johnnie Formation, Death Valley region, California: Precambrian Research, v. 180, p. 113-124, doi: 10.1016/j.precamres.2010.03.007.

U.S. Geological Survey, 1968, Mt. Schader quadrangle, Nevada - Nye County: 7.5 minute series (topographic), scale 1:24,000.

Verdel, C., Wernicke, B.P., and Bowring, S.A., 2011, The Shuram and subsequent Ediacaran carbon isotope excursions from southwest Laurentia, and implications for

environmental stability during the metazoan radiation: Geological Society of America Bulletin, v. 123, no. 7/8, p. 1539-1559, doi: 10.1130/B30369.1.

Walker, J.D., Geissman, J.W., Bowring, S.A., and Babcock, L.E., 2013, The Geological Society of America Geologic Time Scale: Geological Society of America Bulletin, v. 125, n. 3/4, p. 259-272, doi: 10.1130/B30712.1.

Wright, L.A., and Troxel, B.W., 1966, Strata of late Precambrian-Cambrian age, Death Valley region, California-Nevada: American Association of Petroleum Geologists Bulletin, v. 50, n. 5, p. 846-857.

Wright, L.A., and Troxel, B.W., 1984, Geology of the north 1/2 Confidence Hills 15' quadrangle, Inyo County, California: California Division of Mines and Geology Map Sheet 34, scale 1:24000, 1 sheet, 31 p. text.

Xiao, S., Bao, H., Wang, H., Kaufman, A.J., Zhou, C., Li, G., Yuan, X., and Ling, H., 2004, The Neoproterozoic Quruqtagh Group in eastern Chinese Tianshan: Evidence for a post-Marinoan glaciation: Precambrian Research, v. 130, p. 1-26.

Xiao, S., Narbonne, G.M., Zhou, C., Laflamme, M., Grazhdankin, D.V., Moczydlowska-Vidal, M., and Cui, H., 2016, Towards an Ediacaran time scale: Problems, protocols, and prospects: Episodes, v. 39, n. 4, p. 540-555, doi: 10.18814/epiiugs/2016/v39i4/103886.

Yonkee, W.A., Dehler, C.D., Link, P.K., Balgord, E.A., Keeley, J.A., Hayes, D.S., Wells, M.L., Fanning, C.M., and Johnston, S.M., 2014, Tectono-stratigraphic framework of Neoproterozoic to Cambrian strata, west-central U.S.: Protracted rifting, glaciation, and evolution of the North American Cordilleran margin: Earth-Science Reviews, v. 136, p. 59-95, doi: 10.1016/j.earscirev.2014.05.004.

Zhou, C., Xie, G., McFadden, K., Xiao, S., and Yuan, X., 2007, The diversification and extinction of Doushantuo-Pertatataka acritarchs in South China: Causes and biostratigraphic significance: Geological Journal, v. 42, p. 229-262.

**FIGURE CAPTIONS**

Figure 1 (p. 90): Generalized stratigraphic column of Precambrian-Cambrian strata; thicknesses represent sections in the northwest Spring Mountains, Nevada (from Stewart, 1970). Cryogenian-Ediacaran boundary (635 Ma) is based on the interpretation that the Noonday Dolomite is the Marinoan cap carbonate sequence (Petterson et al., 2011) and the definition for the base of the Ediacaran period (Knoll et al., 2004; Knoll et al., 2006; Narbonne et al., 2012). Precambrian-Cambrian boundary (541 Ma) is based on paleontology (Hagadorn and Waggoner, 2000; Corsetti and Hagadorn, 2000). The Noonday Formation and Stirling Formation are generally resistant, cliff-forming units, in contrast to the recessive, slope-forming Johnnie and lower Wood Canyon Formations. The letter C indicates the conglomeratic member of the Johnnie Formation, which fills local valleys incised into the Rainstorm Member.

Figure 2 (p. 91): (A) Google Earth image and (B) corresponding geologic map of Precambrian-Cambrian strata in the northwest Spring Mountains, Nevada, in the vicinity of the type locality of the Johnnie Formation in Johnnie Wash. GF- Grapevine fault; JW- Johnnie Wash; MA- Montgomery anticline; NV-160- Nevada State Highway 160; PF- Paddy's fault. Dotted line labeled d/e indicates the conspicuous surface trace of the contact between informal members D and E of the Johnnie Formation. Data were compiled from Abolins (1999), Burchfiel et al. (1974, 1983), and this study.

Figure 3 (p. 92): Geologic map and cross sections of Johnnie Wash and environs. Definitions of unit labels and the description of map units are given in the Appendix.

Figure 4 (p. 93): Generalized lithostratigraphic column of the Johnnie Formation at its type locality in Johnnie Wash, with thicknesses based on cross sections A - A' and B - B' in Figure 3 for units A through L, and Stewart (1970) for the Rainstorm Member. Roman numerals on left side of column indicate the three sand-rich intervals discussed in text.

Figure 5 (p. 94): Photographs of selected lithostratigraphic elements of the Johnnie Formation. (A) Load cast with folded laminae in sandstone bed, unit B, Johnnie Wash area. Hammer is 28 cm long. (B) Ball-and-pillow structure in unit B, with light-colored siltstone (just above pocket knife) protruding upward between bulbous masses of fine-grained sandstone. Pocket knife is 9 cm long. (C) Gray cherty dolostone, unit F, Johnnie Wash. Pencil is 15 cm long (D) Brown-weathering, laminated dolostone, typical of carbonate beds in units

H through L. Hammer is 28 cm long. (E) Variegated siltstone typical of all units in the Johnnie Formation. Pocket knife is 9 cm long. (F) Johnnie oolite, Johnnie Wash, ooids are 1 - 2 mm in diameter. (G) Large, bulbous mass of orthoquartzite (left of hammer), surrounded by smaller masses lying in a matrix of siltstone, uppermost bed of the Rainstorm Member, Mt. Schader section. Hammer is 33 cm long. (H) Base of orthoquartzite bed in (G), showing load cast structures with underlying siltstone. Hammer is 33 cm long.

Figure 6 (p. 95): Geologic map of the Mt. Schader section, showing measured and sampled transects. Definition of unit labels and description of map units are given in the Appendix.

Figure 7 (p. 96): (A) Detailed lithostratigraphic column of the Mt. Schader section, from unit G of the Johnnie Formation through the lowermost part the A Member of the Stirling Formation, showing thicknesses based on Jacobs staff measurements (transects shown in Figure 6). Detailed description of subunits 1 - 48 are given in the Supplemental Text. (B) and (C), carbon and oxygen isotope ratios, respectively, in carbonate, as a function of stratigraphic position. Numerical values are found in Table S1. VPDB- Vienna Peedee Belemnite

Figure 8 (p. 97): (A) Photograph of tabular planar cross-stratification in unit D, Johnnie Wash. Notebook is 13 cm wide. (B) Equal area stereogram of poles to foreset laminations measured at Locality A (Figure 2A), with bedding tilt removed. Dots are data (n = 65), larger square in circle is the mean vector. Plotted using *Stereonet* software (Allmendinger et al., 2012; Cardozo and Allmendinger, 2013), with Kamb contours at 2σ intervals (Kamb, 1959).

(C) Photograph of steep foreset laminations (bedding parallel to base of photograph), showing 9 cm scale bar at location of petrographic measurements of mean grain size in (D). (D) Mean grain size as a function of stratigraphic height in sample of foreset laminations, showing relatively constant value of 200 μm.

Figure 9 (p. 98): (A) and (B), carbon and oxygen isotope ratios, respectively, in carbonate as a function of stratigraphic position, for units C and F in the Johnnie Wash area. Numerical values are found in Table S1. VPDB-Vienna Peedee Belemnite.

Figure 10 (p. 99): Carbon isotope ratios as function of stratigraphic position, expanding the vertical scale within each carbonate bed, to reveal any intrabed trends. Beds are numbered from bottom to top within a given unit, e.g. Zjj1 is the lowest carbonate bed in unit J. VPDB-Vienna Peedee Belemnite.

Figure 11 (p. 100): Cross plot of $\delta^{18}O$ versus $\delta^{13}C$, color coded by stratigraphic unit, showing linear regression lines. VPDB- Vienna Peedee Belemnite.

Figure 12 (p. 101): Plot showing calculated tectonic subsidence *Y* as a function of observed stratigraphic thickness *S*. Lower curve shows results assuming unit A of the Johnnie Formation at the type locality is immediately underlain by crystalline basement. Error bars show range of estimates of *Y* produced by a ±5 % variation in sediment grain density. Upper curve shows results assuming unit A is underlain by c. 2000 m of hypothetical Pahrump Group strata.

Figure 13 (p. 102): Lithostratigraphic columns of the Johnnie Formation and enveloping Ediacaran-Cambrian formations at three key localities in Nevada and California, indicating the stratigraphic distribution of sand-rich intervals versus siltstone/carbonate-rich intervals. Informal member and unit designations in the southern Nopah and Desert Range sections are after Stewart (1970); note that the informal "Carbonate member" in the Desert Range section is predominantly sand-rich carbonate and fine- to medium-grained orthoquartzite with no siltstone. Bold numbers to the left of the scale bar are ages in Ma as follows: 509, base of Middle Cambrian (Palmer and Halley, 1979); 514 and 520, base of *Bonnia-Olenellus* and *Fallotaspis* trilobite zones respectively (Hunt, 1990; Hollingsworth, 2005); 541 and 550, base of Cambrian and first-appearance datum of cloudinids (Corsetti and Hagadorn, 2000; Smith et al., 2016; Narbonne et al., 2012); 579, 585, and 624, model age estimates from this study; 635, base of Ediacaran (Petterson et al., 2011). Roman numerals indicate sand-rich intervals beginning with unit B of the type Johnnie Formation.

Figure 14 (p. 103): Paleoflow rosettes showing foreset lamination dip directions, corrected for bedding dip. Upper two rosettes compare data from sand-rich interval II (Figure 8B) with data from all sub-unit H strata (p. 224 in Benmore, 1978). Bottom rosette shows data from all pre-Rainstorm orthoquartzites in the Desert Range (p. 221 in Benmore, 1978).

Figure 15 (p. 104): Composite chemostratigraphy of the upper Johnnie Formation, showing carbon isotopic ratios in carbonate from unit H up to the oolite marker horizon in the lowermost Rainstorm Member (Mt. Schader section, this study) and values from just below

the base of the Rainstorm Member to the top of the member (southern Panamint Range, Verdel et al., 2011). VPDB- Vienna Peedee Belemnite.

Figure 16 (p. 105): Chemostratigraphic profiles comparing carbon isotopic data from the Johnnie Formation from unit H through the lowermost Rainstorm Member (ending at the top of the oolite marker bed, Figure 7), with profiles from (A) the Mukhaibah Dome (MD5); and (B) the Buah Dome (BD5) areas of Oman (Osburn et al., 2015). Vertical axis shows measured stratigraphic height in all profiles. Six additional profile comparisons are presented in Figure S3. VPDB- Vienna Peedee Belemnite.

Figure 17 (p. 106): Plot showing an exponential subsidence model $Y(t)$, based on conductive cooling of extended lithosphere (McKenzie, 1978). Plotted on curve are the onset of thermal subsidence at $t = 0$, and two arbitrary points in the history of subsidence. Note that so long as the stratigraphic position of $e(\infty) = 0$ is well defined, the form of the subsidence curve, including the exponential decay constant $\tau$, is uniquely determined, and does not depend on $e(0) = E_0 r$.

Figure 18 (p. 107): Plots showing subsidence data and model for northwest Spring Mountains section of southwest Laurentia: (A) observed subsidence (stratigraphic thickness) $S$ versus tectonic subsidence $Y$; (B) temporal control on tectonic subsidence $Y$ versus time applied to Cambrian and younger points (solid circles), temporal model shown with plus symbols; (C) same as (B), except showing $S$ versus $t$; and (D) same as (C) with axes inverted. Dotted red line and number in (B) show projected age of the base of Johnnie unit A; Dotted red line and

circle in (D) show the amount of additional, hypothetical strata that would be needed below unit A in the Spring Mountains in order for sedimentation to extend linearly back in time to 635 Ma.

## TABLES

| Table 1: Nomenclature of stratigraphic units used in subsidence analysis tables | |
|---|---|
| Stratigraphic unit: can be partitioned/combined formations (Fm) and/or members (Mbr) | Abbreviation |
| **Spring Mountains section** | |
| Carbonate overburden | MzPzco |
| Devils Gate Fm | Ddg |
| Nevada Fm | Dn |
| Laketown Fm (upper 50%) | Dl |
| Laketown Fm (lower 50%) | Sl |
| Ely Springs Fm | Oes |
| Eureka Fm | Oe |
| Pogonip Group (upper third) | Op2 |
| Pogonip Group (lower two thirds) | Op1 |
| Nopah Fm (upper third) | OЄn2 |
| Nopah Fm (lower two thirds) | OЄn1 |
| Dunderberg Fm | Єd |
| Bonanza King Fm (Banded Mountain Mbr, upper 36%) | Єbk2 |
| Bonanza King Fm (Mbrs: Papoose Lake & Banded Mountain, lower 64%) | Єbk1 |
| Carrara Fm (upper two thirds) | Єc2 |
| Carrara Fm (lower third) | Єc1 |
| Zabriskie Fm | Єz |
| Wood Canyon Fm (Ediacaran/Cambrian boundary to top) | ЄZwc2 |
| Wood Canyon Fm (to Ediacaran/Cambrian boundary) | ЄZwc1 |
| Stirling Fm (members A through E) | Zsa - Zse |
| Johnnie Fm (Rainstorm Mbr, oolite bed's base to top of Mbr) | Zjr2 |
| Johnnie Fm (Rainstorm Mbr, base to oolite bed's base) | Zjr1 |
| Johnnie Fm (members A through L) | Zja - Zjl |
| **Pahrump Group substrate (hypothetical)** | |
| Johnnie Fm (Presumed equivalent to the Transitional Mbr of Stewart, 1970) | Zjt |
| Kingston Peak Fm (Mbr: South Park, sub-Mbr: Wildrose) | Zkpw |
| Kingston Peak Fm (Mbr: South Park, sub-Mbr: Thorndike) | Zkpth |
| Kingston Peak Fm (Mbr: South Park, sub-Mbr: Mountain Girl) | Zkpmg |
| Kingston Peak Fm (Mbr: South Park, sub-Mbrs: Sourdough & Middle Park) | Zkpsmp |
| Kingston Peak Fm (Limekiln-Surprise Mbr) | Zkpls |
| Beck Springs Fm/Kingston Peak Fm (lower) | Zbs |
| Horse Thief Springs Fm | Zhs |
| Crystal Springs Fm (upper) | Ycs2 |
| Crystal Springs Fm (lower) | Ycs1 |

| Table 2: Nomenclature of parameters used in delithification and backstripping analysis[1] | |
|---|---|
| $\phi_0$ | Surface porosity (%) |
| c | Porosity depth coefficient ($km^{-1}$) |
| $\rho_{sg}$ | Sediment grain density ($kg\ m^{-3}$) |
| h | Stratigraphic thickness (m) |
| *S* | Cumulative stratigraphic thickness (m) |
| *S** | Delithified/decompacted thickness (m) |
| *Y* | Tectonic subsidence (m) |

[1]Subscripts for *S*, *S**, and *Y*:
ns, no Pahrump Group substrate;
ws, with Pahrump Group substrate;
low, low subsidence from using +5% $\rho_{sg}$;
high, high subsidence from using -5% $\rho_{sg}$.

| Table 3: Parameters used in delithification and backstripping analysis of the Spring Mountains section[1] | | | | | | | | |
|---|---|---|---|---|---|---|---|---|
| Unit | Age[2] (Ma) | Lithology | $\phi_0$ (%) | c ($km^{-1}$) | $\rho_{sg}$ (kg $m^{-3}$) | h (m) | $S_{ns}$ (m) | $S_{ws}$ (m) |
| MzPzco[3] | Ca. 243 | l/d | 43 | 0.58 | 2785 | 3000 | 9720 | 11745 |
| Ddg | 359 | d | 43 | 0.58 | 2710 | 286 | 6720 | 8745 |
| Dn | 383 | d | 43 | 0.58 | 2860 | 286 | 6434 | 8459 |
| Dl | 393 | d | 43 | 0.58 | 2860 | 71.5 | 6148 | 8173 |
| Sl | 419 | d | 43 | 0.58 | 2860 | 71.5 | 6076.5 | 8101.5 |
| Oes | 444 | d | 43 | 0.58 | 2860 | 95 | 6005 | 8030 |
| Oe | 458 | s | 49 | 0.27 | 2650 | 71 | 5910 | 7935 |
| Op2 | - | l | 43 | 0.58 | 2710 | 230 | 5839 | 7864 |
| Op1[4] | 470 | l | 43 | 0.58 | 2710 | 460 | 5609 | 7634 |
| OЄn2 | - | d | 43 | 0.58 | 2860 | 95 | 5149 | 7174 |
| OЄn1 | 485 | d | 43 | 0.58 | 2860 | 191 | 5054 | 7079 |
| Єd | - | sh | 63 | 0.51 | 2720 | 48 | 4863 | 6888 |
| Єbk2 | - | d | 43 | 0.58 | 2860 | 197 | 4815 | 6840 |
| Єbk1 | 497 | d | 43 | 0.58 | 2860 | 637 | 4618 | 6643 |
| Єc2 | - | sh | 63 | 0.51 | 2720 | 286 | 3981 | 6006 |
| Єc1 | 509 | sh | 63 | 0.51 | 2720 | 143 | 3695 | 5720 |
| Єz | - | s | 49 | 0.27 | 2650 | 24 | 3552 | 5577 |
| ЄZwc2 | - | s/slt | 49 | 0.27 | 2650 | 523 | 3528 | 5553 |
| ЄZwc1 | 541 | s/slt | 49 | 0.27 | 2650 | 144 | 3005 | 5030 |
| Zse | - | s | 49 | 0.27 | 2650 | 340 | 2861 | 4886 |
| Zsd[5] | - | d | 46 | 0.43 | 2755 | 10 | 2521 | 4546 |
| Zsc | - | slt/s | 49 | 0.27 | 2650 | 190 | 2511 | 4536 |
| Zsb | - | s/slt | 49 | 0.27 | 2650 | 90 | 2321 | 4346 |
| Zsa | - | s | 49 | 0.27 | 2650 | 369 | 2231 | 4256 |
| Zjr2[6] | - | slt/s/l/d | 47 | 0.37 | 2695 | 250 | 1862 | 3887 |
| Zjr1[7] | - | slt | 49 | 0.27 | 2650 | 17 | 1612 | 3637 |
| Zjl | - | s/slt | 49 | 0.27 | 2650 | 60 | 1595 | 3620 |
| Zjk | - | s/slt | 49 | 0.27 | 2650 | 95 | 1535 | 3560 |
| Zjj | - | s/slt | 49 | 0.27 | 2650 | 190 | 1440 | 3465 |
| Zji | - | s/slt | 49 | 0.27 | 2650 | 55 | 1250 | 3275 |
| Zjh | - | s/slt | 49 | 0.27 | 2650 | 60 | 1195 | 3220 |
| Zjg | - | slt | 49 | 0.27 | 2650 | 135 | 1135 | 3160 |
| Zjf[8] | - | d | 43 | 0.58 | 2860 | 40 | 1000 | 3025 |
| Zje | - | s/slt | 49 | 0.27 | 2650 | 280 | 960 | 2985 |
| Zjd[9] | - | s | 49 | 0.27 | 2650 | 300 | 680 | 2705 |
| Zjc2 | - | slt | 49 | 0.27 | 2650 | 45 | 380 | 2405 |
| Zjc1[10] | - | slt | 49 | 0.27 | 2650 | 50 | 335 | 2360 |
| Zjb[11] | - | s | 49 | 0.27 | 2650 | 160 | 285 | 2310 |
| Zja | - | slt | 49 | 0.27 | 2650 | 125 | 125 | 2150 |
| Zjt[12] | - | d/s | 46 | 0.43 | 2755 | 125 | - | 2025 |
| Zkpw[13] | 635 | ss | 49 | 0.27 | 2650 | 100 | - | 1900 |
| Zkpth | - | d | 43 | 0.58 | 2860 | 100 | - | 1800 |
| Zkpmg | - | s | 49 | 0.27 | 2650 | 100 | - | 1700 |
| Zkpsmp | - | slt | 49 | 0.27 | 2650 | 200 | - | 1600 |
| Zkpls | - | s/cgl | 49 | 0.27 | 2650 | 400 | - | 1400 |
| Zbs | - | d | 43 | 0.58 | 2860 | 200 | - | 1000 |
| Zhs[14] | <787 | s | 49 | 0.27 | 2650 | 200 | - | 800 |
| Ycs2 | >1087 | d | 43 | 0.58 | 2860 | 200 | - | 600 |
| Ycs1[15] | - | s | 49 | 0.27 | 2650 | 400 | - | 400 |

[1]Values from table 9.1 *in* Allen and Allen (2005), Equation 3 *in* Halley and Schmoker (1983), Deer et al. (1992), or weighted averages for lithologic mixtures. Abbreviations for lithology are: s, sandstone; slt, siltstone; l, limestone; d, dolostone; sh, shale; cgl, conglomerate. See Table 2 for parameter definitions.

[2]Ages are at top of unit.

[3]Lithologic ratio used is 50/50; average for $\rho_{sg}$.

[4]Carbonate is mostly limestone (fig. 2 *in* Burchfiel et al., 1974).

[5]Dolostone is sandy (stratigraphic column for Spring Mountains, plate 2 *in* Stewart, 1970).

[6]Shuram excursion ends. Lithologic ratio is slt+s/l/d = 67/16.5/16.5 (table 3 *in* Stewart, 1970).

[7]Shuram excursion begins.
[8]Cherty dolostone.
[9]High-angle cross-bedding.
[10]Onset of thermal subsidence (based on interpretation of ball-and-pillow structure, see text).
[11]Ball-and-pillow structure.
[12]Lithologic ratio is d/s = 50/50.
[13]Age from Petterson et al. (2011).
[14]Maximum age from Mahon et al. (2014).
[15]Minimum age from Heaman and Grotzinger (1992).

Table 4: Results from delithification and backstripping analysis of the Spring Mountains section[1]

| Unit | Age[2] (Ma) | $S_{ns}$ | $S^*_{ns}$ | $Y_{ns,\ low}$ | $Y_{ns}$ | $Y_{ns,\ high}$ | $S_{ws}$ | $S^*_{ws}$ | $Y_{ws,\ low}$ | $Y_{ws}$ | $Y_{ws,\ high}$ |
|---|---|---|---|---|---|---|---|---|---|---|---|
| MzPzco | Ca. 243 | 9720 | 9714 | 2670 | 3193 | 3715 | 11745 | 11736 | 3128 | 3768 | 4406 |
| Ddg | 359 | 6720 | 7489 | 2412 | 2791 | 3169 | 8745 | 9548 | 2905 | 3401 | 3895 |
| Dn | 383 | 6434 | 7246 | 2380 | 2743 | 3105 | 8459 | 9310 | 2878 | 3358 | 3836 |
| Dl | 393 | 6148 | 7002 | 2367 | 2713 | 3058 | 8173 | 9071 | 2871 | 3334 | 3795 |
| Sl | 419 | 6076.5 | 6940 | 2364 | 2706 | 3046 | 8101.5 | 9011 | 2869 | 3328 | 3785 |
| Oes | 444 | 6005 | 6881 | 2361 | 2699 | 3035 | 8030 | 8953 | 2868 | 3322 | 3776 |
| Oe | 458 | 5910 | 6799 | 2357 | 2689 | 3020 | 7935 | 8874 | 2866 | 3315 | 3763 |
| Op2 | - | 5839 | - | - | - | - | 7864 | - | - | - | - |
| Op1 | 470 | 5609 | 6541 | 2320 | 2636 | 2950 | 7634 | 8622 | 2836 | 3269 | 3700 |
| OЄn2 | - | 5149 | - | - | - | - | 7174 | - | - | - | - |
| OЄn1 | 485 | 5054 | 6070 | 2280 | 2564 | 2846 | 7079 | 8167 | 2811 | 3212 | 3611 |
| Єd | - | 4863 | - | - | - | - | 6888 | - | - | - | - |
| Єbk2 | - | 4815 | - | - | - | - | 6840 | - | - | - | - |
| Єbk1 | 497 | 4618 | 5694 | 2264 | 2522 | 2778 | 6643 | 7804 | 2809 | 3183 | 3556 |
| Єc2 | - | 3981 | - | - | - | - | 6006 | - | - | - | - |
| Єc1 | 509 | 3695 | 4798 | 2125 | 2327 | 2528 | 5720 | 6949 | 2710 | 3029 | 3347 |
| Єz | - | 3552 | - | - | - | - | 5577 | - | - | - | - |
| ЄZwc2 | - | 3528 | - | - | - | - | 5553 | - | - | - | - |
| ЄZwc1 | 541 | 3005 | 4024 | 1844 | 2009 | 2173 | 5030 | 6220 | 2475 | 2757 | 3037 |
| Zse | - | 2861 | 3865 | 1786 | 1943 | 2100 | 4886 | 6072 | 2428 | 2702 | 2975 |
| Zsd | - | 2521 | 3481 | 1642 | 1781 | 1919 | 4546 | 5718 | 2313 | 2570 | 2824 |
| Zsc | - | 2511 | 3469 | 1638 | 1777 | 1914 | 4536 | 5708 | 2311 | 2566 | 2821 |
| Zsb | - | 2321 | 3250 | 1553 | 1682 | 1809 | 4346 | 5507 | 2245 | 2490 | 2735 |
| Zsa | - | 2231 | 3144 | 1512 | 1635 | 1758 | 4256 | 5411 | 2213 | 2454 | 2693 |
| Zjr2 | - | 1862 | 2706 | 1337 | 1441 | 1544 | 3887 | 5018 | 2083 | 2304 | 2523 |
| Zjr1 | - | 1612 | 2400 | 1221 | 1311 | 1399 | 3637 | 4748 | 2004 | 2210 | 2415 |
| Zjl | - | 1595 | 2379 | 1212 | 1301 | 1388 | 3620 | 4730 | 1997 | 2203 | 2407 |
| Zjk | - | 1535 | 2303 | 1179 | 1264 | 1349 | 3560 | 4663 | 1973 | 2176 | 2377 |
| Zjj | - | 1440 | 2179 | 1125 | 1204 | 1284 | 3465 | 4556 | 1936 | 2133 | 2329 |
| Zji | - | 1250 | 1930 | 1012 | 1082 | 1150 | 3275 | 4343 | 1859 | 2046 | 2231 |
| Zjh | - | 1195 | 1856 | 978 | 1045 | 1110 | 3220 | 4280 | 1836 | 2020 | 2203 |
| Zjg | - | 1135 | 1775 | 941 | 1004 | 1066 | 3160 | 4212 | 1812 | 1992 | 2171 |
| Zjf | - | 1000 | 1589 | 853 | 909 | 964 | 3025 | 4058 | 1756 | 1929 | 2101 |
| Zje | - | 960 | 1537 | 835 | 889 | 941 | 2985 | 4015 | 1747 | 1918 | 2087 |
| Zjd | - | 680 | 1132 | 633 | 671 | 709 | 2705 | 3689 | 1624 | 1779 | 1933 |
| Zjc2 | - | 380 | 664 | 385 | 406 | 427 | 2405 | 3331 | 1486 | 1624 | 1762 |
| Zjc1 | - | 335 | 591 | 344 | 363 | 382 | 2360 | 3278 | 1465 | 1601 | 1736 |
| Zjb | - | 285 | 507 | 297 | 313 | 329 | 2310 | 3217 | 1441 | 1574 | 1707 |
| Zja | - | 125 | 230 | 138 | 145 | 152 | 2150 | 3024 | 1365 | 1489 | 1612 |
| Zjt | - | - | - | - | - | - | 2025 | 2871 | 1304 | 1422 | 1538 |
| Zkpw | 635 | - | - | - | - | - | 1900 | 2722 | 1255 | 1365 | 1475 |
| Zkpth | - | - | - | - | - | - | 1800 | 2597 | 1204 | 1308 | 1412 |
| Zkpmg | - | - | - | - | - | - | 1700 | 2480 | 1173 | 1271 | 1368 |
| Zkpsmp | - | - | - | - | - | - | 1600 | 2349 | 1116 | 1209 | 1300 |
| Zkpls | - | - | - | - | - | - | 1400 | 2086 | 1000 | 1081 | 1162 |
| Zbs | - | - | - | - | - | - | 1000 | 1546 | 756 | 815 | 873 |
| Zhs | <787 | - | - | - | - | - | 800 | 1288 | 669 | 716 | 762 |
| Ycs2 | >1087 | - | - | - | - | - | 600 | 993 | 523 | 558 | 593 |
| Ycs1 | - | - | - | - | - | - | 400 | 707 | 408 | 431 | 453 |

[1]See Table 2 for parameter definitions. For subscript “ns,” *S* was measured relative to the base of Zja, and for “ws,” relative to the base of Ycs1.
[2]Ages are at top of unit.

| Table 5: Estimates for the time constant $\tau$[1] | | | | | | | | |
|---|---|---|---|---|---|---|---|---|
| Model | *Y*(541) | *Y*(509) | *Y*(393) | *Y*(383) | *Y*(c. 388)[2] | $\tau$ (m.y.) | SE[3] begin (Ma) | SE[3] end (Ma) |
| $Y_{ns}$ | 2009 | 2327 | 2713 | 2743 | 2728 | 55 | 578 | 573 |
| $Y_{ns}$[4] | 1646 | 1964 | 2350 | 2380 | 2365 | 55 | 578 | 573 |
| $Y_{ws}$ | 2757 | 3029 | 3334 | 3358 | 3346 | 52 | 575 | 570 |
| | | | | | | | | |
| $Y_{ns, low}$ | 1844 | 2125 | 2367 | 2380 | 2374 | 42 | 574 | 569 |
| $Y_{ns}$ | 2009 | 2327 | 2713 | 2743 | 2728 | 55 | 578 | 573 |
| $Y_{ns, high}$ | 2173 | 2528 | 3058 | 3105 | 3082 | 65 | 581 | 575 |
| | | | | | | | | |
| $Y_{ns, low}$[4] | 1500 | 1781 | 2023 | 2036 | 2030 | 42 | 574 | 569 |
| $Y_{ns}$[4] | 1646 | 1964 | 2350 | 2380 | 2365 | 55 | 578 | 573 |
| $Y_{ns, high}$[4] | 1791 | 2146 | 2676 | 2723 | 2700 | 65 | 581 | 575 |
| | | | | | | | | |
| $Y_{ws, low}$ | 2475 | 2710 | 2871 | 2878 | 2875 | 36 | 569 | 566 |
| $Y_{ws}$ | 2757 | 3029 | 3334 | 3358 | 3346 | 52 | 575 | 570 |
| $Y_{ws, high}$ | 3037 | 3347 | 3795 | 3836 | 3816 | 63 | 578 | 573 |

[1]Units for $\tau$ are millions of years (my). Units for all *Y* values are in meters (m).
[2]Mean value of *Y*(393 Ma) and *Y*(383 Ma).
[3]SE = Shuram excursion.
[4]*Y* values were adjusted by assuming a zero datum that represents a specific point in the stratigraphic column inferred to represent cessation of mechanical stretching and inception of passive-margin thermal subsidence.

| Table 6: All ages modeled using no substrate | | | | | | | | | | |
|---|---|---|---|---|---|---|---|---|---|---|
| | | Model ages (Ma) | | | | | | | | |
| | | $\tau$ = 55 m.y. | | | $\tau$ = 60 m.y. | | | $\tau$ = 65 m.y. | | |
| Unit | Age[1] (Ma) | Min | Int | Max | Min | Int | Max | Min | Int | Max |
| MzPzco | Ca. 243 | - | - | - | - | - | - | - | - | - |
| Ddg | 359 | - | - | - | - | - | - | - | - | - |
| Dn | 383 | - | - | - | - | - | - | - | - | - |
| Dl | 393 | 341 | 328 | 303 | 323 | 309 | 281 | 305 | 289 | 260 |
| Sl | 419 | 363 | 349 | 323 | 347 | 332 | 303 | 331 | 314 | 283 |
| Oes | 444 | 378 | 364 | 337 | 363 | 348 | 319 | 348 | 332 | 300 |
| Oe | 458 | 393 | 381 | 352 | 380 | 366 | 335 | 366 | 352 | 317 |
| Op1 | 470 | 435 | 428 | 415 | 425 | 418 | 404 | 416 | 407 | 393 |
| OЄn1 | 485 | 467 | 460 | 446 | 460 | 452 | 437 | 453 | 445 | 429 |
| Єbk1 | 497 | 481 | 472 | 455 | 475 | 466 | 447 | 470 | 460 | 439 |
| Єc1 | 509 | 514 | 509 | 499 | 511 | 506 | 496 | 509 | 503 | 492 |
| ЄZwc1 | 541 | 541 | 541 | 541 | 541 | 541 | 541 | 541 | 541 | 541 |
| Zse | - | 545 | 546 | 547 | 546 | 546 | 547 | 546 | 547 | 548 |
| Zsd | - | 555 | 556 | 559 | 556 | 558 | 560 | 557 | 559 | 562 |
| Zsc | - | 555 | 556 | 559 | 556 | 558 | 561 | 557 | 559 | 562 |
| Zsb | - | 560 | 562 | 565 | 561 | 563 | 567 | 563 | 565 | 569 |
| Zsa | - | 562 | 564 | 568 | 564 | 566 | 570 | 565 | 568 | 573 |
| Zjr2 | - | 570 | 573 | 578 | 573 | 576 | 581 | 575 | 579 | 585 |
| Zjr1 | - | 575 | 578 | 584 | 578 | 582 | 588 | 581 | 585 | 592 |
| Zjl | - | 575 | 579 | 584 | 578 | 582 | 588 | 581 | 586 | 592 |
| Zjk | - | 576 | 580 | 586 | 580 | 584 | 590 | 583 | 587 | 594 |
| Zjj | - | 579 | 582 | 588 | 582 | 586 | 592 | 585 | 590 | 597 |
| Zji | - | 582 | 587 | 593 | 586 | 591 | 598 | 590 | 595 | 602 |
| Zjh | - | 584 | 588 | 594 | 587 | 592 | 599 | 591 | 596 | 604 |
| Zjg | - | 585 | 589 | 596 | 589 | 593 | 601 | 593 | 598 | 606 |
| Zjf | - | 588 | 592 | 599 | 592 | 597 | 604 | 596 | 601 | 610 |
| Zje | - | 588 | 593 | 600 | 592 | 597 | 605 | 597 | 602 | 610 |
| Zjd | - | 594 | 599 | 606 | 599 | 604 | 612 | 603 | 609 | 618 |
| Zjc2 | - | 600 | 605 | 614 | 605 | 611 | 620 | 611 | 617 | 627 |
| Zjc1 | - | 601 | 606 | 615 | 606 | 612 | 622 | 612 | 618 | 628 |
| Zjb | - | 602 | 608 | 616 | 607 | 614 | 623 | 613 | 620 | 630 |
| Zja | - | 605 | 611 | 620 | 611 | 618 | 627 | 617 | 624 | 635 |
| (base) | - | 608 | 614 | 623 | 614 | 621 | 631 | 620 | 628 | 639 |

[1]Ages are at top of unit.

**FIGURES**

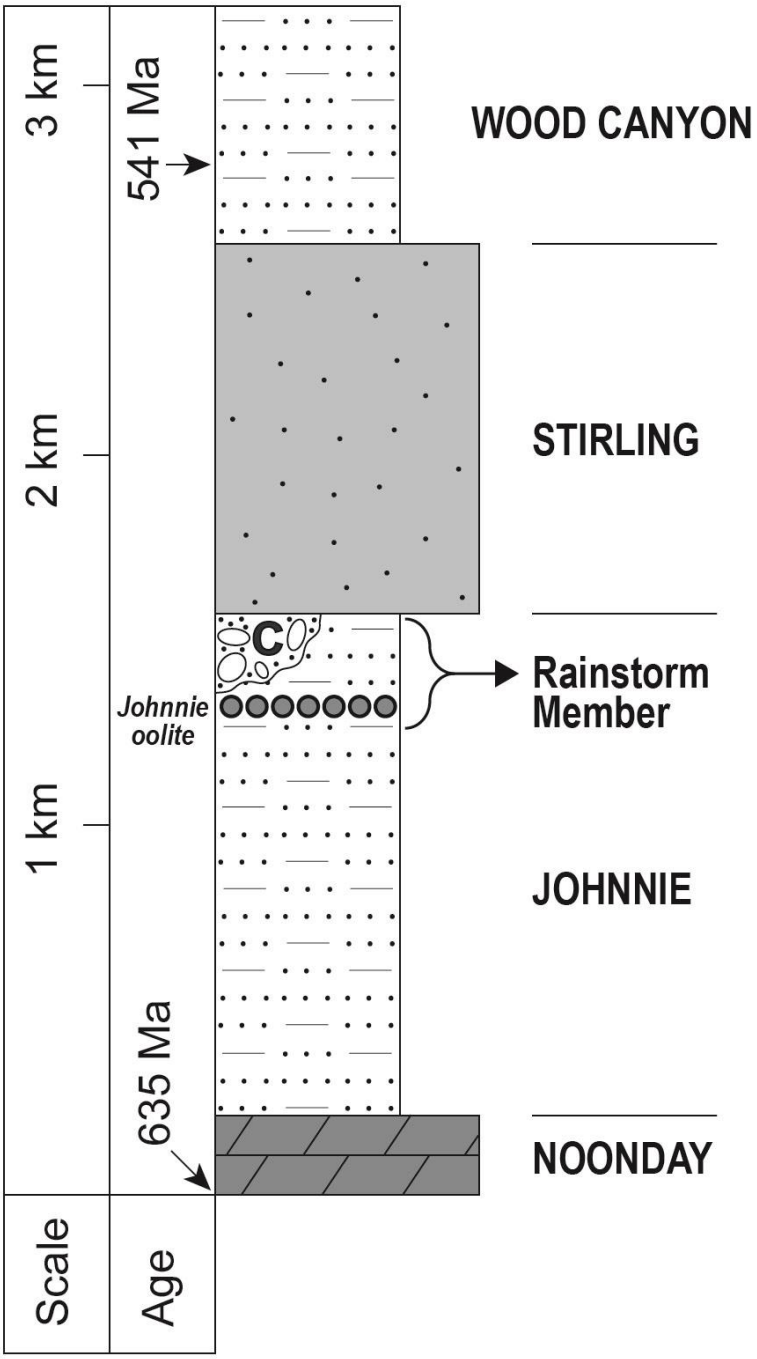


Figure 1

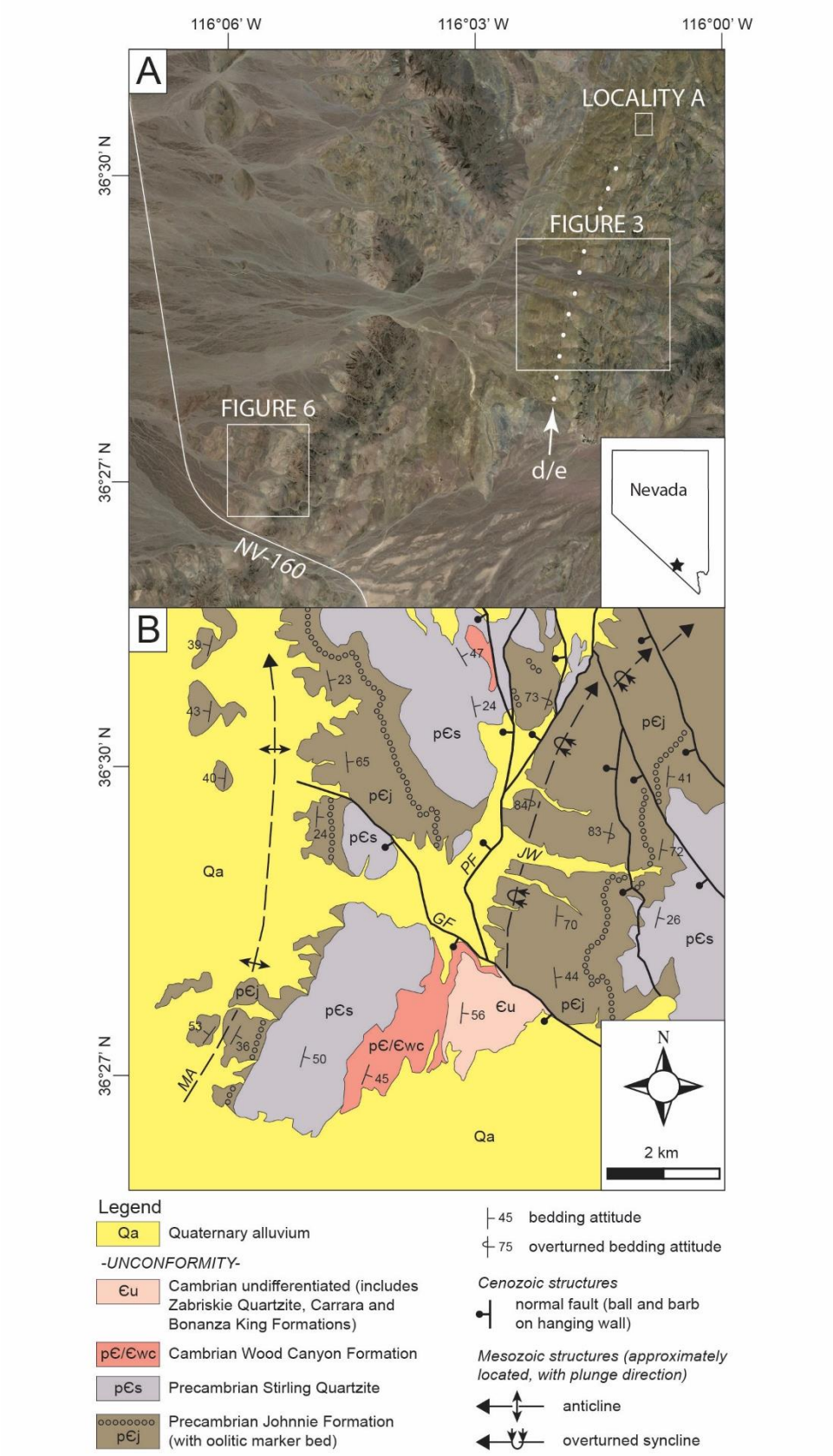
116°06' W
116°03' W
116°00' W
36°30' N
36°27' N
A
LOCALITY A
FIGURE 3
FIGURE 6
d/e
Nevada
NV-160
B
pЄs
pЄj
Qa
PF
JW
GF
MA
pЄ/Єwc
Єu
N
2 km
Legend
Qa Quaternary alluvium
-UNCONFORMITY-
Єu Cambrian undifferentiated (includes Zabriskie Quartzite, Carrara and Bonanza King Formations)
pЄ/Єwc Cambrian Wood Canyon Formation
pЄs Precambrian Stirling Quartzite
pЄj Precambrian Johnnie Formation (with oolitic marker bed)
45 bedding attitude
75 overturned bedding attitude
Cenozoic structures
normal fault (ball and barb on hanging wall)
Mesozoic structures (approximately located, with plunge direction)
anticline
overturned syncline

Figure 2

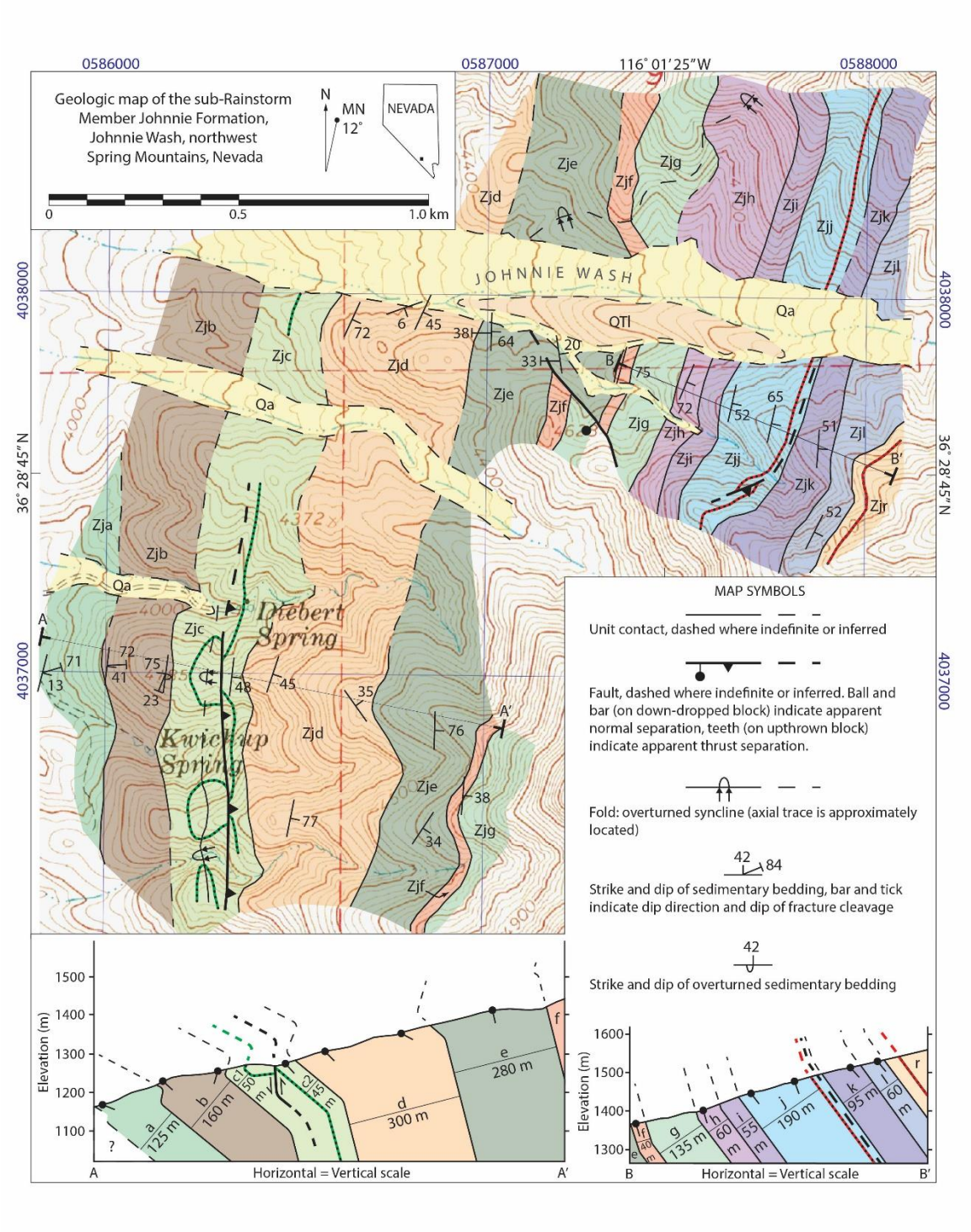
Geologic map of the sub-Rainstorm Member Johnnie Formation, Johnnie Wash, northwest Spring Mountains, Nevada
N
MN 12°
NEVADA
0
0.5
1.0 km
0586000
0587000
116° 01' 25"W
0588000
4038000
4037000
36° 28' 45"N
JOHNNIE WASH
Qa
QTl
Zja
Zjb
Zjc
Zjd
Zje
Zjf
Zjg
Zjh
Zji
Zjj
Zjk
Zjl
Zjr
Diebert Spring
Kwichup Spring
A
A'
B
B'
MAP SYMBOLS
Unit contact, dashed where indefinite or inferred
Fault, dashed where indefinite or inferred. Ball and bar (on down-dropped block) indicate apparent normal separation, teeth (on upthrown block) indicate apparent thrust separation.
Fold: overturned syncline (axial trace is approximately located)
Strike and dip of sedimentary bedding, bar and tick indicate dip direction and dip of fracture cleavage
Strike and dip of overturned sedimentary bedding
Elevation (m)
1500
1400
1300
1200
1100
a 125 m
b 160 m
c 50 m
d 300 m
e 280 m
f
Horizontal = Vertical scale
1600
1500
1400
1300
g 135 m
h 60 m
i 55 m
j 190 m
k 95 m
l 60 m
r
Horizontal = Vertical scale

Figure 3

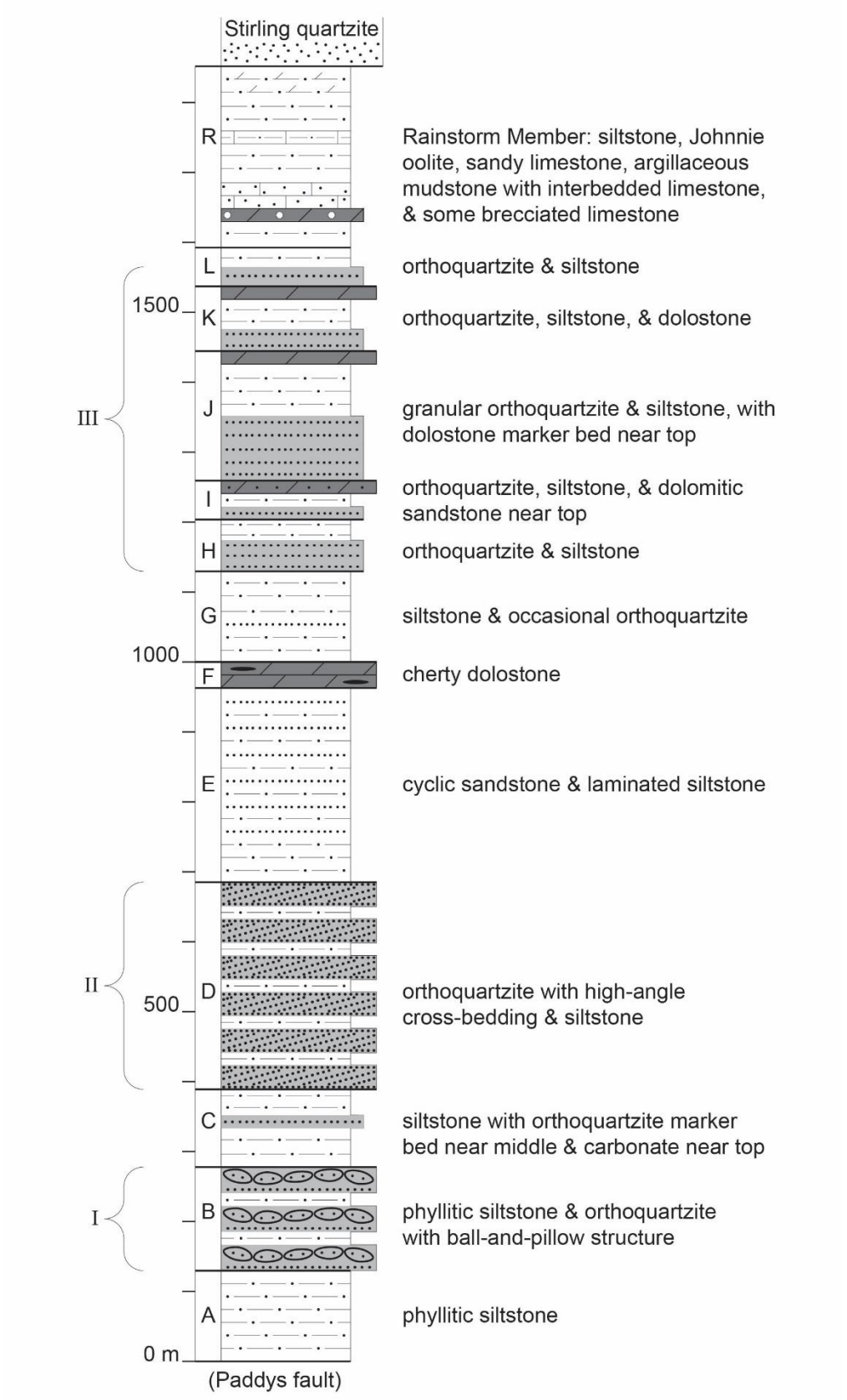
Stirling quartzite
R
Rainstorm Member: siltstone, Johnnie oolite, sandy limestone, argillaceous mudstone with interbedded limestone, & some brecciated limestone
L
orthoquartzite & siltstone
1500
K
orthoquartzite, siltstone, & dolostone
III
J
granular orthoquartzite & siltstone, with dolostone marker bed near top
I
orthoquartzite, siltstone, & dolomitic sandstone near top
H
orthoquartzite & siltstone
G
siltstone & occasional orthoquartzite
1000
F
cherty dolostone
E
cyclic sandstone & laminated siltstone
II
500
D
orthoquartzite with high-angle cross-bedding & siltstone
C
siltstone with orthoquartzite marker bed near middle & carbonate near top
I
B
phyllitic siltstone & orthoquartzite with ball-and-pillow structure
A
phyllitic siltstone
0 m
(Paddys fault)

Figure 4


Figure 5

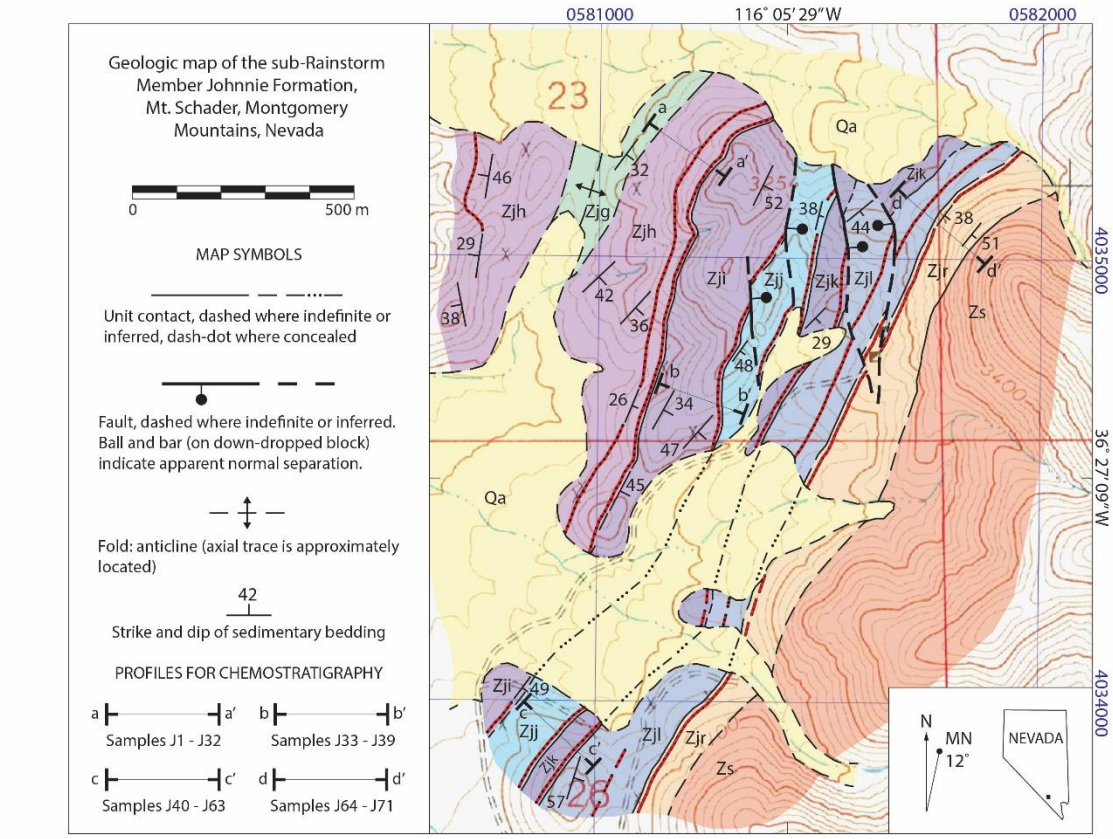
Geologic map of the sub-Rainstorm Member Johnnie Formation, Mt. Schader, Montgomery Mountains, Nevada
0
500 m
MAP SYMBOLS
Unit contact, dashed where indefinite or inferred, dash-dot where concealed
Fault, dashed where indefinite or inferred. Ball and bar (on down-dropped block) indicate apparent normal separation.
Fold: anticline (axial trace is approximately located)
42
Strike and dip of sedimentary bedding
PROFILES FOR CHEMOSTRATIGRAPHY
a a' Samples J1 - J32
b b' Samples J33 - J39
c c' Samples J40 - J63
d d' Samples J64 - J71
0581000
116° 05' 29"W
0582000
4035000
36° 27' 09"W
4034000
Qa
Zjh
Zjg
Zji
Zjj
Zjk
Zjl
Zjr
Zs
23
28
N
MN
12°
NEVADA

Figure 6

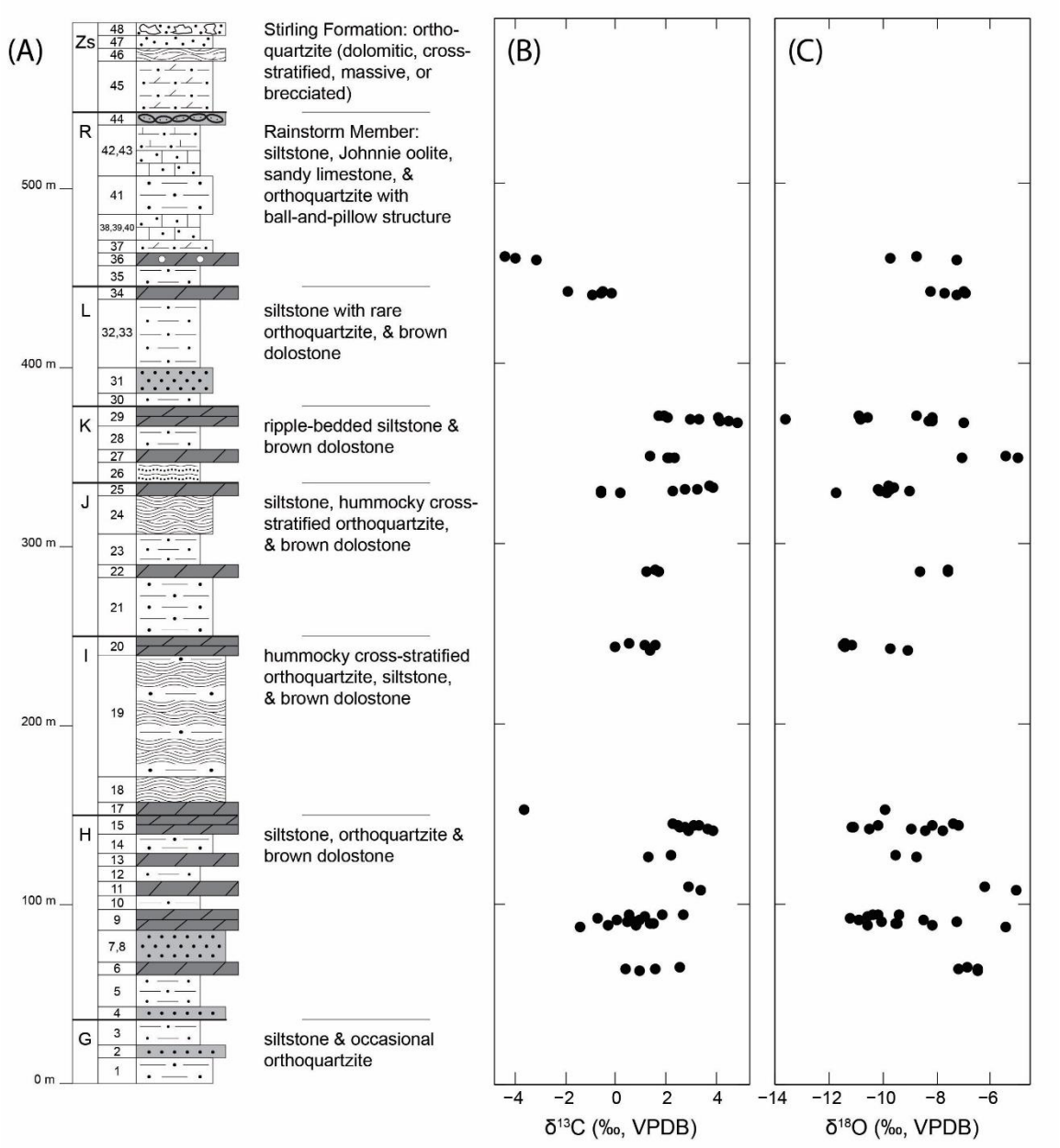
(A)
(B)
(C)
Zs
R
L
K
J
I
H
G
48
47
46
45
44
42,43
41
38,39,40
37
36
35
34
32,33
31
30
29
28
27
26
25
24
23
22
21
20
19
18
17
15
14
13
12
11
10
9
7,8
6
5
4
3
2
1
500 m
400 m
300 m
200 m
100 m
0 m
Stirling Formation: ortho-quartzite (dolomitic, cross-stratified, massive, or brecciated)
Rainstorm Member: siltstone, Johnnie oolite, sandy limestone, & orthoquartzite with ball-and-pillow structure
siltstone with rare orthoquartzite, & brown dolostone
ripple-bedded siltstone & brown dolostone
siltstone, hummocky cross-stratified orthoquartzite, & brown dolostone
hummocky cross-stratified orthoquartzite, siltstone, & brown dolostone
siltstone, orthoquartzite & brown dolostone
siltstone & occasional orthoquartzite
−4
−2
0
2
4
δ13C (‰, VPDB)
−14
−12
−10
−8
−6
δ18O (‰, VPDB)

Figure 7

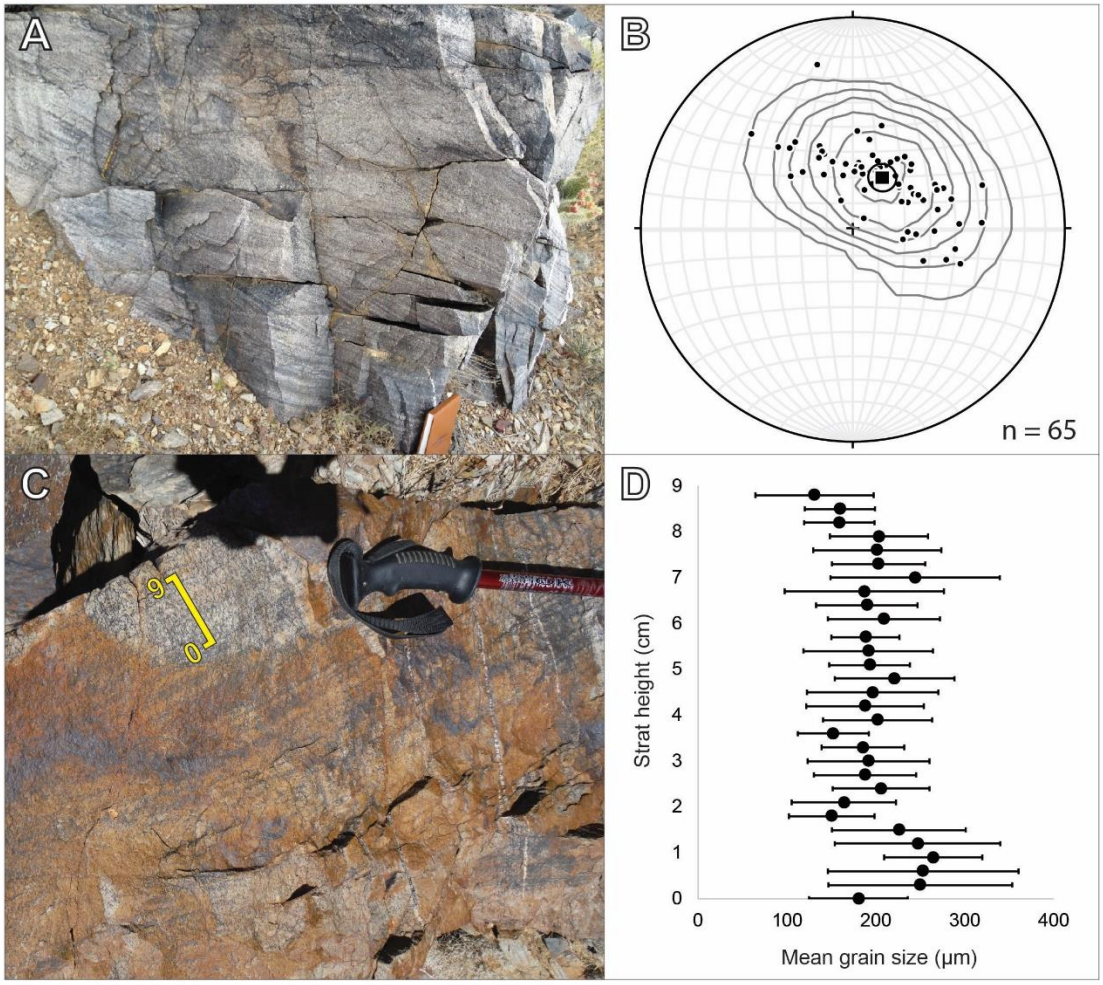
A
B
n = 65
C
9
0
D
Strat height (cm)
0
1
2
3
4
5
6
7
8
9
0
100
200
300
400
Mean grain size (μm)

Figure 8

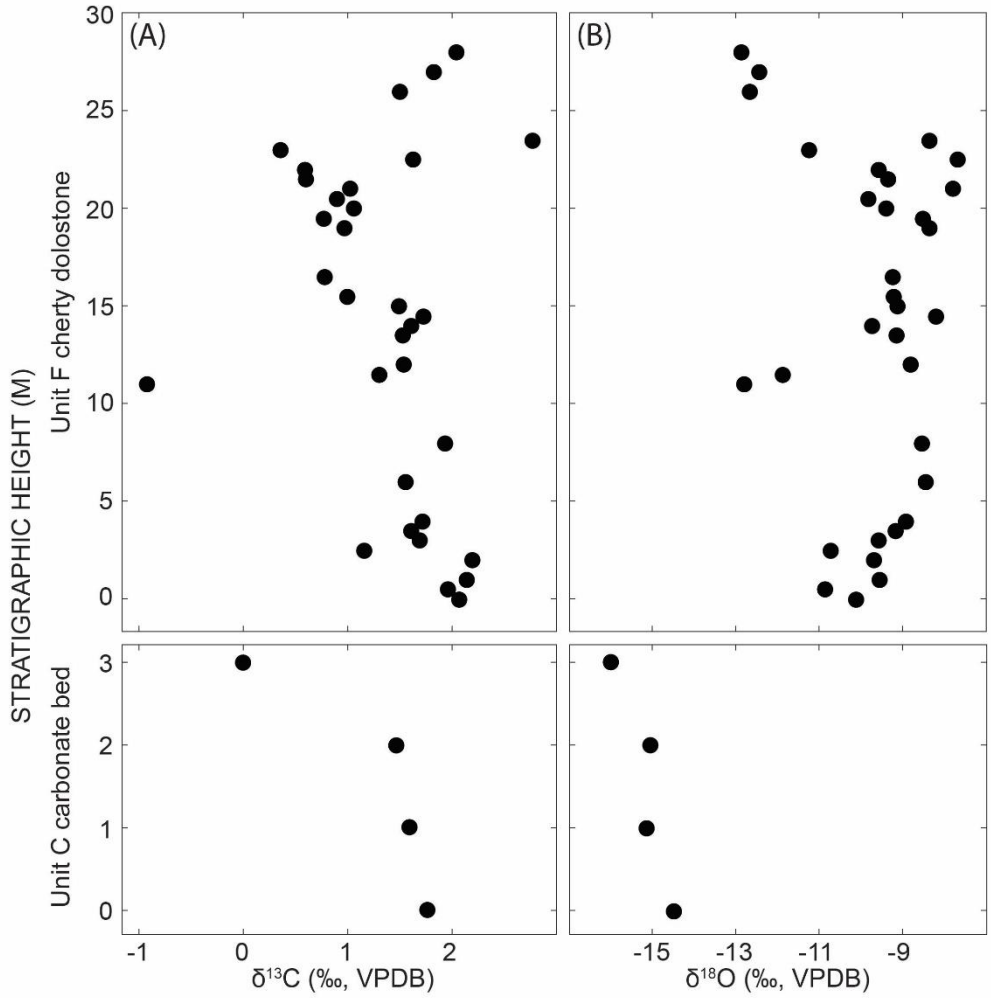
(A)
(B)
STRATIGRAPHIC HEIGHT (M)
Unit F cherty dolostone
Unit C carbonate bed
30
25
20
15
10
5
0
3
2
1
0
-1
0
1
2
-15
-13
-11
-9
δ13C (‰, VPDB)
δ18O (‰, VPDB)

Figure 9

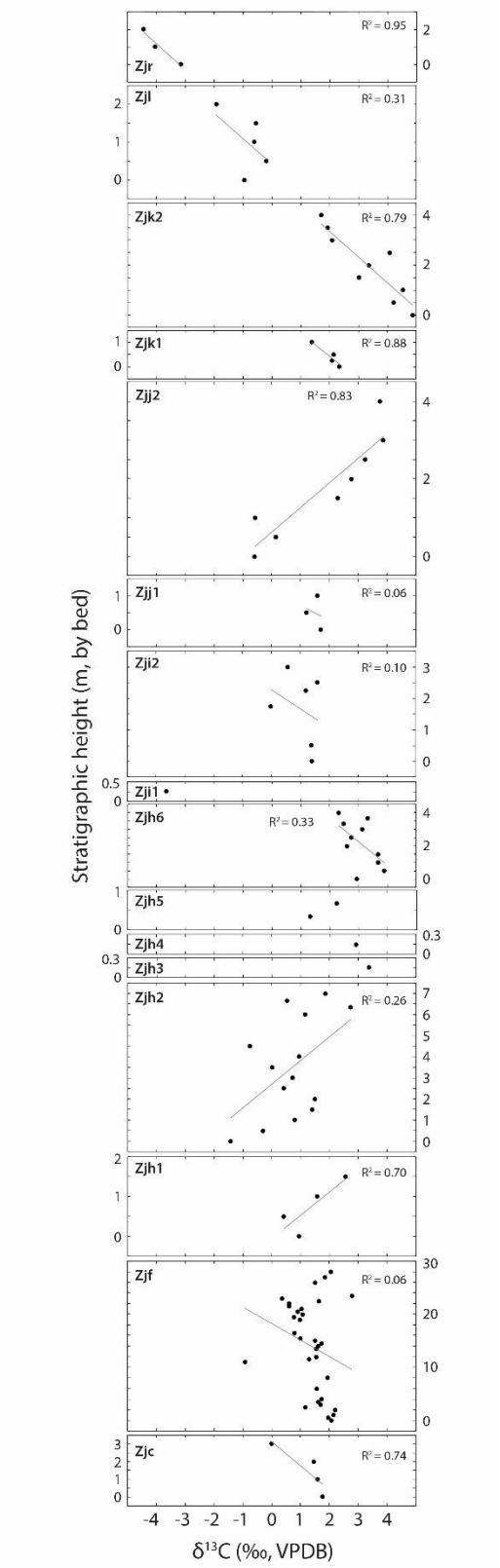
Zjr
R² = 0.95
Zjl
R² = 0.31
Zjk2
R² = 0.79
Zjk1
R² = 0.88
Zjj2
R² = 0.83
Zjj1
R² = 0.06
Zji2
R² = 0.10
Zji1
Zjh6
R² = 0.33
Zjh5
Zjh4
Zjh3
Zjh2
R² = 0.26
Zjh1
R² = 0.70
Zjf
R² = 0.06
Zjc
R² = 0.74
Stratigraphic height (m, by bed)
δ13C (‰, VPDB)

Figure 10

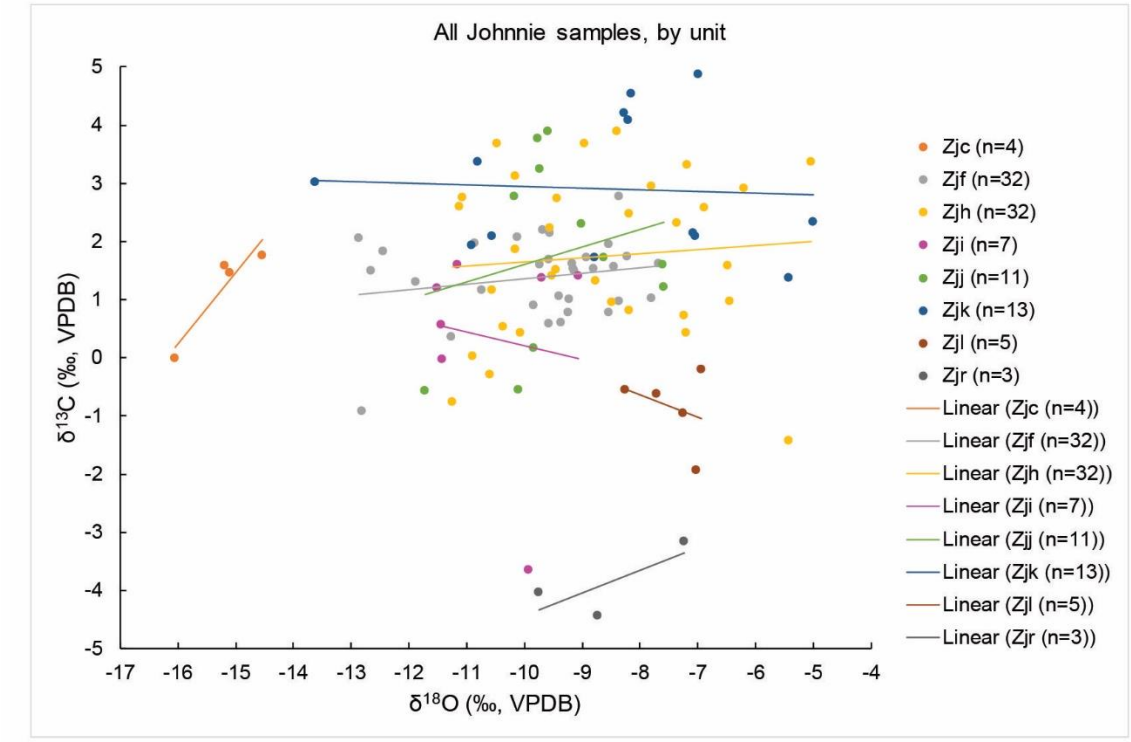
All Johnnie samples, by unit
δ13C (‰, VPDB)
δ18O (‰, VPDB)
5
4
3
2
1
0
-1
-2
-3
-4
-5
-17
-16
-15
-14
-13
-12
-11
-10
-9
-8
-7
-6
-5
-4
Zjc (n=4)
Zjf (n=32)
Zjh (n=32)
Zji (n=7)
Zjj (n=11)
Zjk (n=13)
Zjl (n=5)
Zjr (n=3)
Linear (Zjc (n=4))
Linear (Zjf (n=32))
Linear (Zjh (n=32))
Linear (Zji (n=7))
Linear (Zjj (n=11))
Linear (Zjk (n=13))
Linear (Zjl (n=5))
Linear (Zjr (n=3))

Figure 11

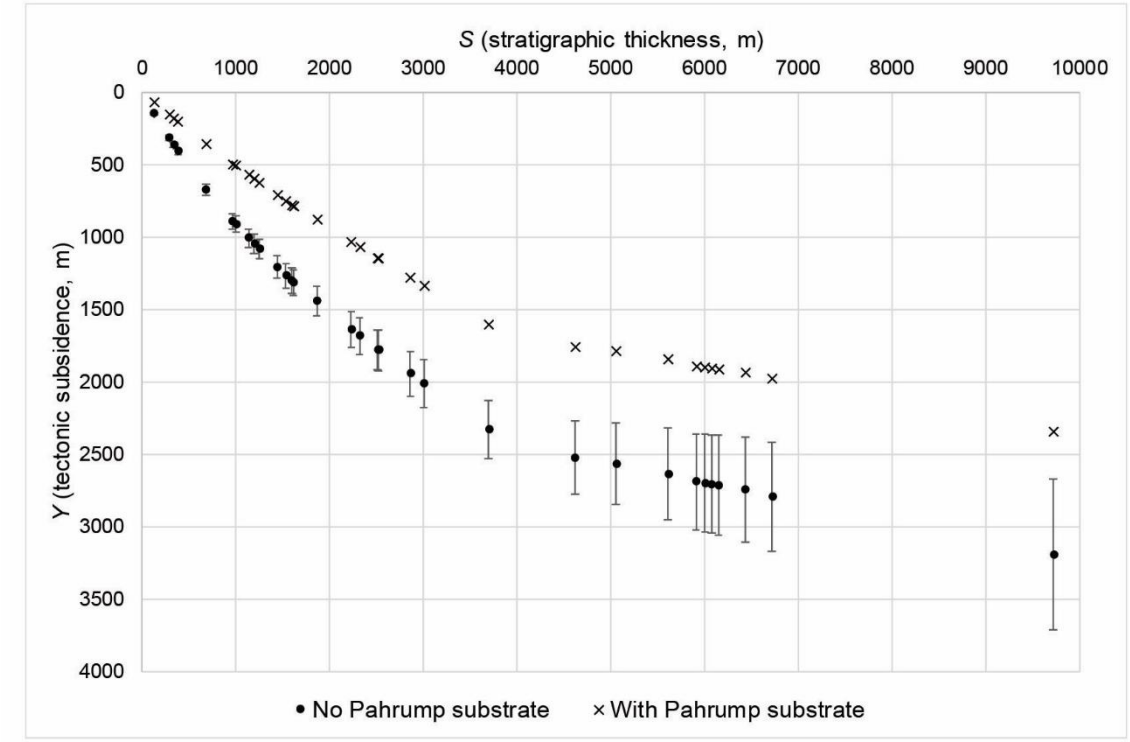
S (stratigraphic thickness, m)
0
1000
2000
3000
4000
5000
6000
7000
8000
9000
10000
Y (tectonic subsidence, m)
0
500
1000
1500
2000
2500
3000
3500
4000
• No Pahrump substrate
× With Pahrump substrate

Figure 12

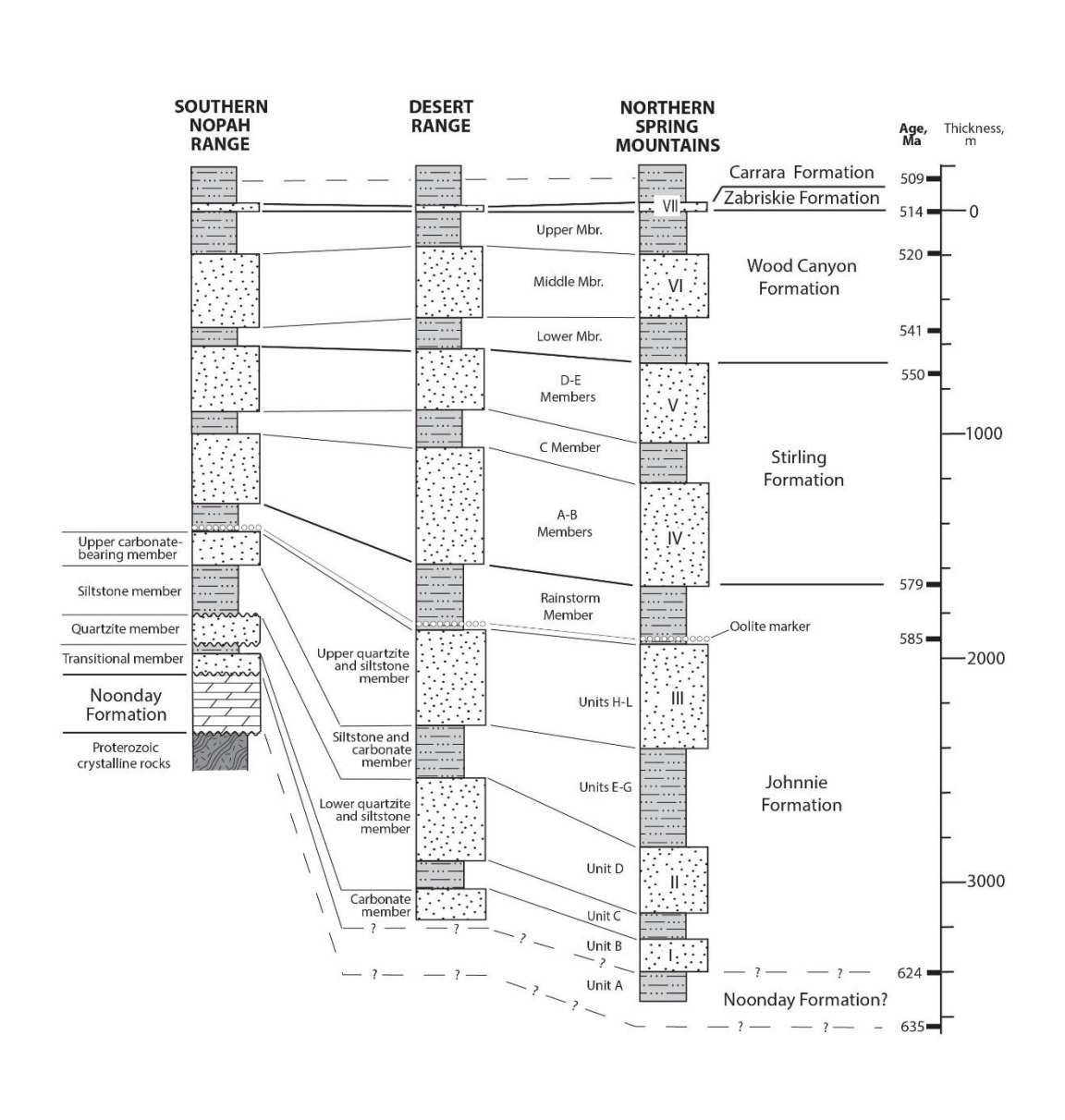
SOUTHERN NOPAH RANGE
DESERT RANGE
NORTHERN SPRING MOUNTAINS
Age, Ma
Thickness, m
Carrara Formation
Zabriskie Formation
Upper Mbr.
Middle Mbr.
Lower Mbr.
D-E Members
C Member
A-B Members
Rainstorm Member
Oolite marker
Upper quartzite and siltstone member
Siltstone and carbonate member
Lower quartzite and siltstone member
Carbonate member
Units H-L
Units E-G
Unit D
Unit C
Unit B
Unit A
Wood Canyon Formation
Stirling Formation
Johnnie Formation
Noonday Formation?
VII
VI
V
IV
III
II
I
Upper carbonate-bearing member
Siltstone member
Quartzite member
Transitional member
Noonday Formation
Proterozoic crystalline rocks
509
514
520
541
550
579
585
624
635
0
1000
2000
3000

Figure 13

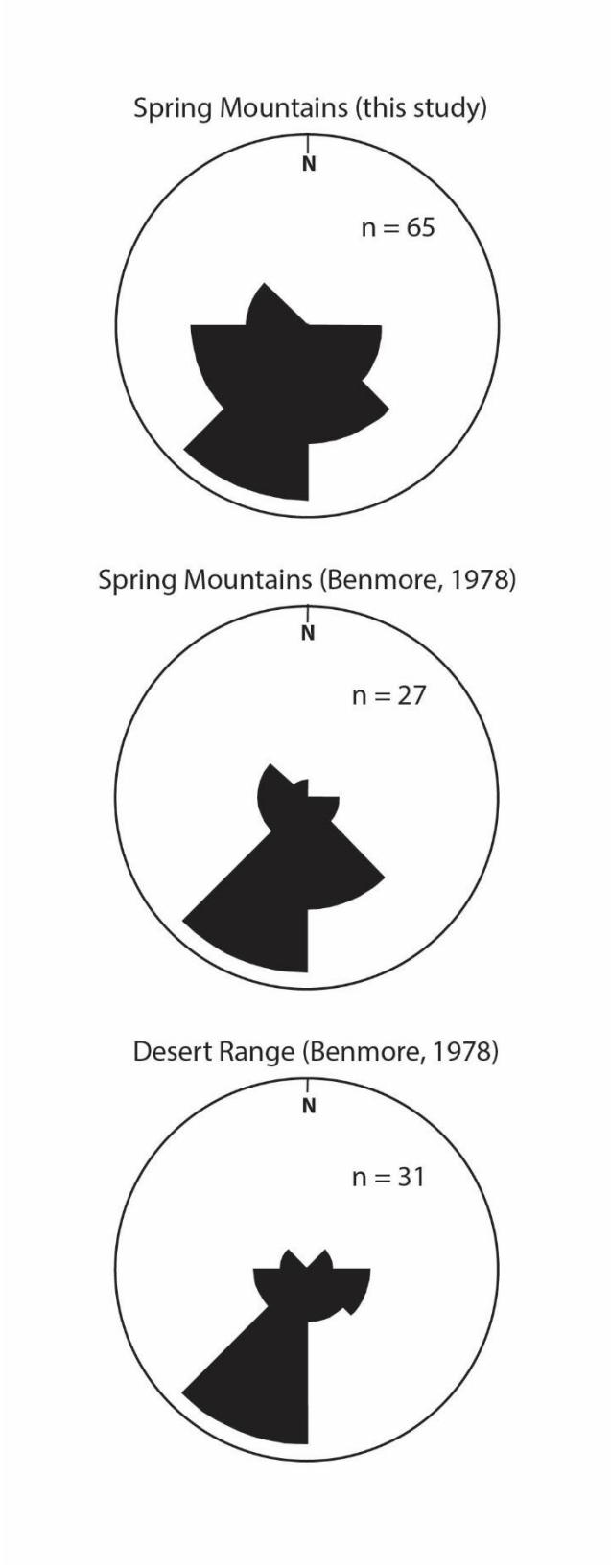
Spring Mountains (this study)
N
n = 65
Spring Mountains (Benmore, 1978)
N
n = 27
Desert Range (Benmore, 1978)
N
n = 31

Figure 14

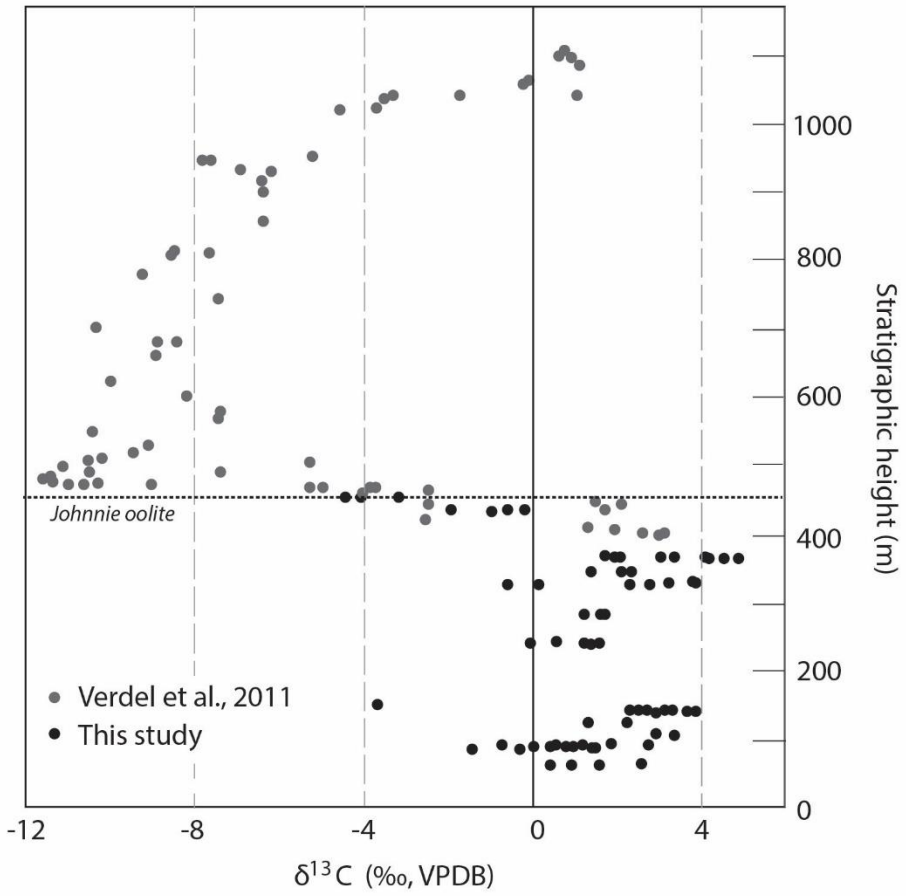
1000
800
600
400
200
0
Stratigraphic height (m)
Johnnie oolite
Verdel et al., 2011
This study
-12
-8
-4
0
4
δ13C (‰, VPDB)

Figure 15

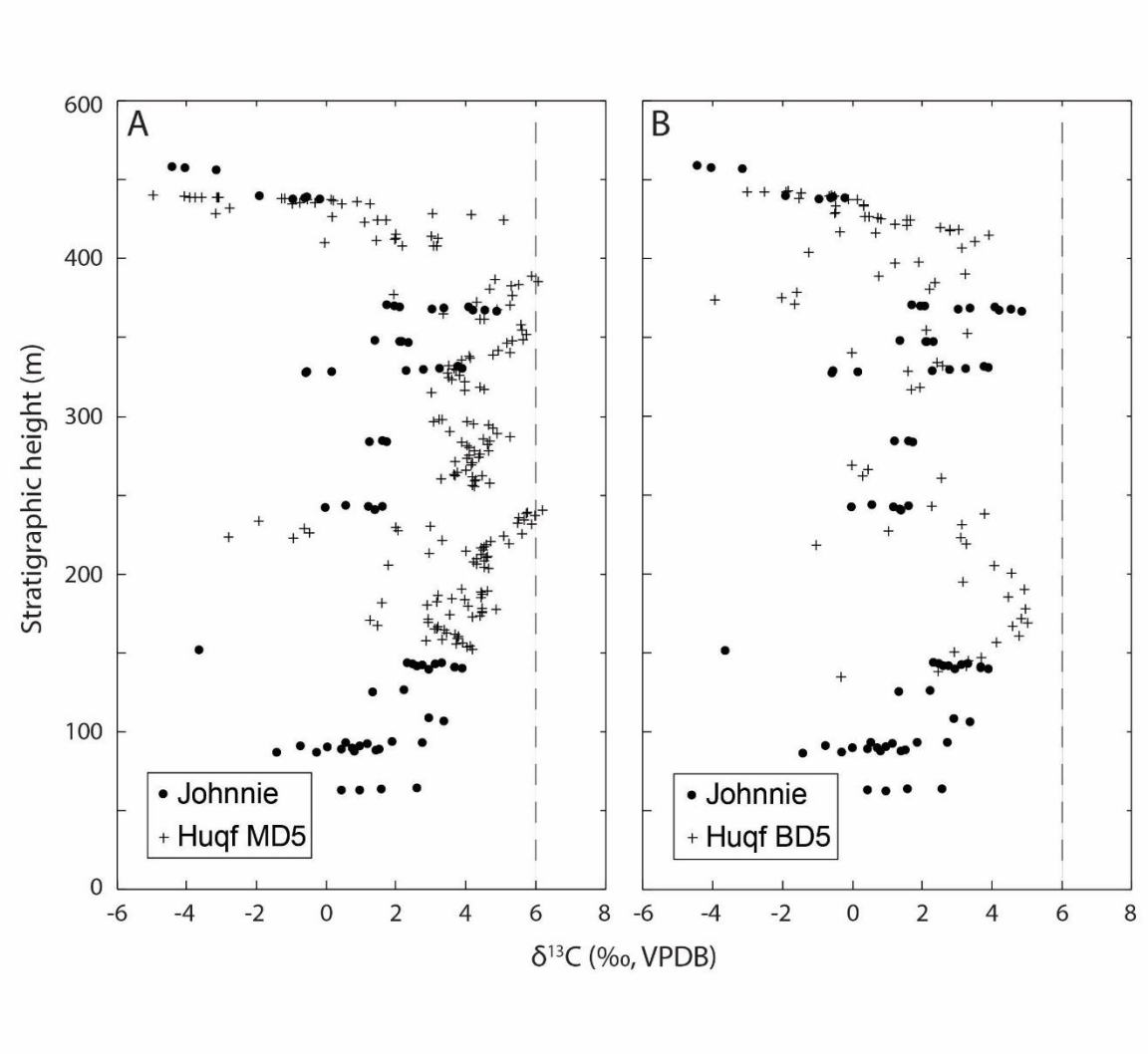
A
B
Stratigraphic height (m)
600
400
300
200
100
0
-6
-4
-2
0
2
4
6
8
Johnnie
Huqf MD5
Johnnie
Huqf BD5
δ13C (‰, VPDB)

Figure 16

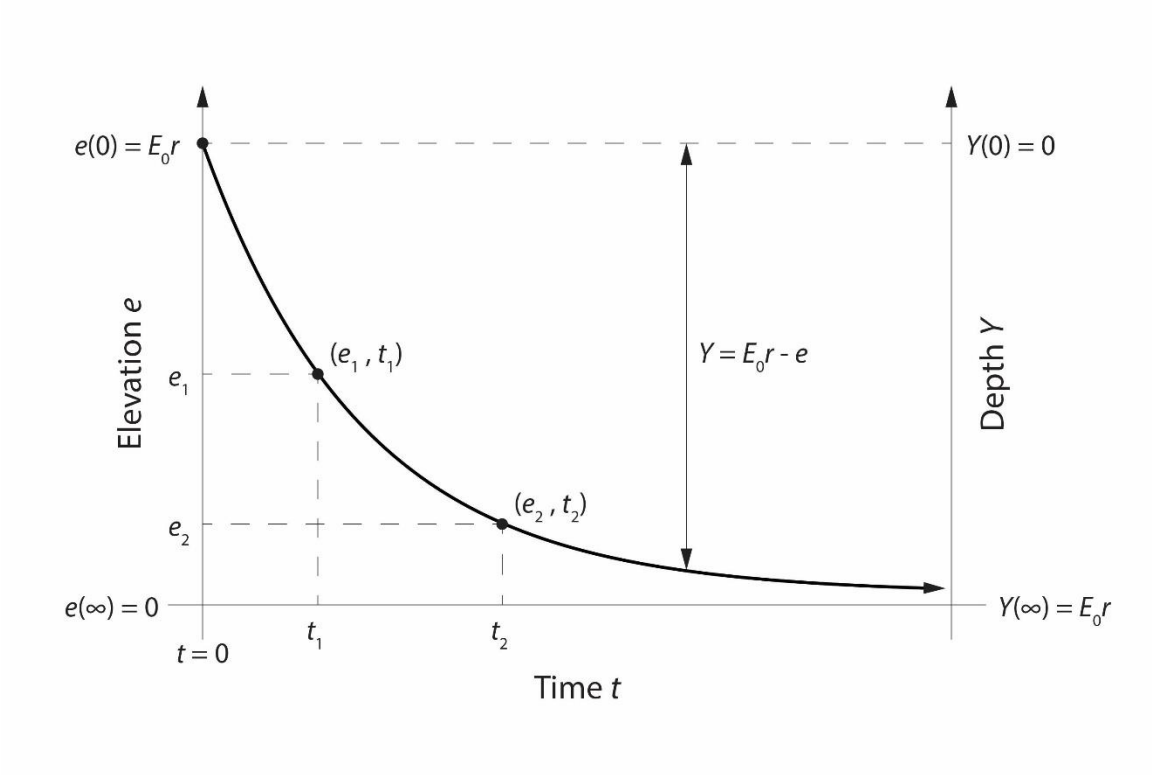
e(0) = E0r
Y(0) = 0
Elevation e
Depth Y
(e1 , t1)
Y = E0r - e
e1
(e2 , t2)
e2
e(∞) = 0
Y(∞) = E0r
t = 0
t1
t2
Time t

Figure 17

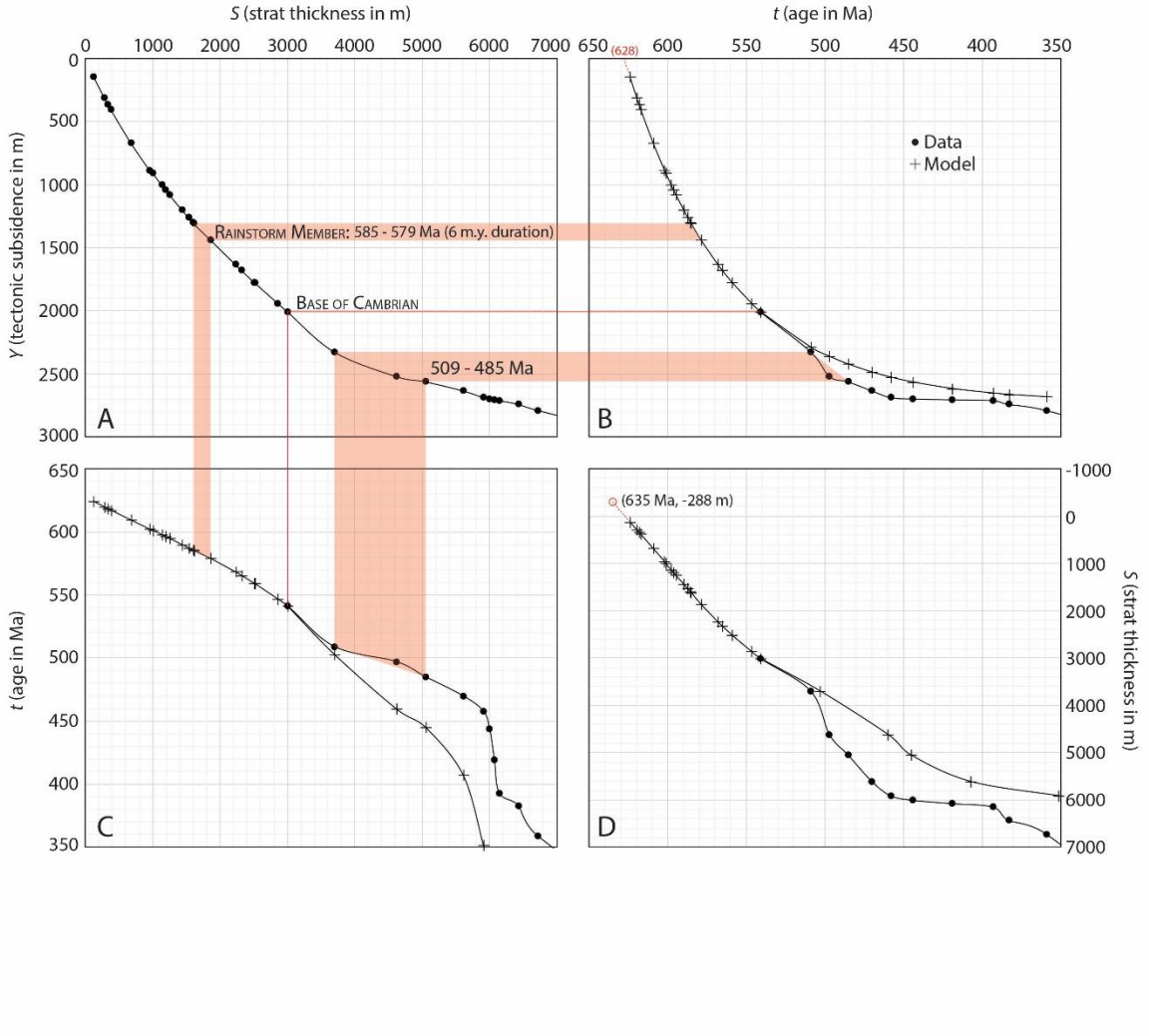
S (strat thickness in m)
t (age in Ma)
Y (tectonic subsidence in m)
RAINSTORM MEMBER: 585 - 579 Ma (6 m.y. duration)
BASE OF CAMBRIAN
509 - 485 Ma
• Data
+ Model
(628)
(635 Ma, -288 m)
A
B
C
D

Figure 18

## SUPPLEMENTAL ITEMS

### Figure Captions

Figure S1 (p. 114): (A) Google Earth image looking c. 60° down-dip to the east along section B - B' in Figure 3, showing traces of mapped unit boundaries (dashed lines) for units E through L and the Rainstorm Member, using unit designations from the Appendix. Width of view at level of Zji is c. 400 m. (B) Google Earth image looking c. 40° down-dip to the east along section A - A' in Figure 3, showing traces of mapped unit boundaries for units A through I. Width of view at unit D/E boundary is c. 1200 m.

Figure S2 (pp. 115-130): Plots of $\delta^{13}C$ and $\delta^{18}O$ versus stratigraphic position with side-by-side cross plots of $\delta^{18}O$ versus $\delta^{13}C$, for each individual carbonate interval designated in Figure 10 of the main text.

Figure S3 (pp. 131-138): Chemostratigraphic profiles comparing carbon isotopic data from the Johnnie Formation from unit H through the lowermost Rainstorm Member (ending at the top of the oolite marker bed, Figure 7) with profiles from the Buah Dome (BD1, BD4, BD5, BD6); Khufai Dome (KDW); and Mukhaibah Dome (MD5, MD6, MDE) areas of Oman (Osburn et al., 2015). Vertical axis shows measured stratigraphic height, from the Mt. Schader section, in all profiles.

Figure S4 (p. 139): Plot showing tectonic subsidence data and models as a function of age (small points and curves, respectively), showing the effect of varying sediment grain density on estimates for the age and duration of the Shuram excursion (large points). Red: high-density; blue: intermediate density; green: low density.

Figure S5 (p. 140): Plot showing tectonic subsidence data and models as a function of age (points and curves, respectively), showing the effect of varying the exponential time constant $\tau$. Models are fit to the 541 Ma data point and assume intermediate sediment grain density.

Figure S6 (p. 141): Plot showing calculated tectonic subsidence $Y$ as a function of observed stratigraphic thickness $S$ for the backstripping and delithification model that includes a hypothetical Pahrump Group substrate below the lowest exposed Johnnie Formation strata (unit A) in the Spring Mountains section. Error bars show range of estimates of $Y$ produced by a ±5 % variation in sediment grain density.

**Tables**

| Table S1: Chemostratigraphy results | | | | | | |
|---|---|---|---|---|---|---|
| Unit | Sample | Stratigraphic position (m) | Bed position (m) | $\delta^{13}C$ (‰, VPDB) | $\delta^{18}O$ (‰, VPDB) | Notes |
| Zjc collection site* located at 36°30'35.05" N, 116°00'58.55" W (within rectangle labeled "Locality A" in Figure 2A) | | | | | | |
| Zjc | J72 | - | 0.00 | 1.8 | -14.5 | |
| | J73 | - | 1.00 | 1.6 | -15.2 | |
| | J74 | - | 2.00 | 1.5 | -15.1 | |
| | J75 | - | 3.00 | 0.0 | -16.0 | |
| Zjf collected along a transect beginning at 36°28'53.96" N, 116°01'30.13" W; ending at 36°28'53.79" N, 116°01'28.97" W (at the beginning of cross section line B-B' in Figure 3: Johnnie Wash geologic map) | | | | | | |

| | | | | | | |
|---|---|---|---|---|---|---|
| Zjf | J76 | - | 0.00 | 2.1 | -10.1 | |
| | J77 | - | 0.50 | 2.0 | -10.9 | |
| | J78 | - | 1.00 | 2.1 | -9.6 | |
| | J79 | - | 2.00 | 2.2 | -9.7 | |
| | J80 | - | 2.50 | 1.2 | -10.7 | |
| | J81 | - | 3.00 | 1.7 | -9.6 | |
| | J82 | - | 3.50 | 1.6 | -9.2 | |
| | J83 | - | 4.00 | 1.7 | -8.9 | |
| | J84 | - | 6.00 | 1.6 | -8.4 | |
| | J85 | - | 8.00 | 1.9 | -8.5 | |
| | J86 | - | 11.00 | -0.9 | -12.8 | |
| | J87 | - | 11.50 | 1.3 | -11.9 | |
| | J88 | - | 12.00 | 1.5 | -8.8 | |
| | J89 | - | 13.50 | 1.5 | -9.2 | |
| | J90 | - | 14.00 | 1.6 | -9.7 | |
| | J91 | - | 14.50 | 1.7 | -8.2 | |
| | J92 | - | 15.00 | 1.5 | -9.1 | |
| | J93 | - | 15.50 | 1.0 | -9.2 | |
| | J94 | - | 16.50 | 0.8 | -9.2 | |
| | J95 | - | 19.00 | 1.0 | -8.4 | |
| | J96 | - | 19.50 | 0.8 | -8.5 | |
| | J97 | - | 20.00 | 1.1 | -9.4 | |
| | J98 | - | 20.50 | 0.9 | -9.8 | |
| | J99 | - | 21.00 | 1.0 | -7.8 | |
| | J100 | - | 21.50 | 0.6 | -9.4 | |
| | J101 | - | 22.00 | 0.6 | -9.6 | |
| | J102 | - | 22.50 | 1.6 | -7.7 | |
| | J103 | - | 23.00 | 0.4 | -11.3 | |
| | J104 | - | 23.50 | 2.8 | -8.4 | |
| | J105 | - | 26.00 | 1.5 | -12.7 | |
| | J106 | - | 27.00 | 1.8 | -12.4 | |
| | J107 | - | 28.00 | 2.0 | -12.9 | |
| Transect a-a’ in Figure 6: Mt. Schader geologic map (begins at 36°27'31.70" N, 116°05'43.38" W; ends at 36°27'30.30" N, 116°05'33.92" W) | | | | | | |
| Zjh | J1 | 63.00 | 0.00 | 1.0 | -6.5 | |
| | J2 | 63.50 | 0.50 | 0.4 | -7.2 | |
| | J3 | 64.00 | 1.00 | 1.6 | -6.5 | |
| | J4 | 64.50 | 1.50 | 2.6 | -6.9 | |
| | J5 | 87.00 | 0.00 | -1.4 | -5.4 | |
| | J6 | 87.50 | 0.50 | -0.3 | -10.6 | |
| | J7 | 88.00 | 1.00 | 0.8 | -8.2 | |
| | J8 | 88.50 | 1.50 | 1.4 | -9.5 | |
| | J9 | 89.00 | 2.00 | 1.5 | -9.5 | |
| | J10 | 89.50 | 2.50 | 0.4 | -10.1 | |
| | J11 | 90.00 | 3.00 | 0.7 | -7.2 | |
| | J12 | 90.50 | 3.50 | 0.0 | -10.9 | |
| | J13 | 91.00 | 4.00 | 1.0 | -8.5 | |
| | J14 | 91.50 | 4.50 | -0.8 | -11.2 | |
| | J15 | 93.00 | 6.00 | 1.2 | -10.6 | |
| | J16 | 93.33 | 6.33 | 2.7 | -9.4 | |
| | J17 | 93.66 | 6.66 | 0.5 | -10.4 | |

| | | | | | | |
|---|---|---|---|---|---|---|
| | J18 | 94.00 | 7.00 | 1.9 | -10.2 | |
| | J19 | 107.00 | - | 3.4 | -5.0 | |
| | J20 | 109.00 | - | 2.9 | -6.2 | |
| | J21 | 125.75 | - | 1.3 | -8.8 | |
| | J22 | 126.75 | - | 2.2 | -9.6 | |
| | J23 | 140.00 | 0.00 | 2.9 | -7.8 | |
| | J24 | 140.50 | 0.50 | 3.9 | -8.4 | |
| | J25 | 141.00 | 1.00 | 3.7 | -9.0 | |
| | J26 | 141.50 | 1.50 | 3.7 | -10.5 | |
| | J27 | 142.00 | 2.00 | 2.6 | -11.1 | |
| | J28 | 142.50 | 2.50 | 2.7 | -11.1 | |
| | J29 | 143.00 | 3.00 | 3.1 | -10.2 | |
| | J30 | 143.33 | 3.33 | 2.5 | -8.2 | |
| | J31 | 143.66 | 3.66 | 3.3 | -7.2 | |
| | J32 | 144.00 | 4.00 | 2.3 | -7.4 | |
| Transect b-b’ in Figure 6: Mt. Schader geologic map (begins at 36°27'18.37" N, 116°05'39.60" W; ends at 36°27'17.54" N, 116°05'33.18" W) | | | | | | |
| Zji | J33 | 152.00 | - | -3.7 | -9.9 | |
| | J34 | 241.00 | 0.00 | 1.4 | -9.1 | |
| | J35 | 241.50 | 0.50 | 1.4 | -9.7 | |
| | J36 | 242.75 | 1.75 | 0.0 | -11.4 | |
| | J37 | 243.25 | 2.25 | 1.2 | -11.5 | |
| | J38 | 243.50 | 2.50 | 1.6 | -11.2 | |
| | J39 | 244.00 | 3.00 | 0.6 | -11.4 | |
| Transect c-c’ in Figure 6: Mt. Schader geologic map (begins at 36°26'50.85" N, 116°05'53.02" W; ends at 36°26'45.94" N, 116°05'46.85" W) | | | | | | |
| Zjj | J40 | 284.00 | 0.00 | 1.7 | -8.6 | |
| | J41 | 284.50 | 0.50 | 1.2 | -7.6 | |
| | J42 | 285.00 | 1.00 | 1.6 | -7.6 | |
| | J43 | 328.00 | 0.00 | -0.6 | -11.7 | |
| | J44 | 328.50 | 0.50 | 0.2 | -9.8 | |
| | J45 | 329.00 | 1.00 | -0.6 | -10.1 | |
| | J46 | 329.50 | 1.50 | 2.3 | -9.0 | |
| | J47 | 330.00 | 2.00 | 2.8 | -10.2 | |
| | J48 | 330.50 | 2.50 | 3.2 | -9.7 | |
| | J49 | 331.00 | 3.00 | 3.9 | -9.6 | |
| | J50 | 332.00 | 4.00 | 3.8 | -9.8 | |
| Zjk | J51 | 347.50 | 0.00 | 2.3 | -5.0 | |
| | J52 | 347.75 | 0.25 | 2.1 | -7.0 | |
| | J53 | 348.00 | 0.50 | 2.1 | -7.1 | |
| | J54 | 348.50 | 1.00 | 1.4 | -5.4 | |
| | J55 | 367.00 | 0.00 | 4.9 | -7.0 | |
| | J56 | 367.50 | 0.50 | 4.2 | -8.3 | |
| | J57 | 368.00 | 1.00 | 4.5 | -8.2 | |
| | J58 | 368.50 | 1.50 | 3.0 | -13.6 | |
| | J59 | 369.00 | 2.00 | 3.4 | -10.8 | |
| | J60 | 369.50 | 2.50 | 4.1 | -8.2 | |
| | J61 | 370.00 | 3.00 | 2.1 | -10.6 | |
| | J62 | 370.50 | 3.50 | 1.9 | -10.9 | |
| | J63 | 371.00 | 4.00 | 1.7 | -8.8 | |

| Transect d-d' in Figure 6: Mt. Schader geologic map (begins at 36°27'28.71" N, 116°05'16.42" W; ends at 36°27'24.47" N, 116°05'10.44" W) | | | | | | |
|---|---|---|---|---|---|---|
| Zjl | J64 | 438.00 | 0.00 | -1.0 | -7.3 | |
| | J65 | 438.50 | 0.50 | -0.2 | -6.9 | |
| | J66 | 439.00 | 1.00 | -0.6 | -7.7 | |
| | J67 | 439.50 | 1.50 | -0.6 | -8.3 | |
| | J68 | 440.00 | 2.00 | -1.9 | -7.0 | |
| Zjr | J69 | 457.00 | 0.00 | -3.2 | -7.2 | Johnnie oolite |
| | J70 | 458.00 | 1.00 | -4.0 | -9.8 | |
| | J71 | 459.00 | 2.00 | -4.4 | -8.7 | |
| *All locations recorded using GPS with the WGS84 coordinate system | | | | | | |

| Table S2: All ages modeled using hypothetical Pahrump Group substrate | | | | | | | | | | |
|---|---|---|---|---|---|---|---|---|---|---|
| | | Model ages (Ma) | | | | | | | | |
| | | $\tau$ = 55 my | | | $\tau$ = 60 my | | | $\tau$ = 65 my | | |
| Unit | Age (Ma) | Min | Int | Max | Min | Int | Max | Min | Int | Max |
| MzPzco | ~243 | - | - | - | - | - | - | - | - | - |
| Ddg | 359 | - | - | - | - | - | - | - | - | - |
| Dn | 383 | - | - | - | - | - | - | - | - | - |
| Dl | 393 | 342 | 327 | 288 | 324 | 307 | 265 | 306 | 288 | 242 |
| Sl | 419 | 364 | 349 | 310 | 348 | 332 | 289 | 331 | 314 | 268 |
| Oes | 444 | 378 | 365 | 318 | 363 | 349 | 298 | 348 | 333 | 278 |
| Oe | 458 | 393 | 379 | 332 | 380 | 364 | 313 | 366 | 350 | 294 |
| Op1 | 470 | 436 | 429 | 413 | 427 | 419 | 401 | 417 | 409 | 390 |
| OЄn1 | 485 | 468 | 460 | 440 | 461 | 452 | 431 | 454 | 445 | 422 |
| Єbk1 | 497 | 481 | 470 | 442 | 475 | 464 | 433 | 470 | 457 | 424 |
| Єc1 | 509 | 513 | 507 | 492 | 511 | 504 | 488 | 508 | 501 | 483 |
| ЄZwc1 | 541 | 541 | 541 | 541 | 541 | 541 | 541 | 541 | 541 | 541 |
| Zse | - | 545 | 546 | 547 | 546 | 546 | 548 | 546 | 547 | 548 |
| Zsd | - | 554 | 556 | 560 | 556 | 558 | 561 | 557 | 559 | 563 |
| Zsc | - | 554 | 556 | 560 | 556 | 558 | 562 | 557 | 559 | 563 |
| Zsb | - | 559 | 562 | 566 | 561 | 563 | 568 | 562 | 565 | 571 |
| Zsa | - | 561 | 564 | 569 | 563 | 566 | 571 | 565 | 568 | 574 |
| Zjr2 | - | 569 | 572 | 579 | 571 | 575 | 582 | 574 | 578 | 585 |
| Zjr1 | - | 573 | 577 | 584 | 576 | 580 | 588 | 579 | 584 | 592 |
| Zjl | - | 574 | 577 | 584 | 577 | 581 | 588 | 580 | 584 | 592 |
| Zjk | - | 575 | 579 | 586 | 578 | 582 | 590 | 581 | 586 | 594 |
| Zjj | - | 577 | 581 | 588 | 580 | 584 | 592 | 583 | 588 | 596 |
| Zji | - | 580 | 585 | 592 | 584 | 589 | 597 | 587 | 592 | 602 |
| Zjh | - | 581 | 586 | 594 | 585 | 590 | 598 | 588 | 594 | 603 |
| Zjg | - | 582 | 587 | 595 | 586 | 591 | 600 | 590 | 595 | 605 |
| Zjf | - | 584 | 589 | 598 | 588 | 594 | 603 | 592 | 598 | 608 |
| Zje | - | 585 | 590 | 598 | 589 | 594 | 603 | 593 | 599 | 608 |
| Zjd | - | 590 | 595 | 604 | 594 | 600 | 609 | 598 | 605 | 615 |
| Zjc2 | - | 594 | 600 | 609 | 599 | 605 | 616 | 604 | 611 | 622 |
| Zjc1 | - | 595 | 601 | 610 | 600 | 606 | 617 | 605 | 612 | 623 |
| Zjb | - | 596 | 602 | 611 | 601 | 607 | 618 | 606 | 613 | 624 |
| Zja | - | 598 | 604 | 614 | 603 | 610 | 621 | 609 | 616 | 627 |
| Zjt | - | 600 | 606 | 616 | 605 | 612 | 623 | 611 | 618 | 630 |
| Zkpw | 635 | 602 | 608 | 618 | 607 | 614 | 625 | 613 | 620 | 632 |
| Zkpth | - | 603 | 609 | 620 | 609 | 615 | 627 | 614 | 622 | 634 |
| Zkpmg | - | 604 | 610 | 621 | 610 | 617 | 628 | 615 | 623 | 635 |
| Zkpsmp | - | 605 | 612 | 622 | 611 | 618 | 630 | 617 | 625 | 637 |
| Zkpls | - | 608 | 615 | 626 | 615 | 622 | 634 | 621 | 629 | 641 |
| Zbs | - | 614 | 621 | 633 | 621 | 628 | 641 | 627 | 636 | 649 |
| Zhs | <787 | 616 | 623 | 635 | 623 | 631 | 643 | 630 | 638 | 652 |
| Ycs2 | >1087 | 619 | 627 | 638 | 626 | 634 | 647 | 633 | 642 | 656 |
| Ycs1 | - | 621 | 629 | 641 | 629 | 637 | 650 | 636 | 645 | 659 |
| (base) | - | 628 | 637 | 649 | 636 | 645 | 659 | 644 | 654 | 669 |

**Figures**

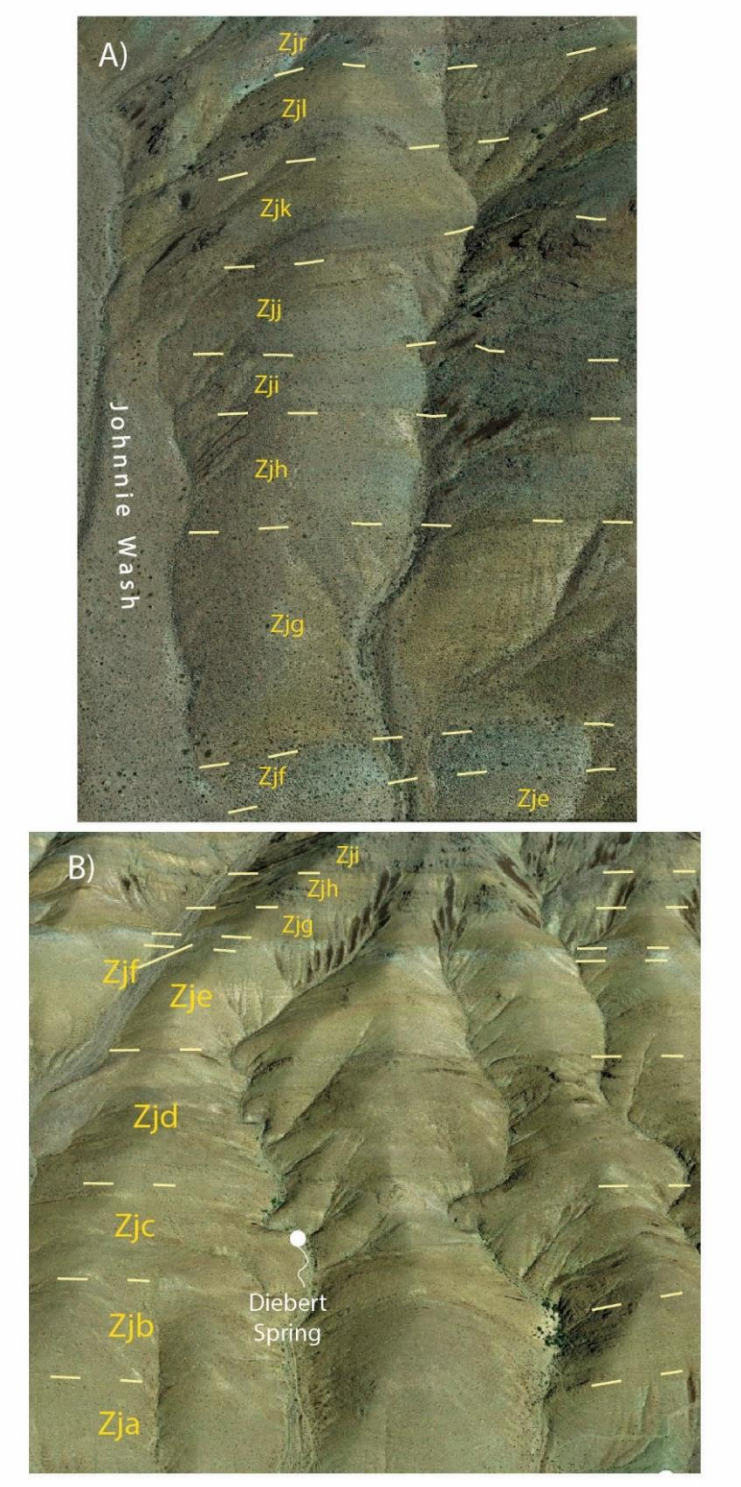


Figure S1

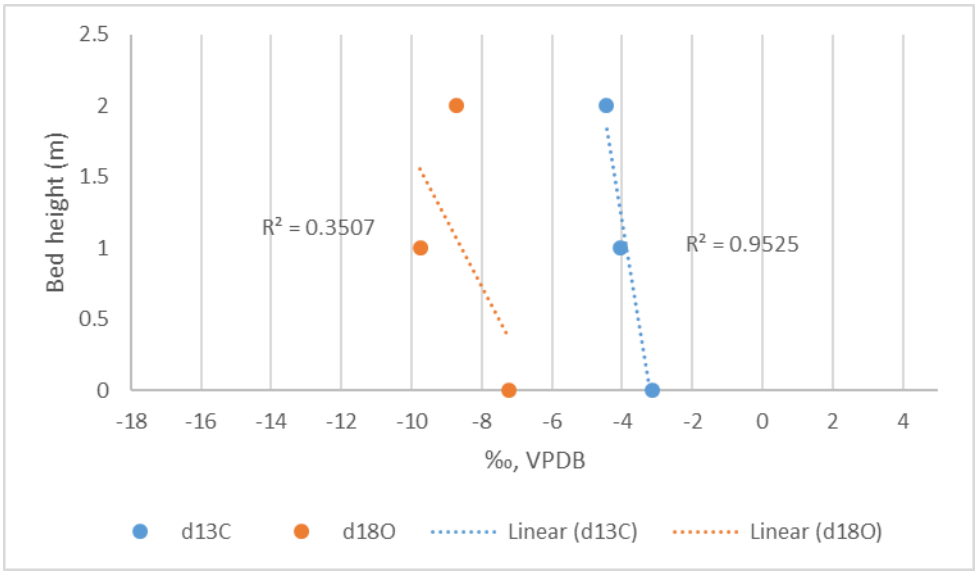


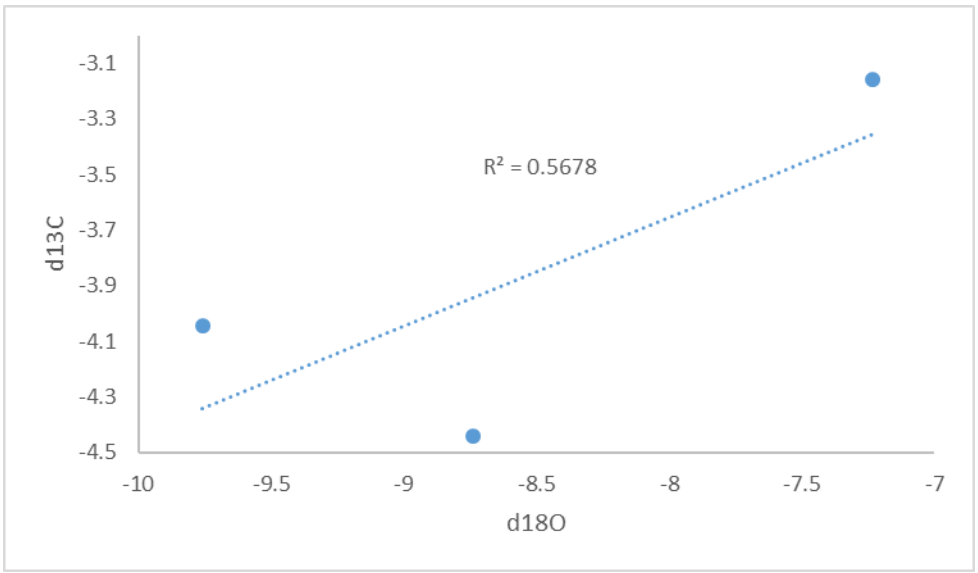


Figure S2: Zjr (j69-71)

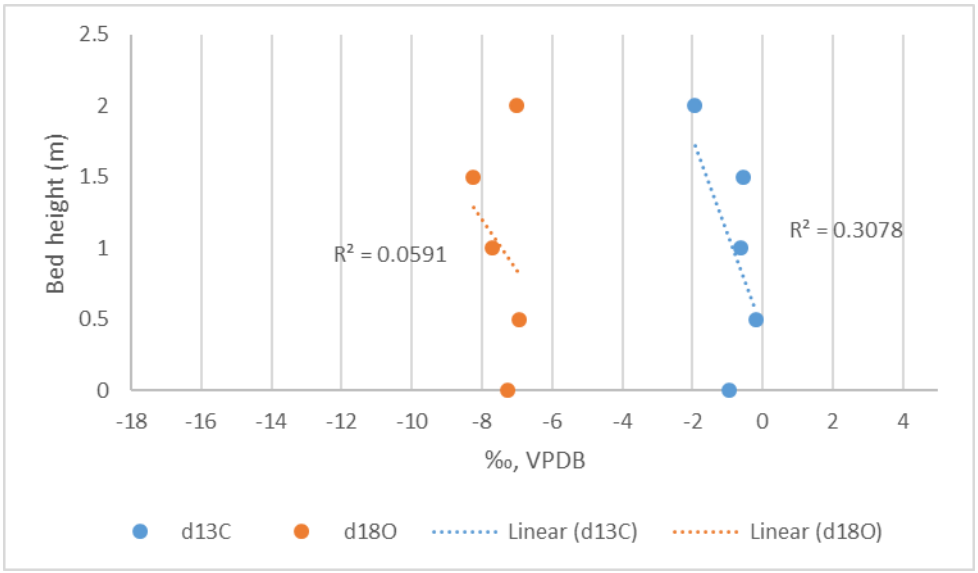


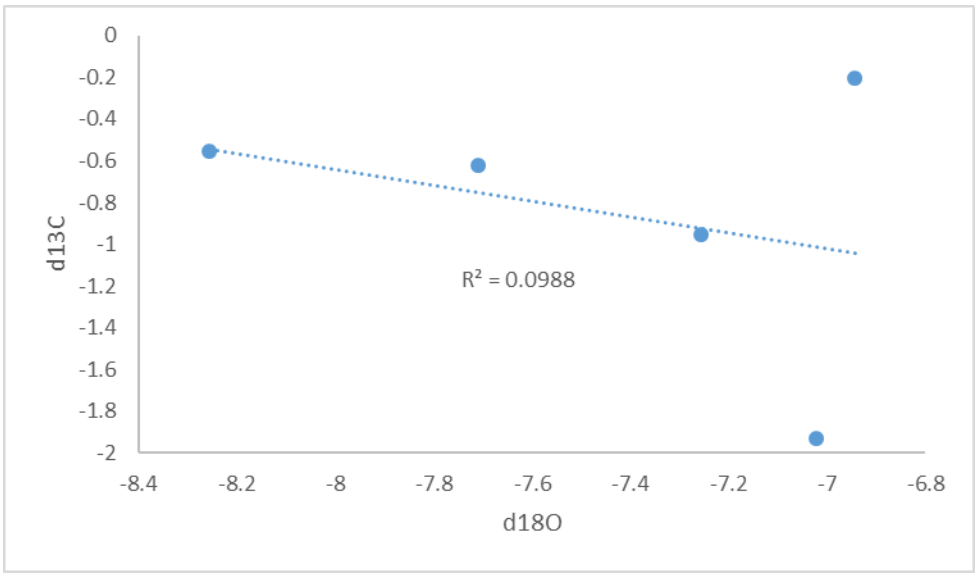


Figure S2: Zjl (j64-68)

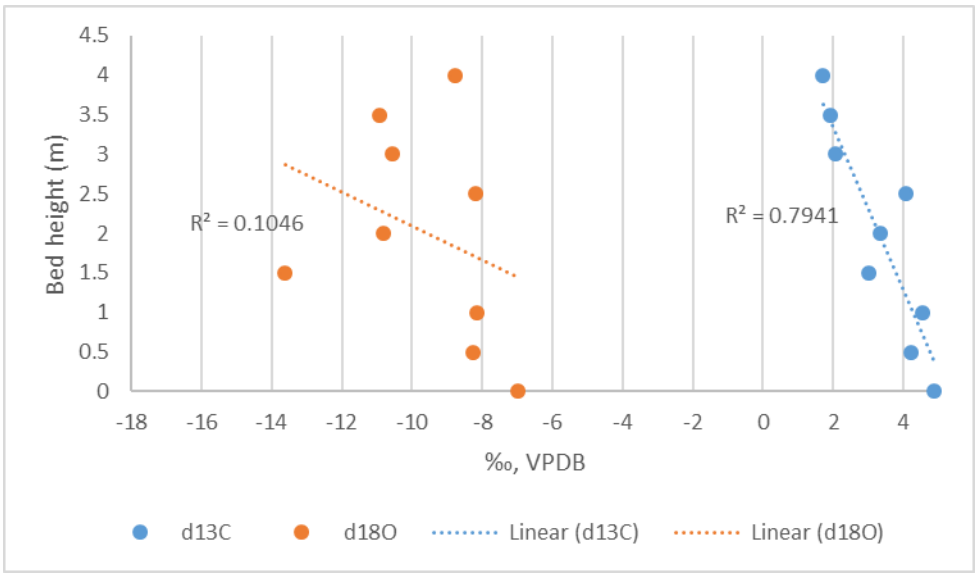


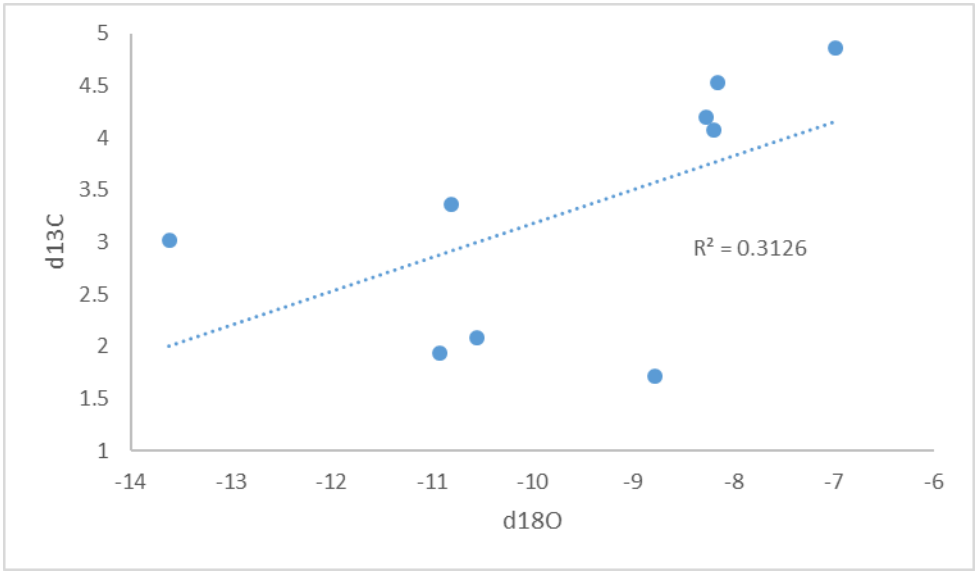


Figure S2: Zjk2 (j55-63)

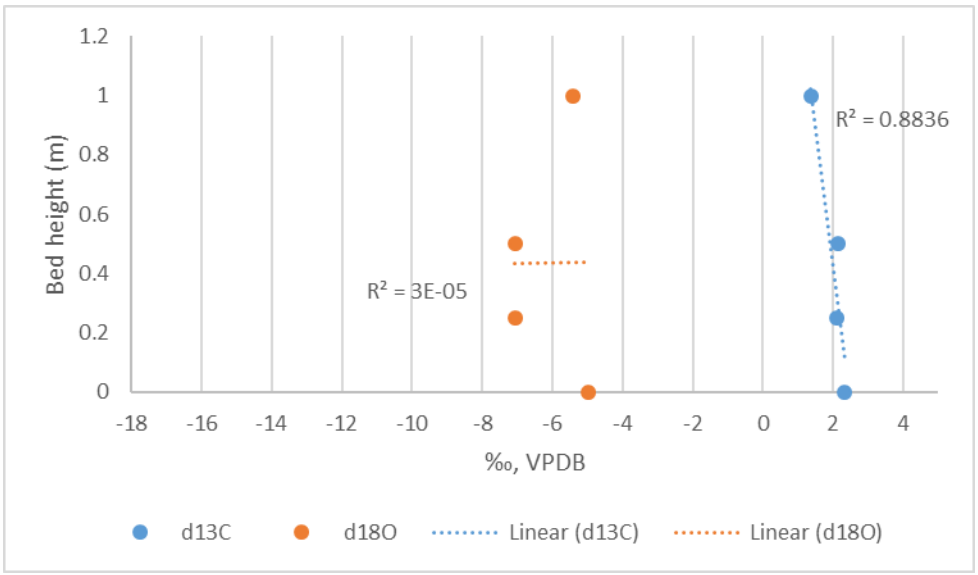


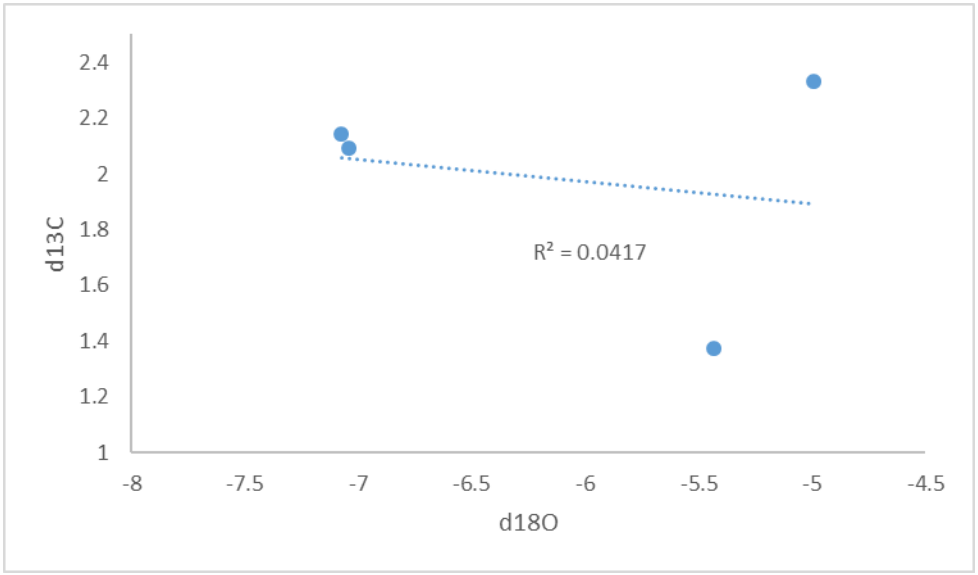


Figure S2: Zjk1 (j51-54)

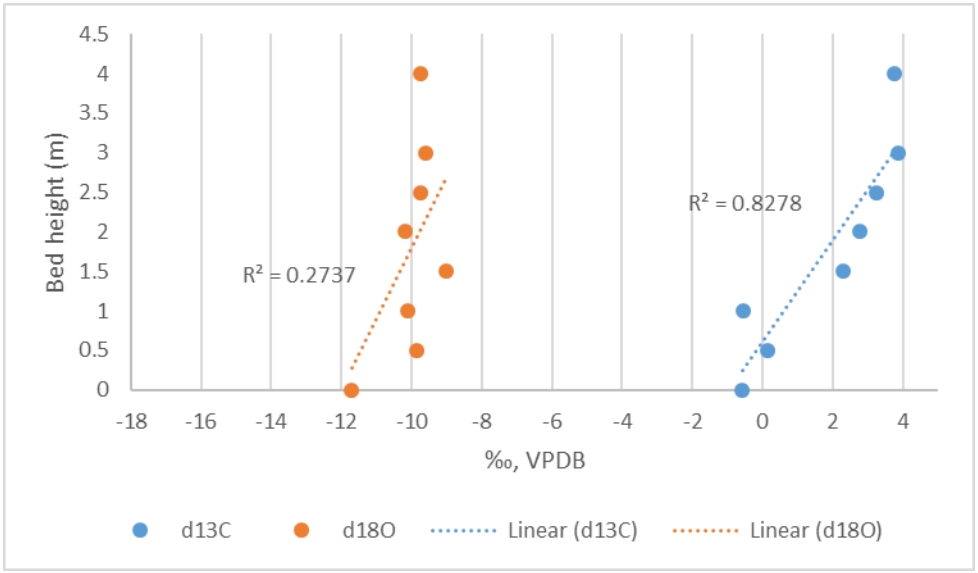


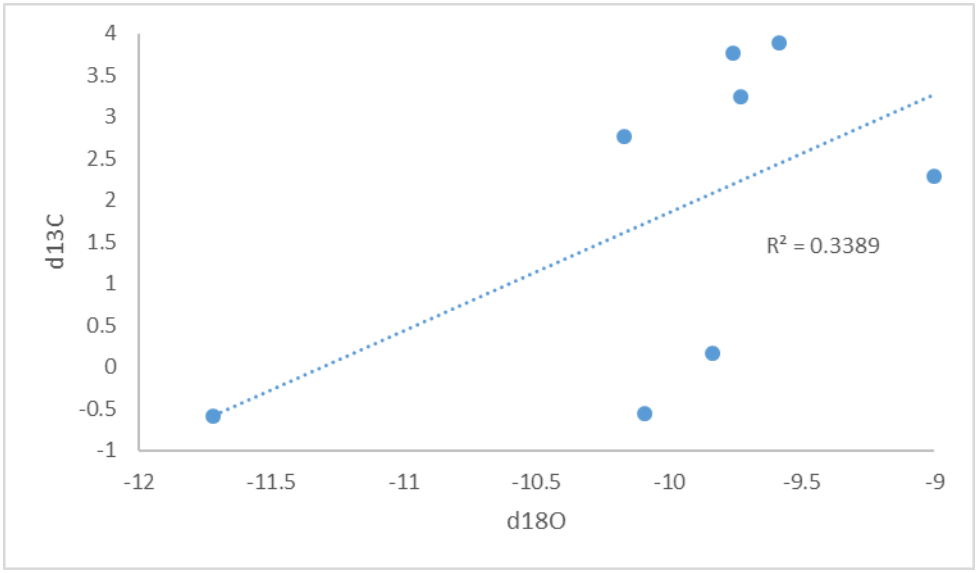


Figure S2: Zjj2 (j43-50)

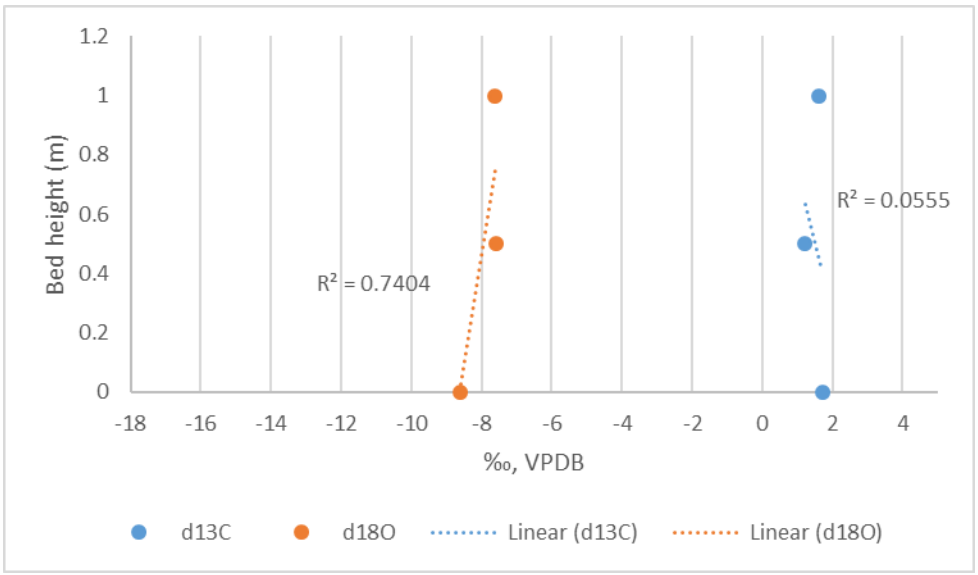


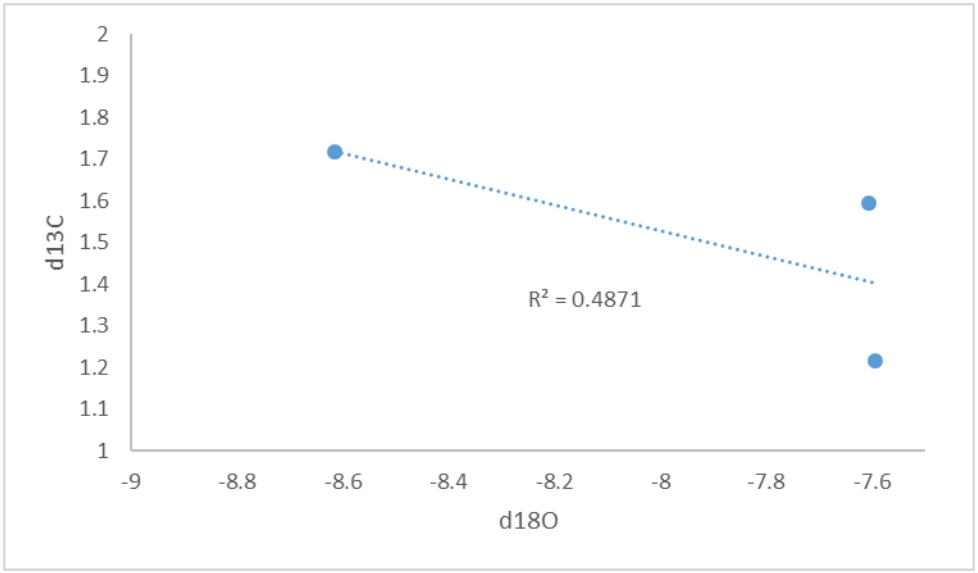


Figure S2: Zjj1 (j40-42)

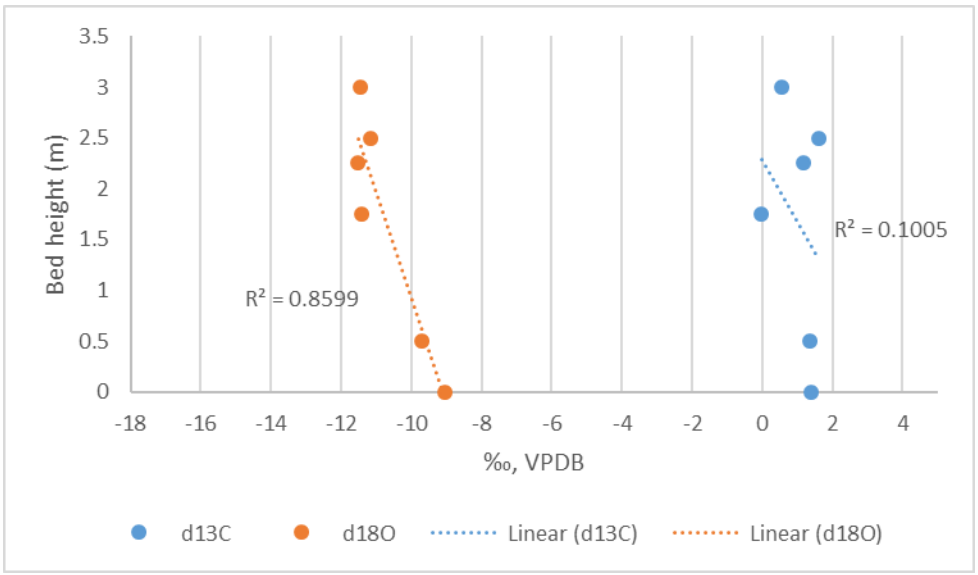


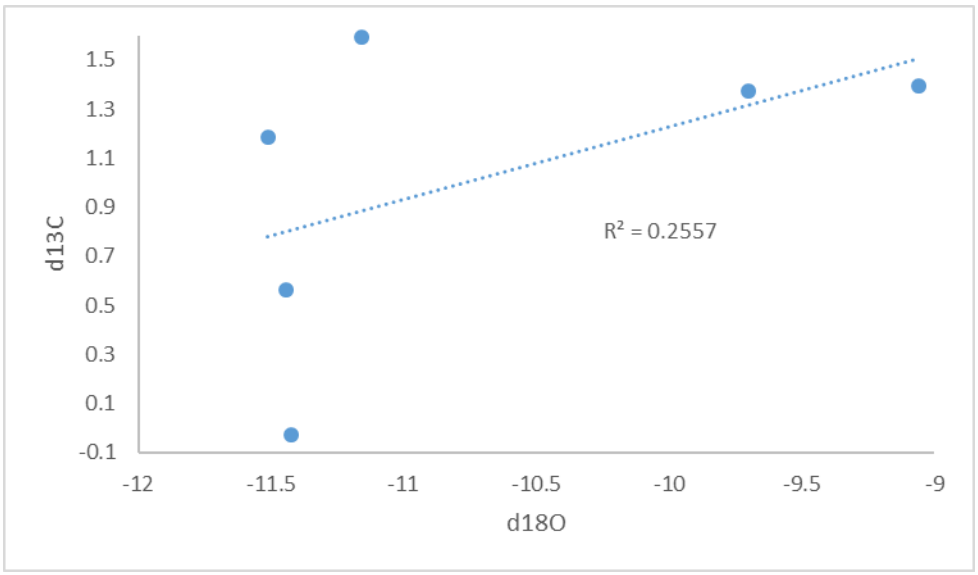


Figure S2: Zji2 (j34-39)

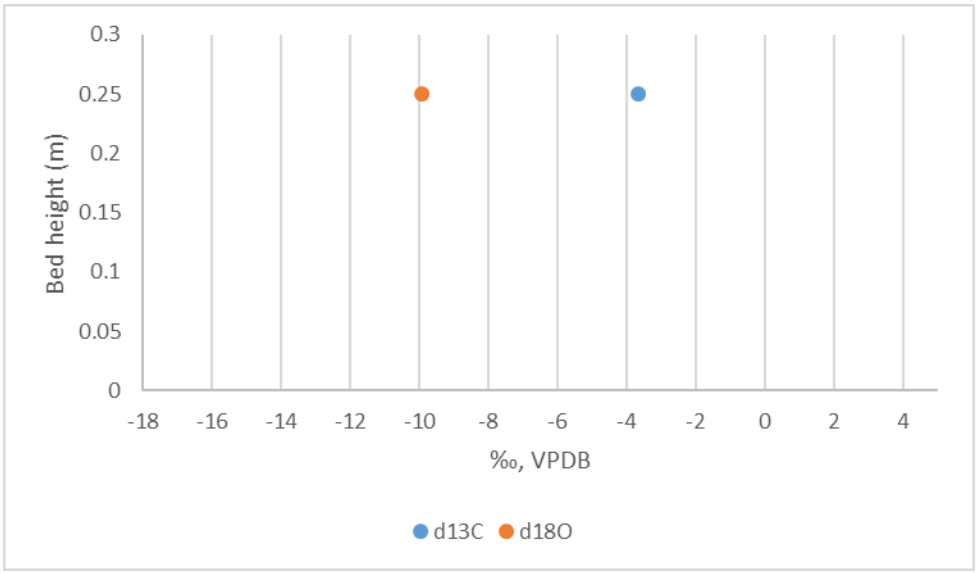


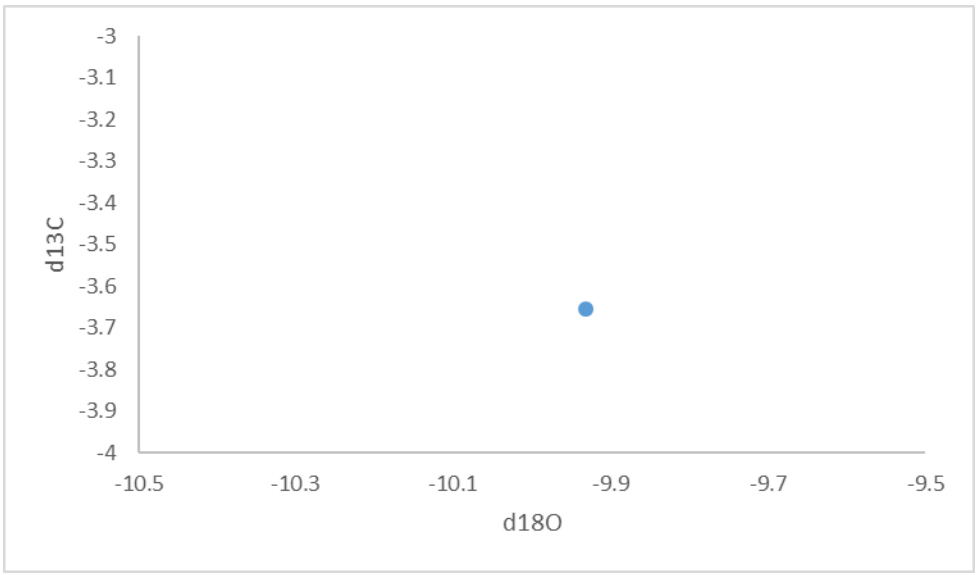


Figure S2: Zji1 (j33)

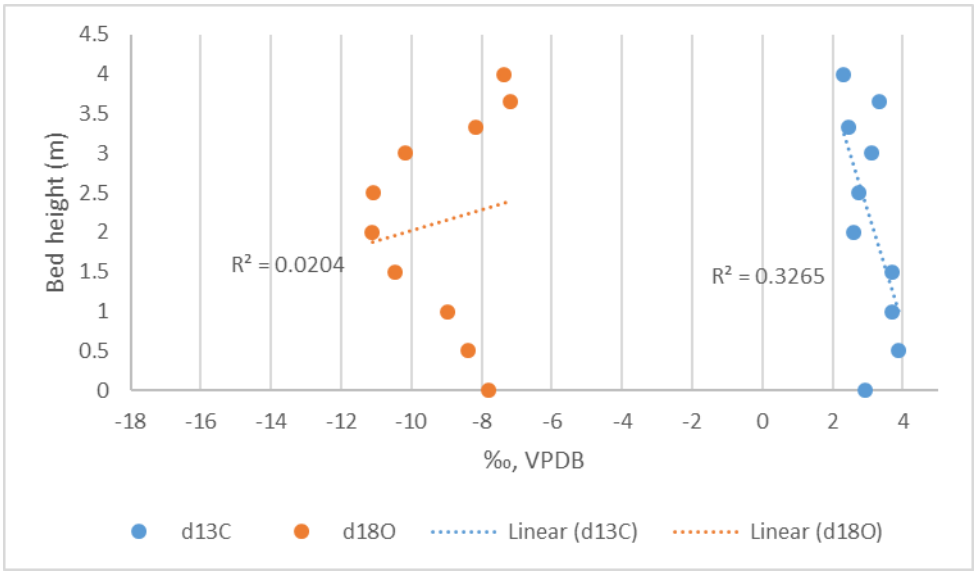


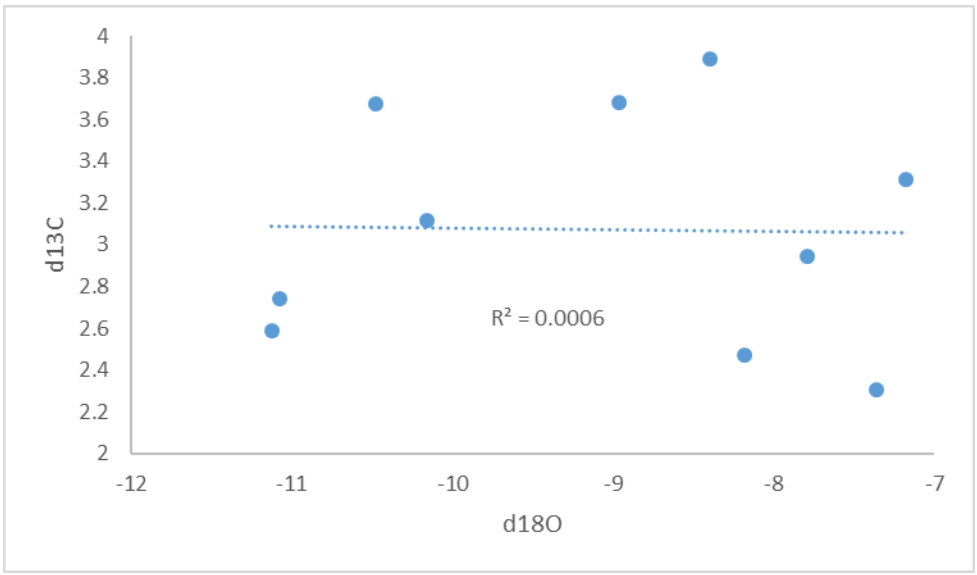


Figure S2: Zjh6 (j23-32)

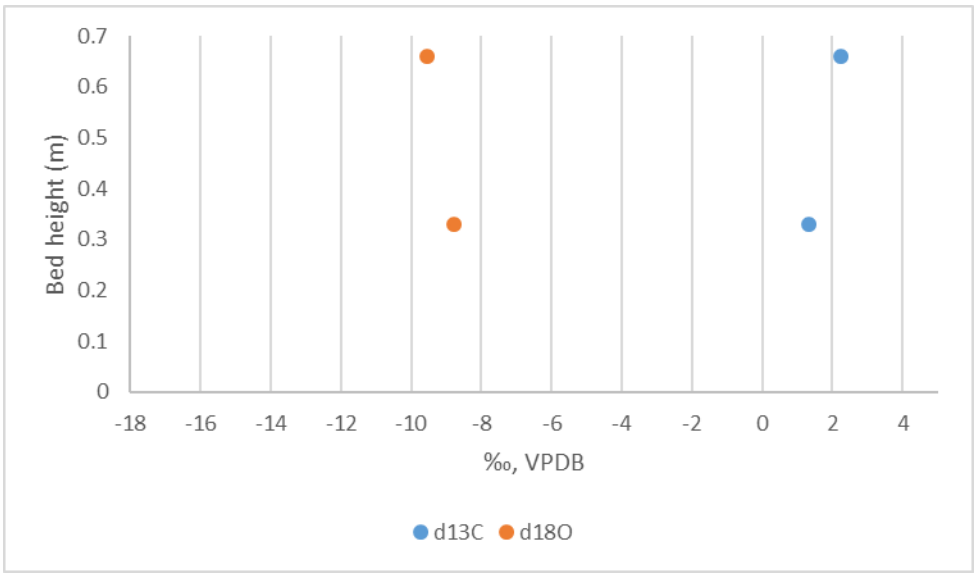


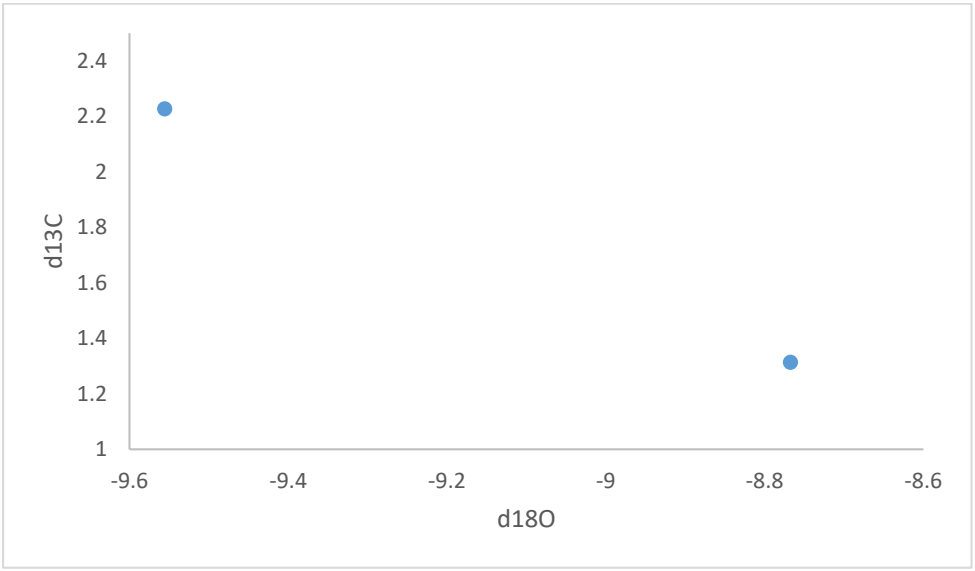


Figure S2: Zjh5 (j21-22)

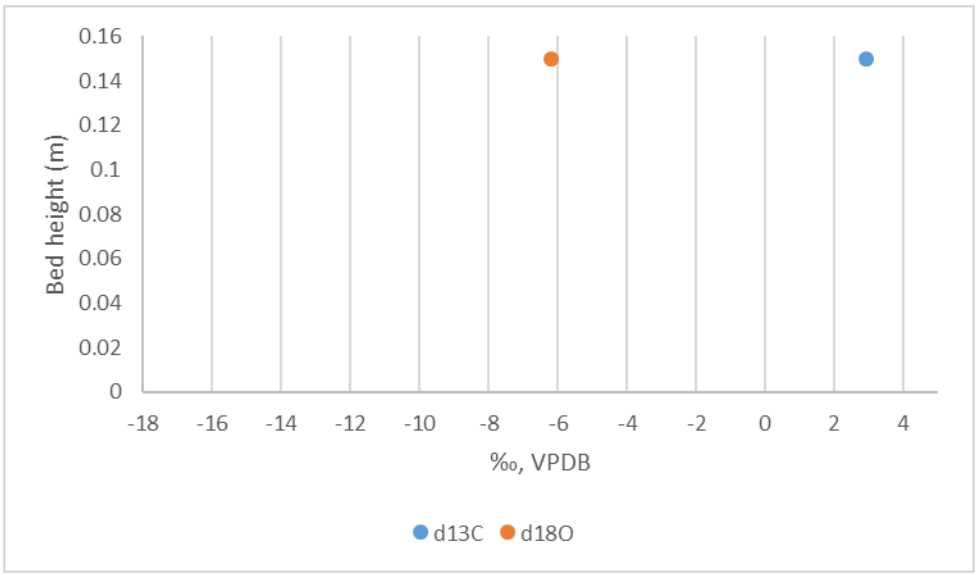


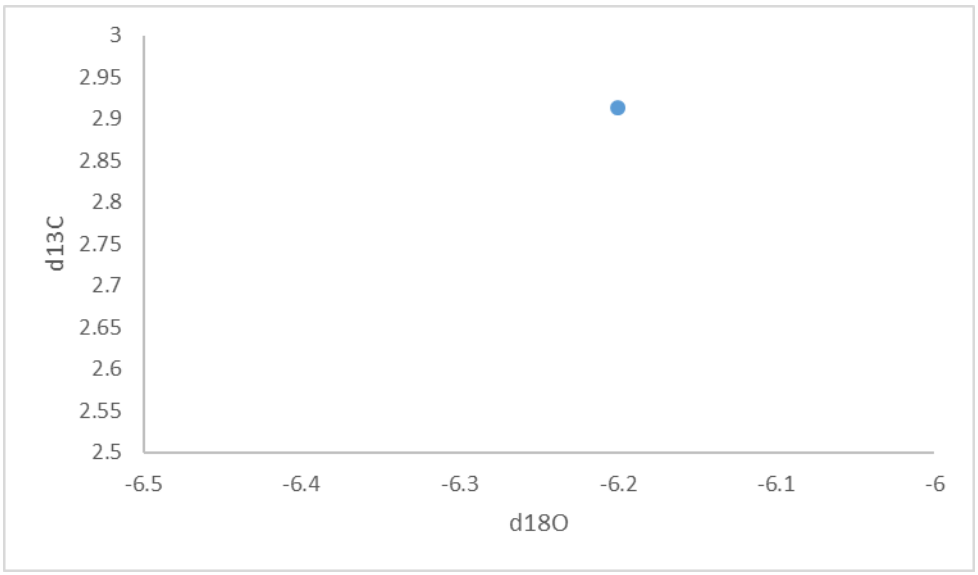


Figure S2: Zjh4 (j20)

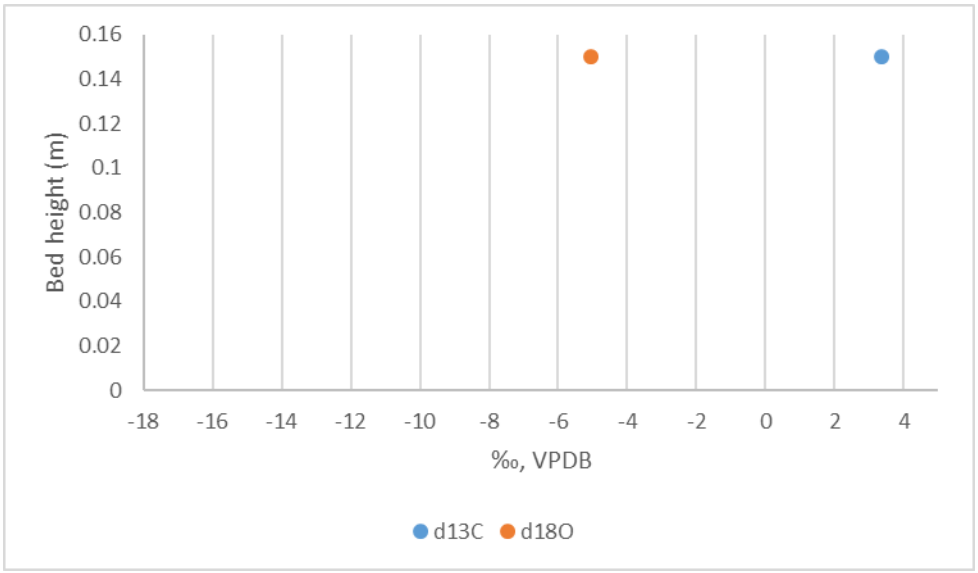


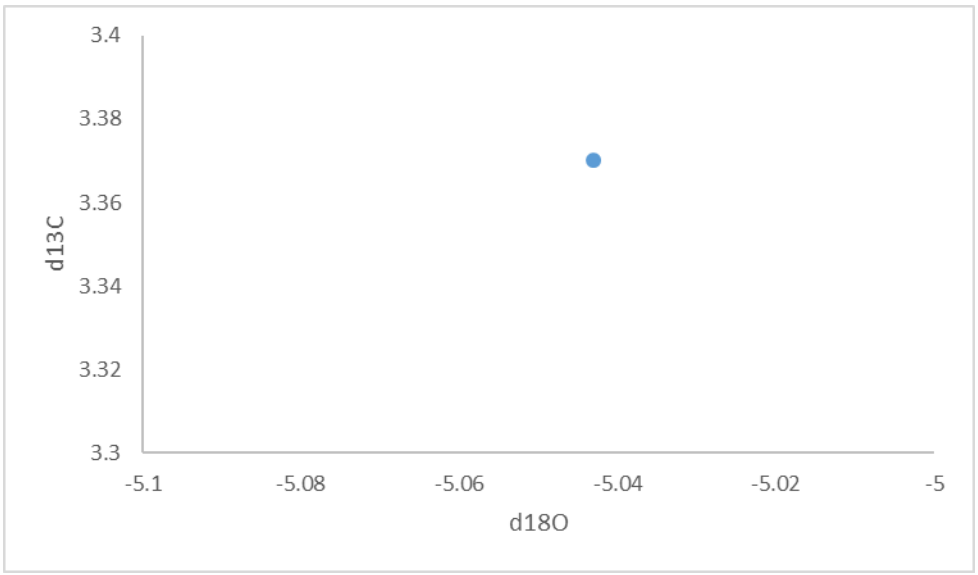


Figure S2: Zjh3 (j19)

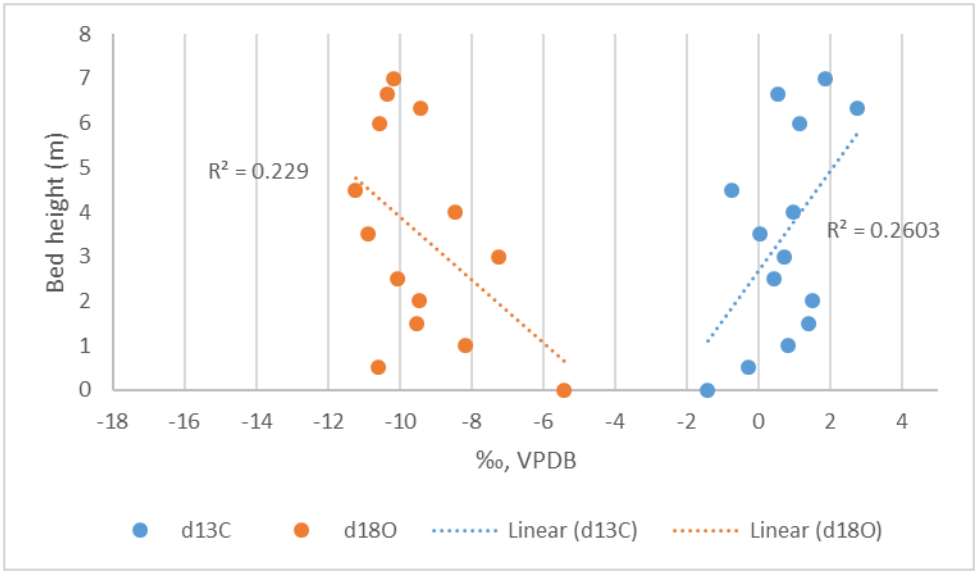


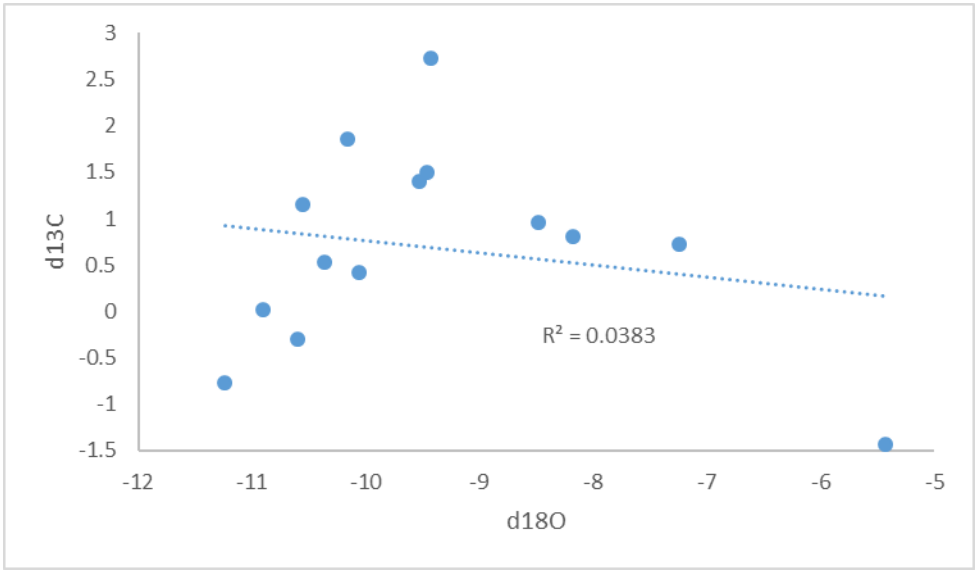


Figure S2: Zjh2 (j5-18)

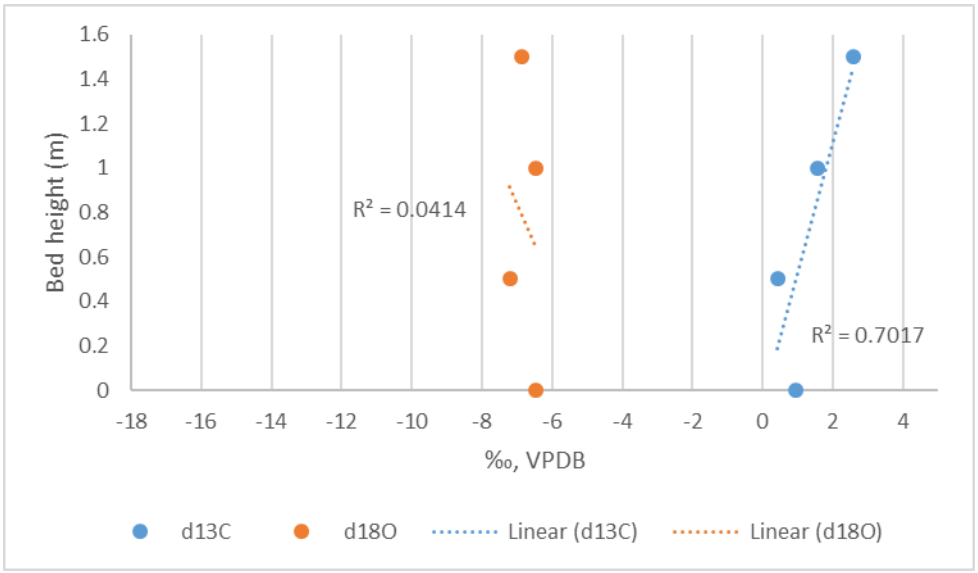


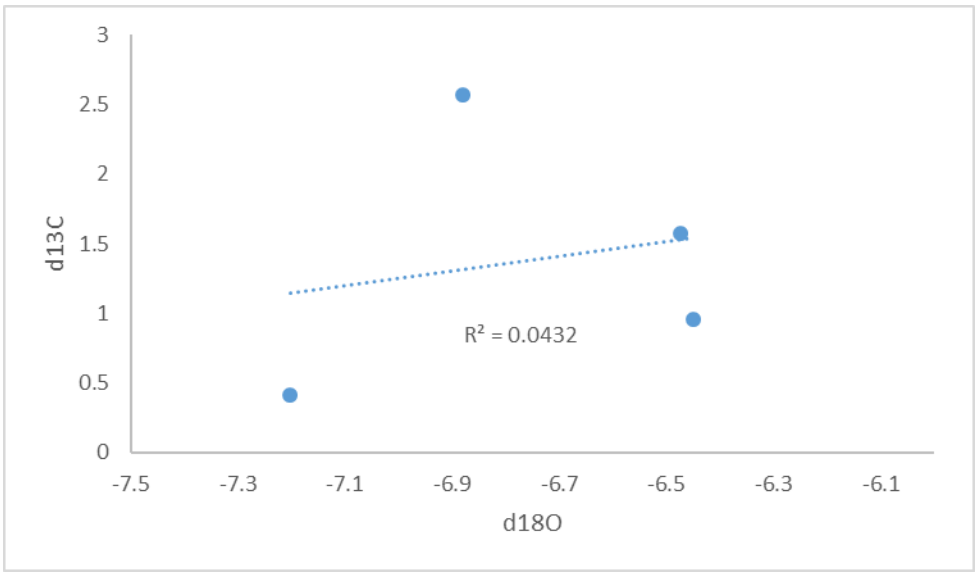


Figure S2: Zjh1 (j1-4)

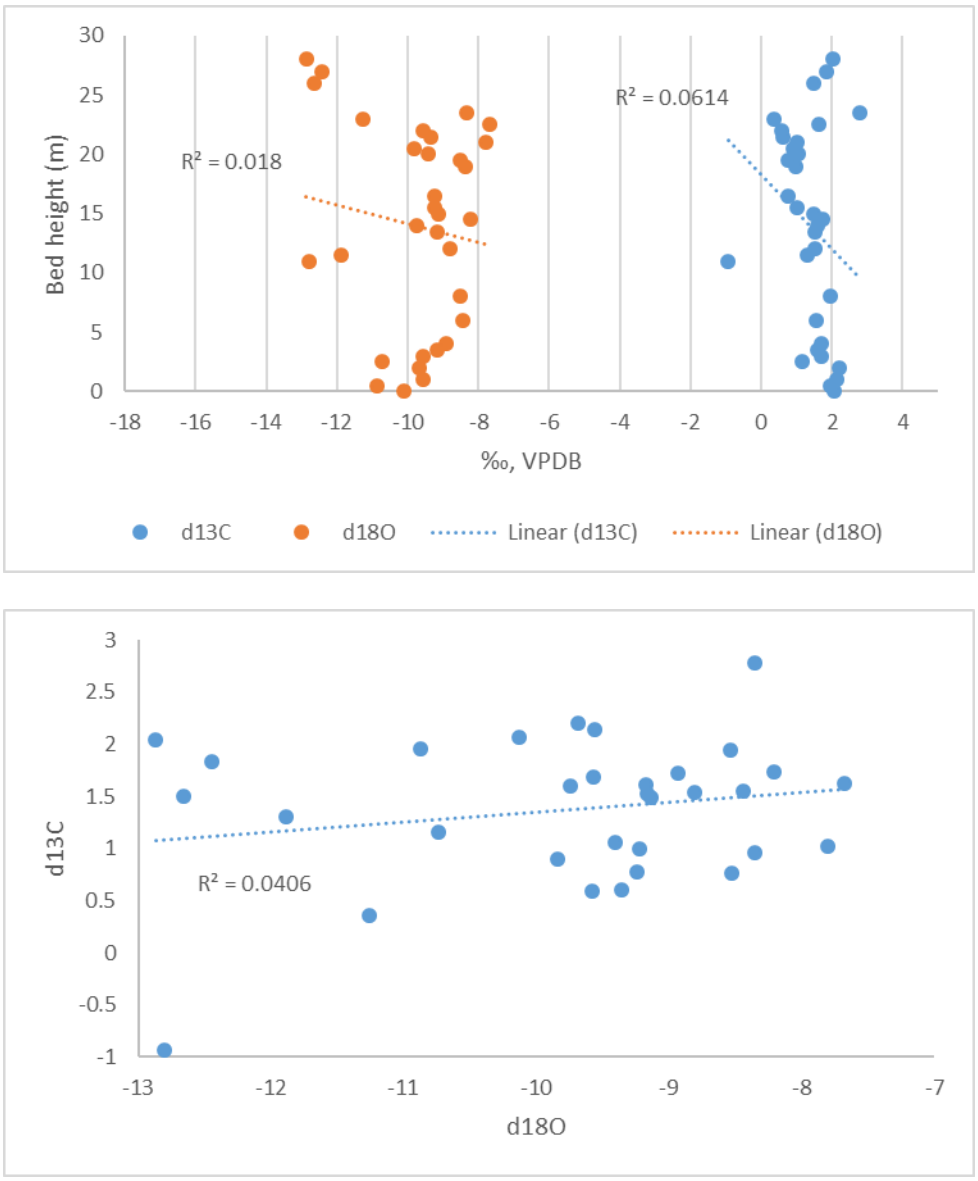


Figure S2: Zjf (j76-107)

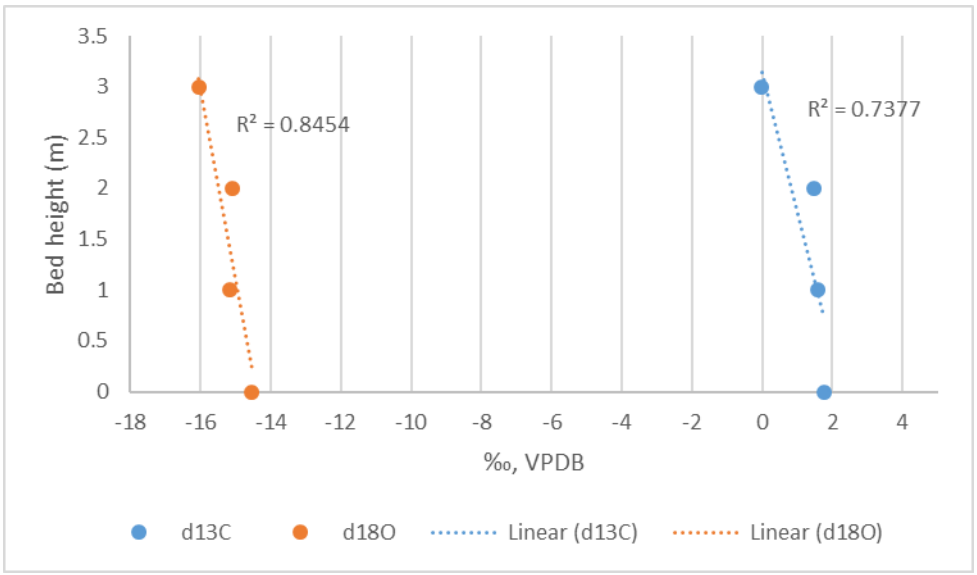


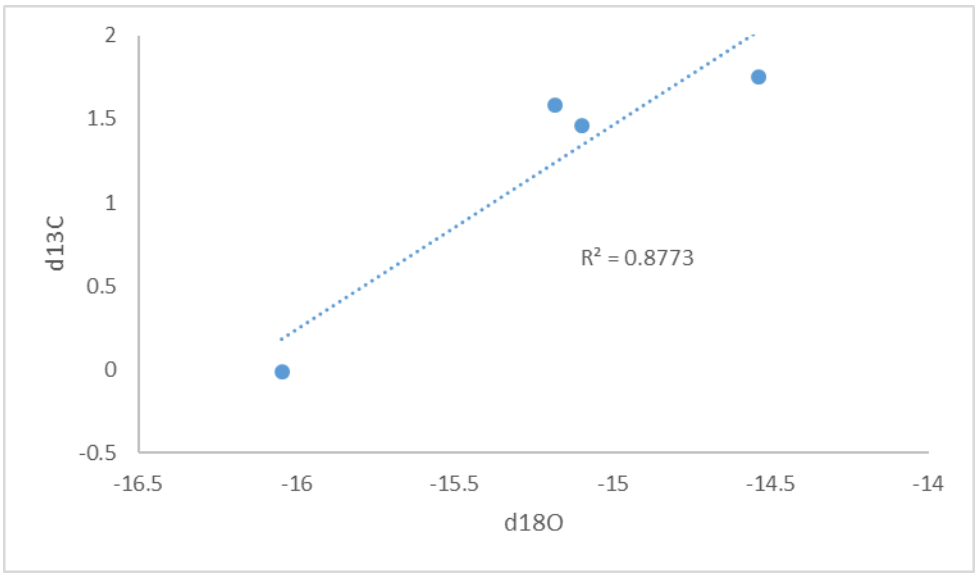


Figure S2: Zjc (j72-75)

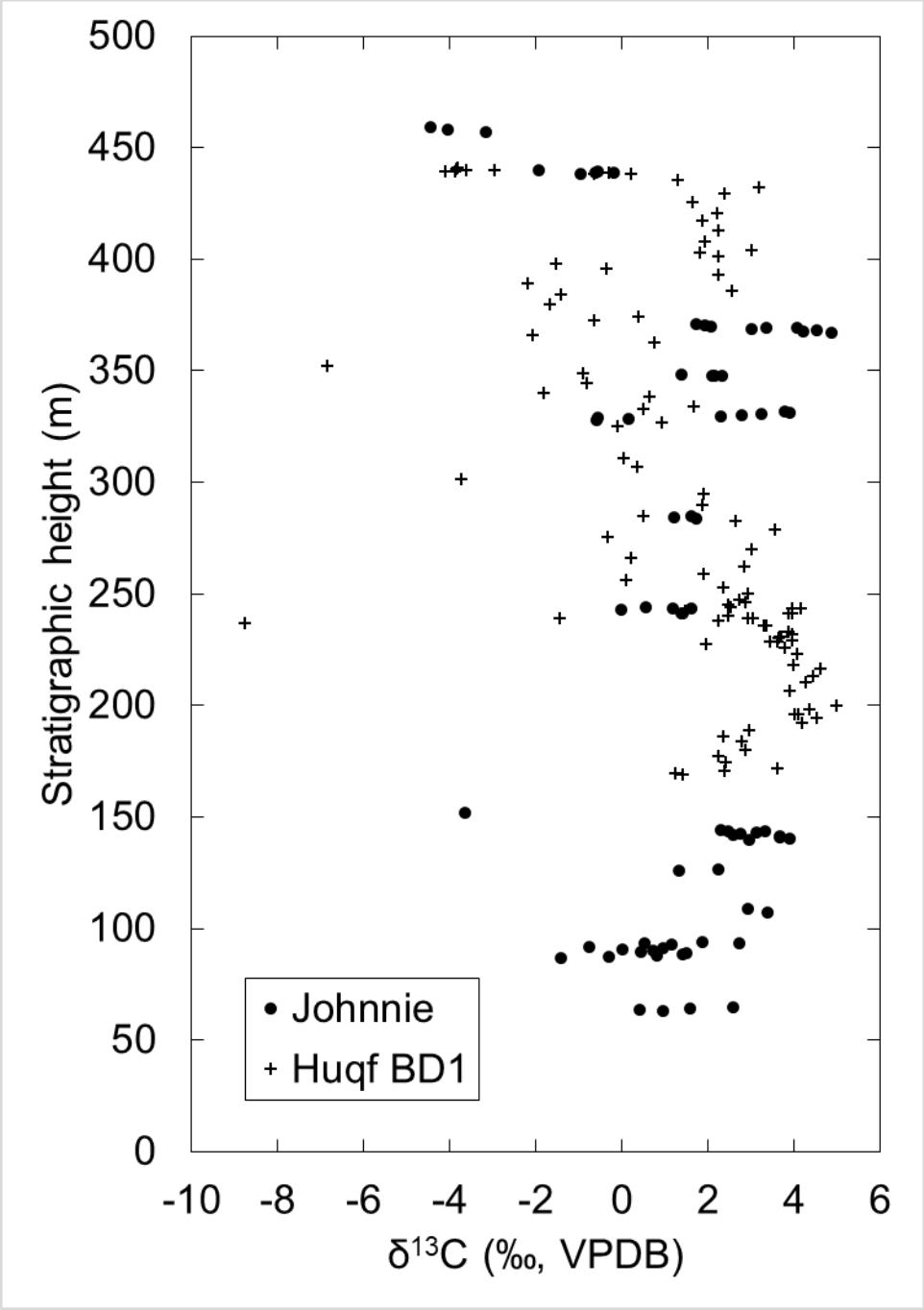


Figure S3: BD1

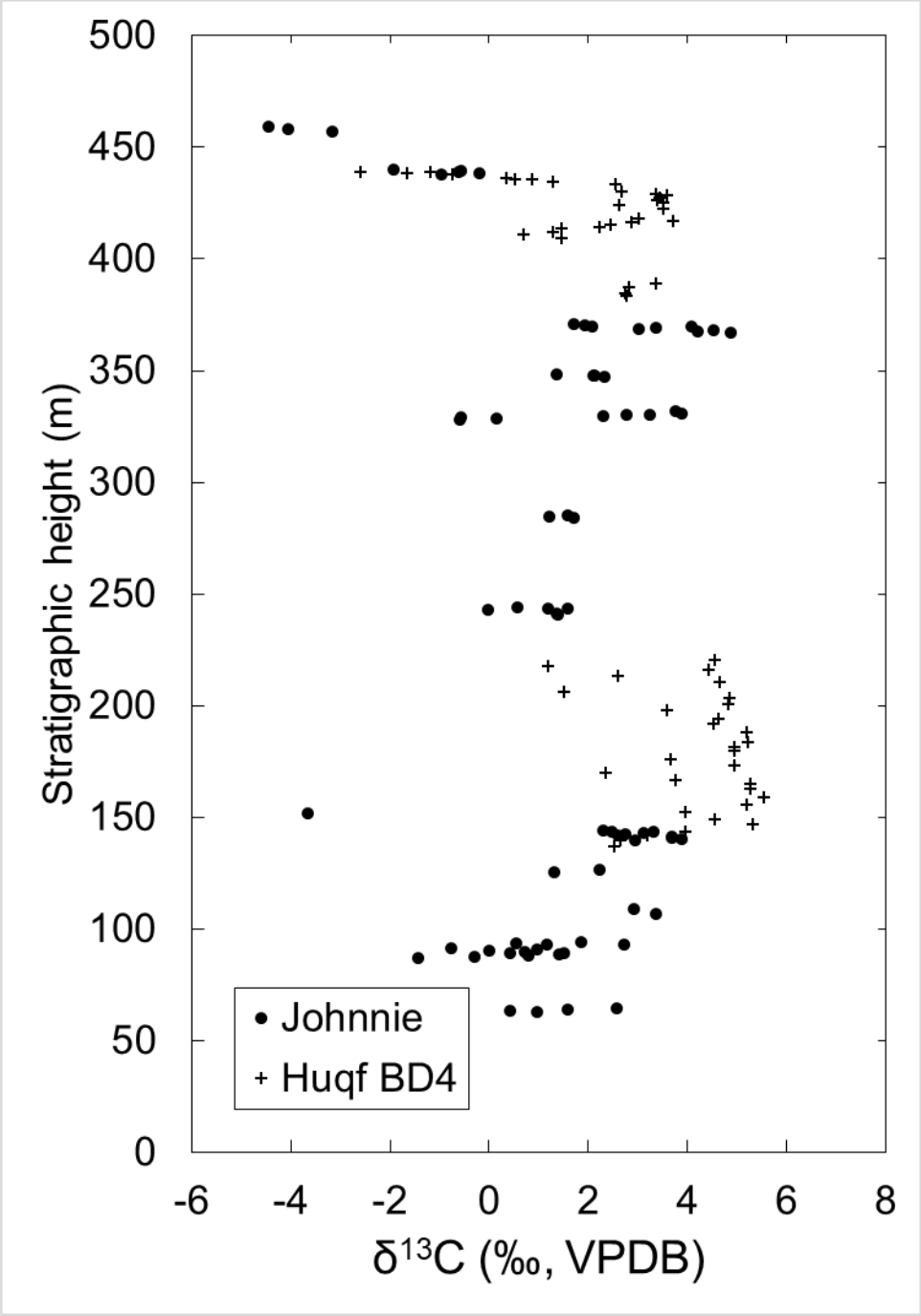


Figure S3: BD4

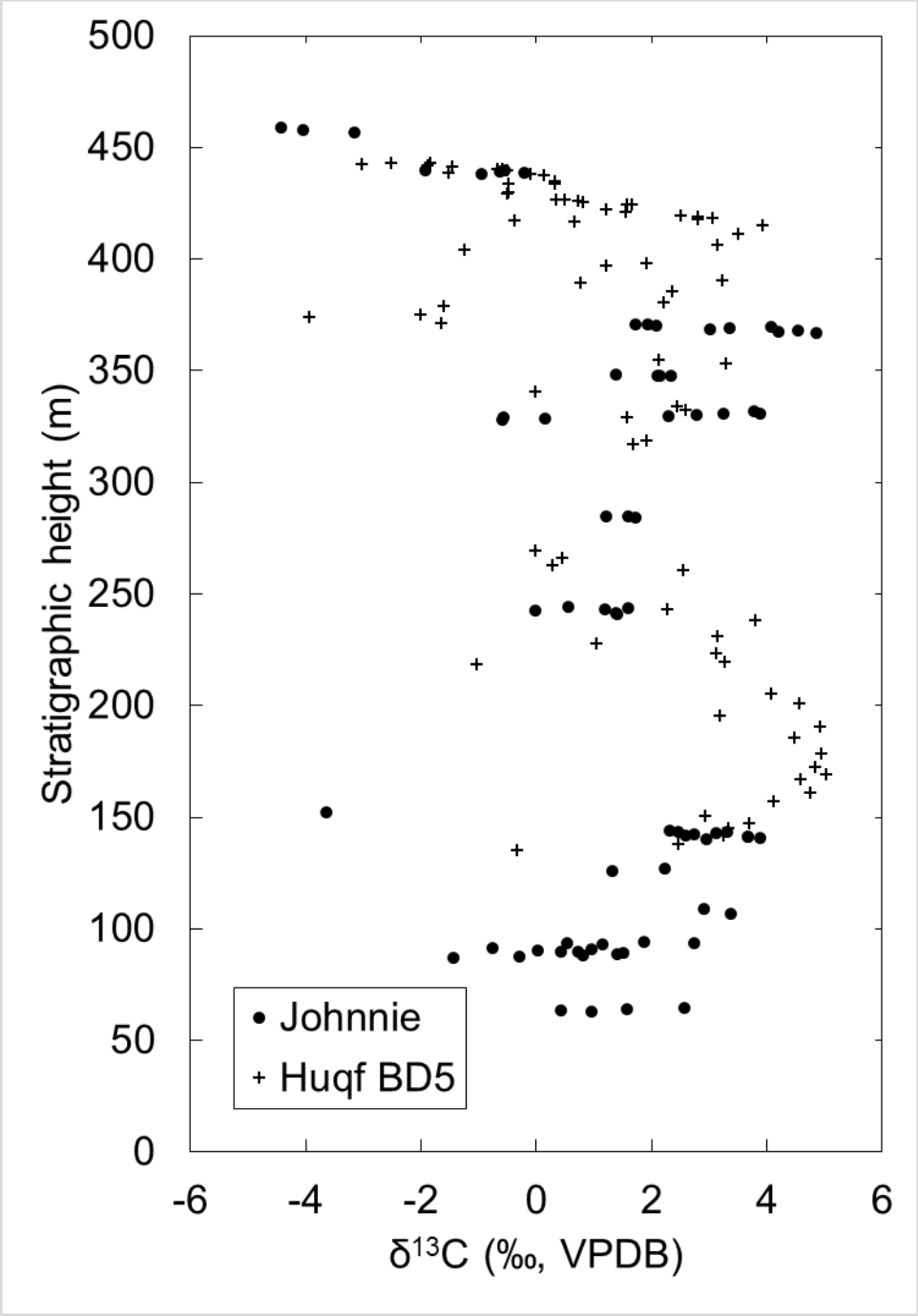


Figure S3: BD5

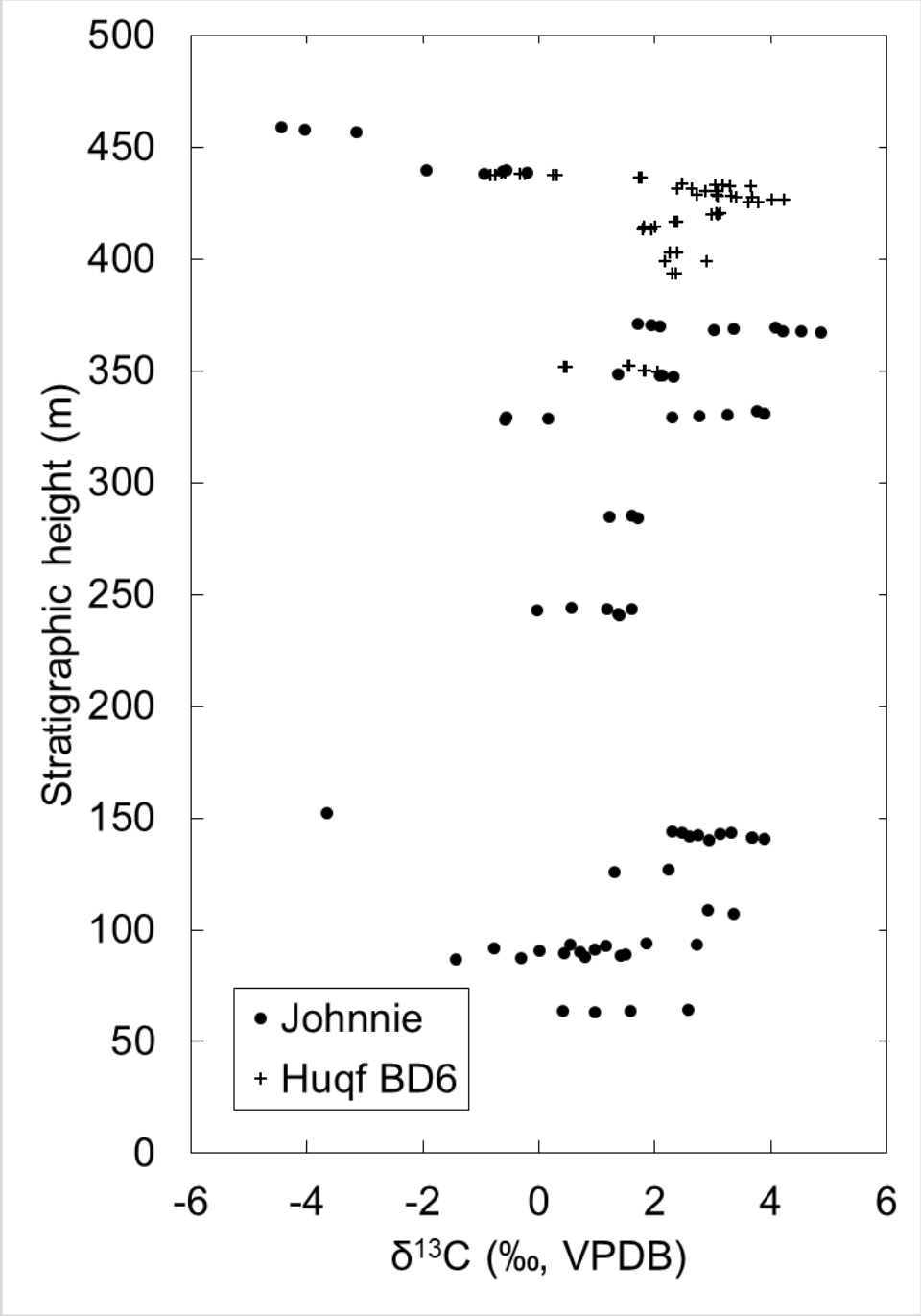


Figure S3: BD6

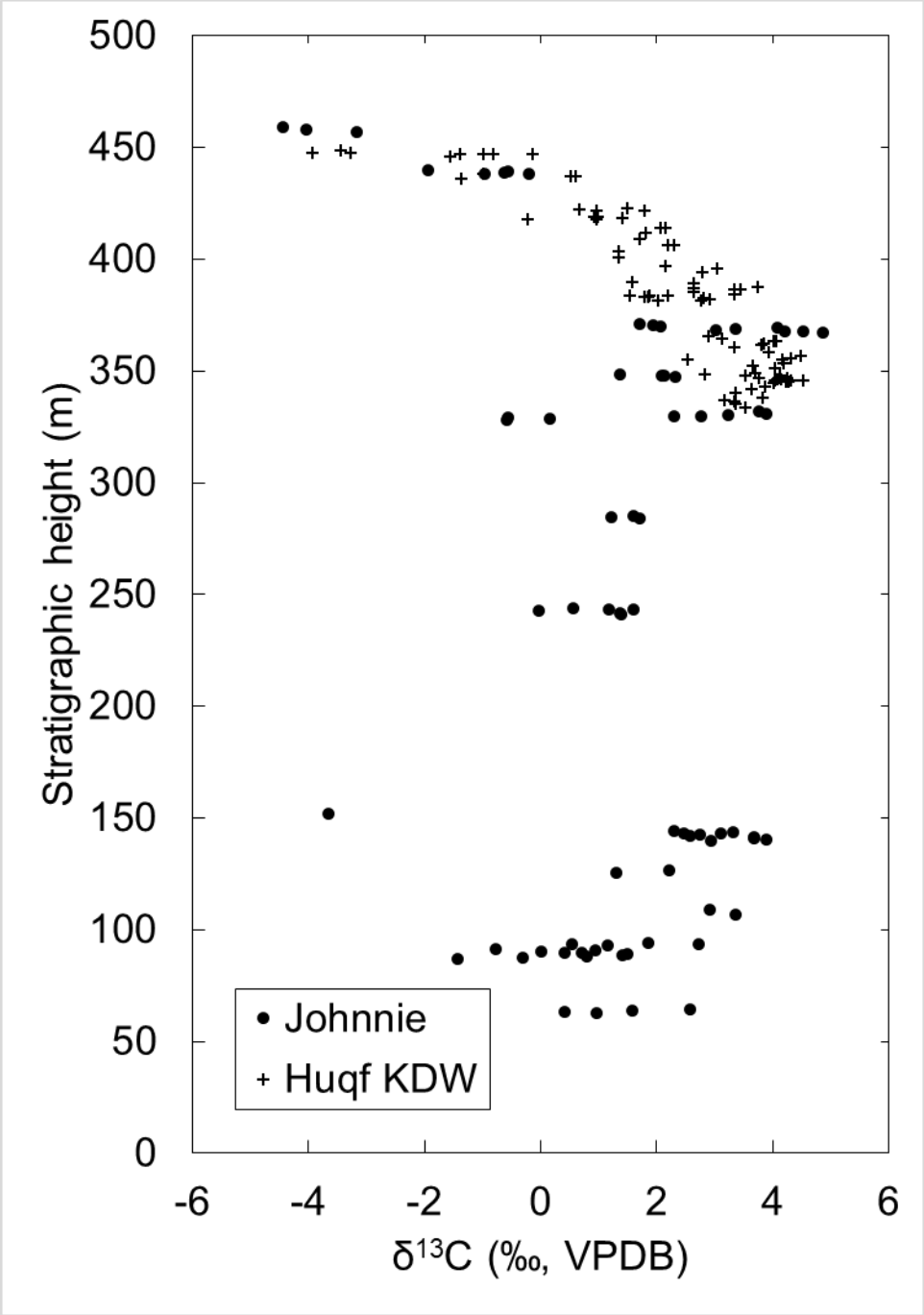


Figure S3: KDW

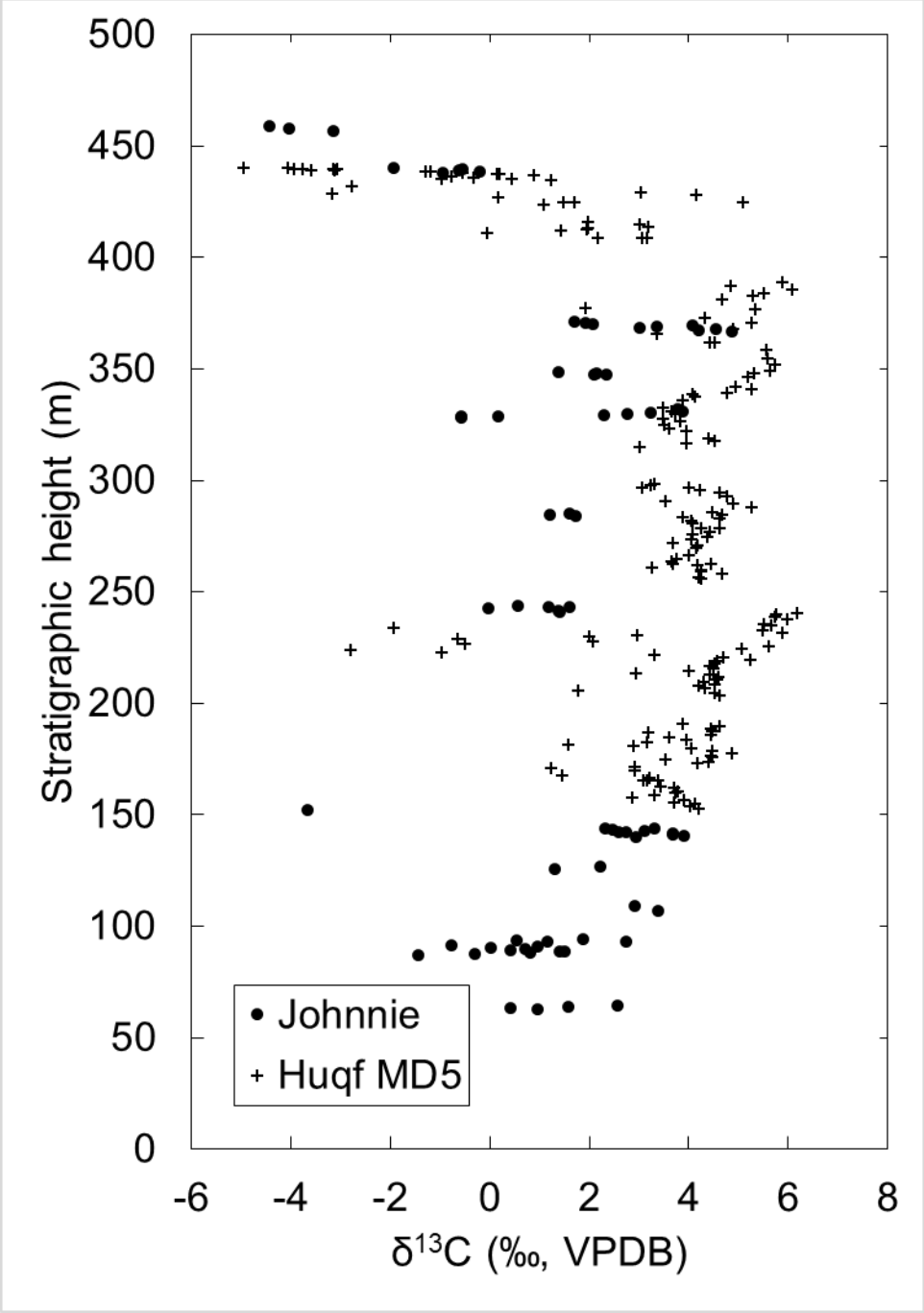


Figure S3: MD5

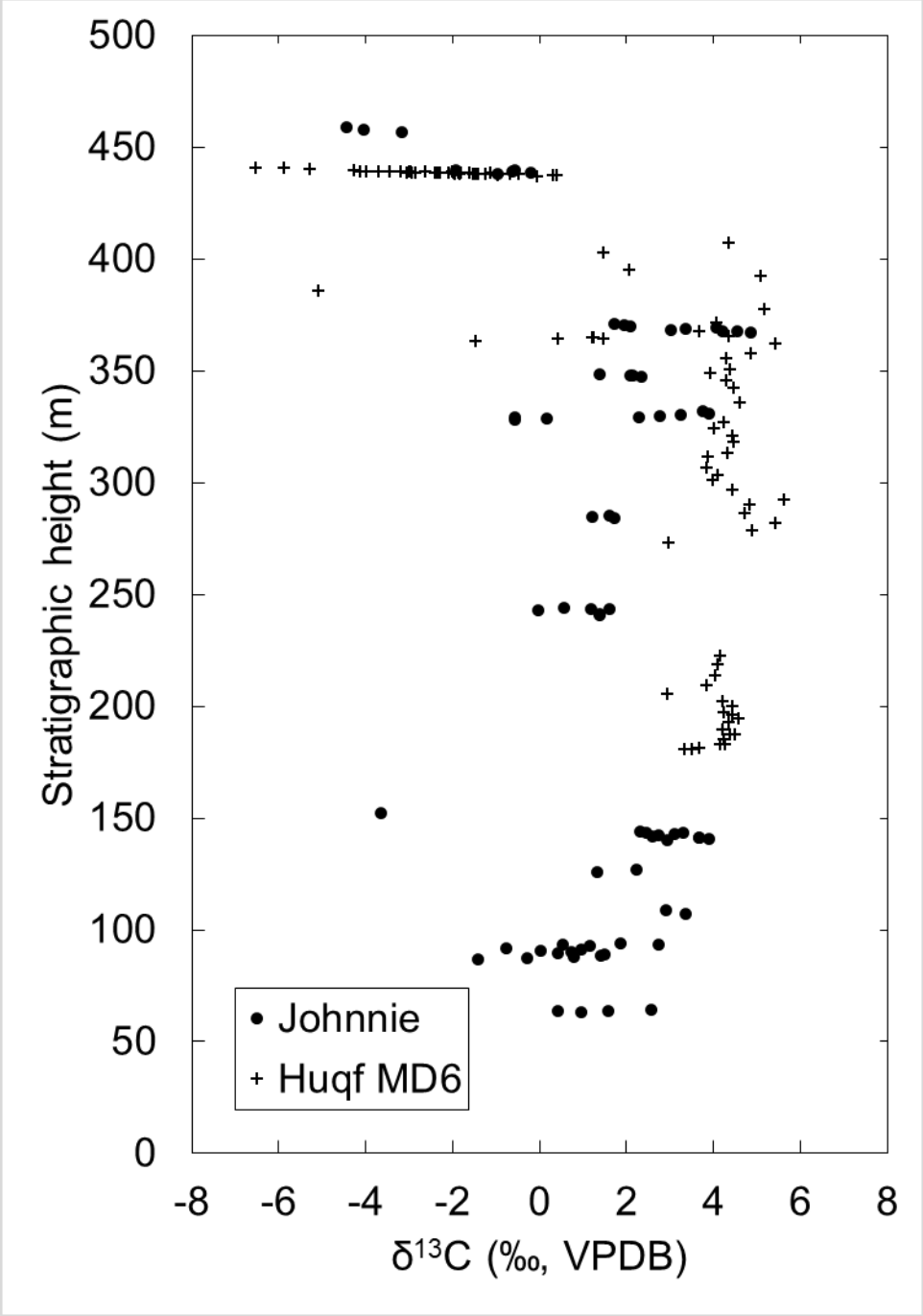


Figure S3: MD6

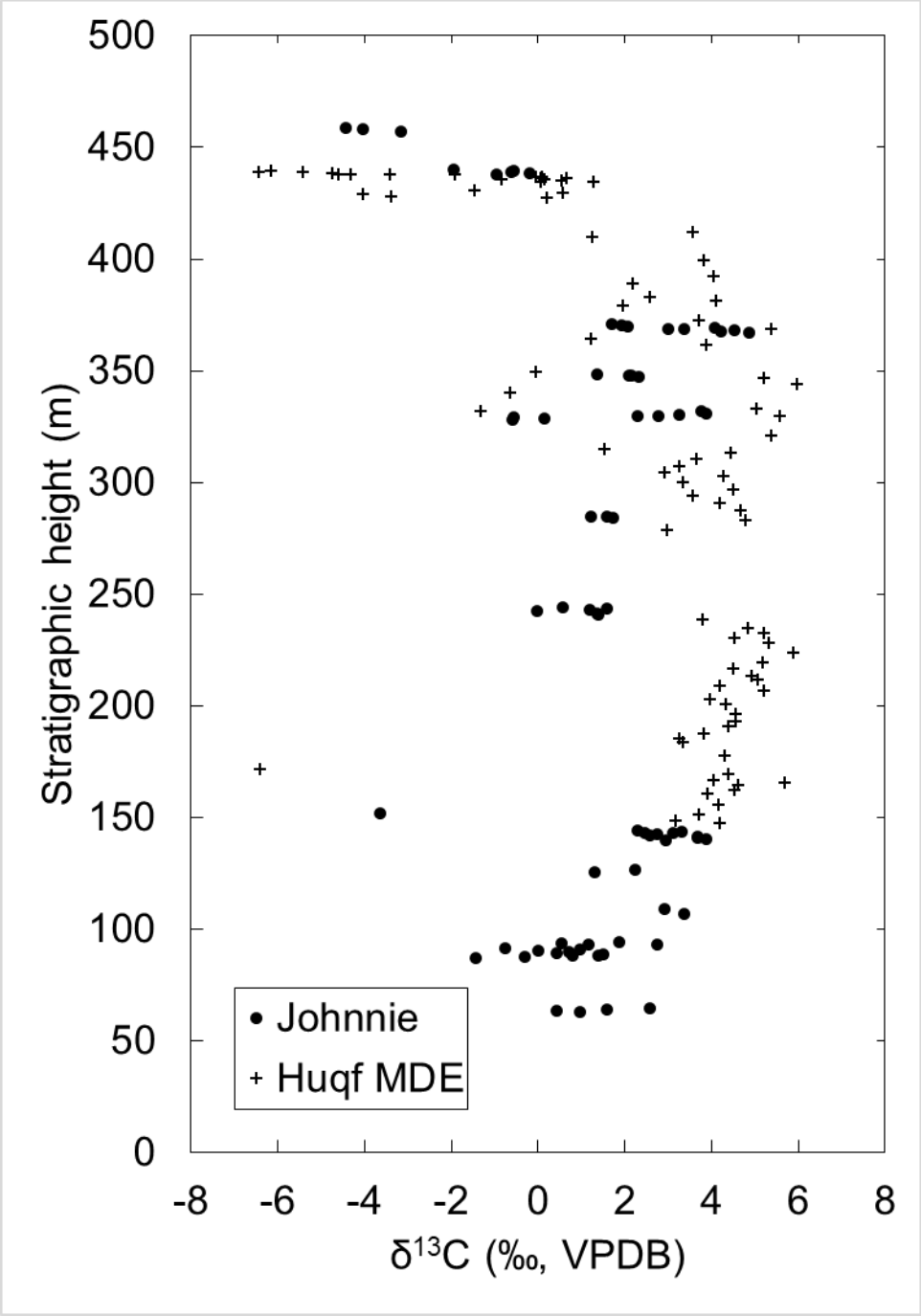


Figure S3: MDE

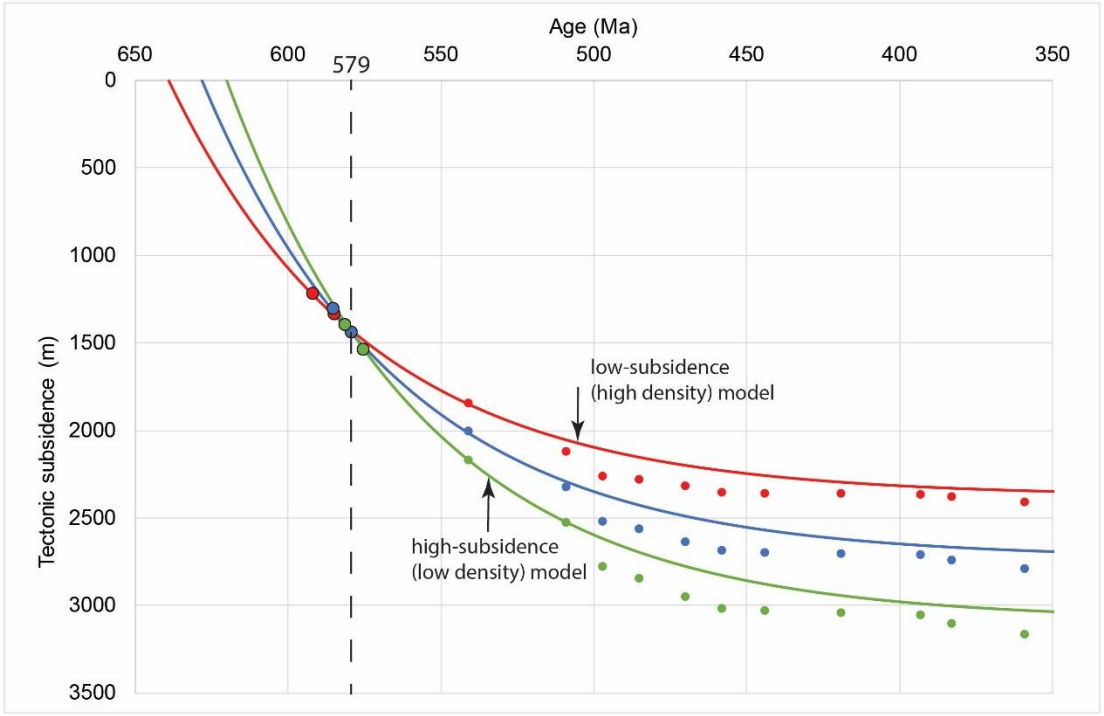
Age (Ma)
650
600
579
550
500
450
400
350
0
500
1000
1500
2000
2500
3000
3500
Tectonic subsidence (m)
low-subsidence
(high density) model
high-subsidence
(low density) model

Figure S4

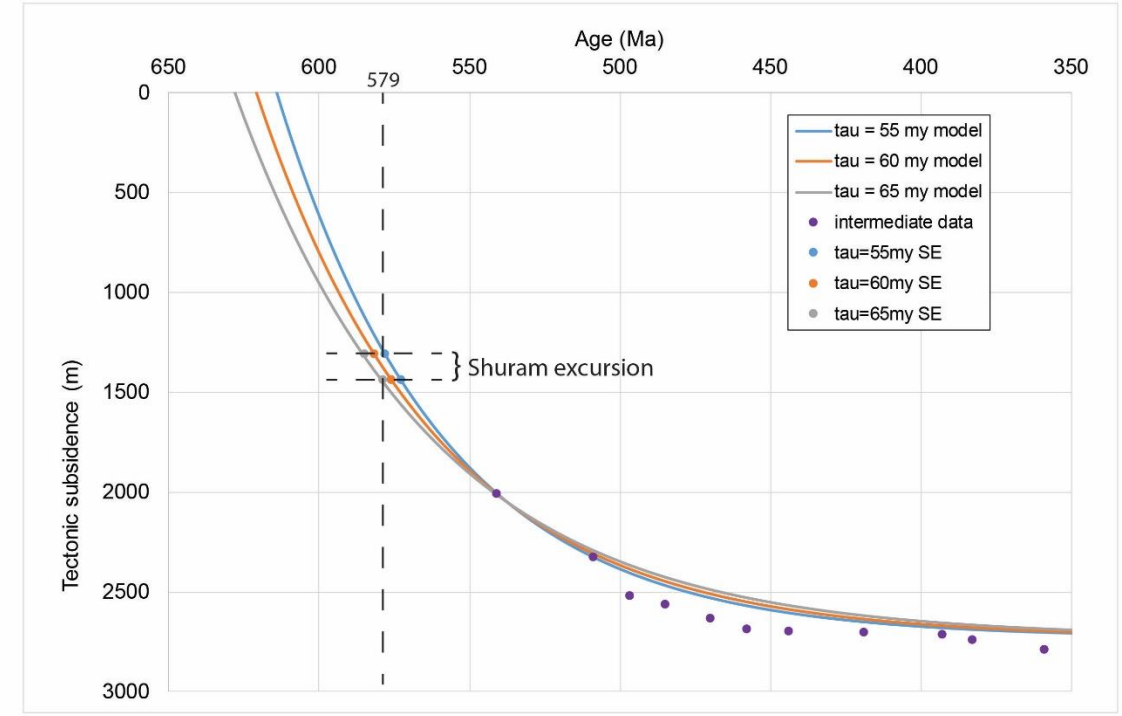
Age (Ma)
650
600
579
550
500
450
400
350
0
500
1000
1500
2000
2500
3000
Tectonic subsidence (m)
tau = 55 my model
tau = 60 my model
tau = 65 my model
intermediate data
tau=55my SE
tau=60my SE
tau=65my SE
} Shuram excursion

Figure S5

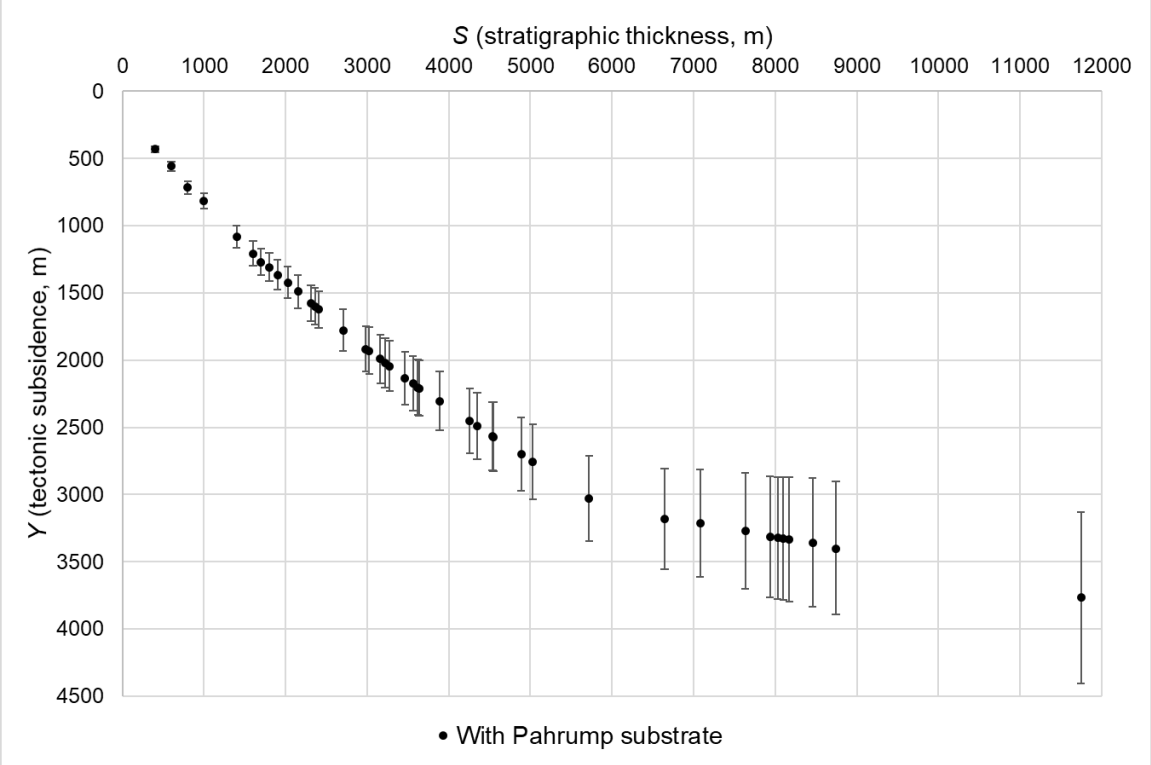
S (stratigraphic thickness, m)
0
1000
2000
3000
4000
5000
6000
7000
8000
9000
10000
11000
12000
Y (tectonic subsidence, m)
0
500
1000
1500
2000
2500
3000
3500
4000
4500
With Pahrump substrate

Figure S6

**Supplemental Text**

Lithologic descriptions regarding the Mt. Schader stratigraphic section for the Ediacaran Johnnie Formation, Montgomery Mountains, Nevada

Thickness of stratigraphic units were measured with a Jacob's staff and recorded to the nearest 1/4 or 1/3 of a meter. Care was taken to avoid structural complexities (i.e. by moving to locations where faults and/or folds are not present). Color names and numerical designations were recorded using a Geological Society of America Rock Color Chart with genuine Munsell® color chips. Grain sizes were recorded using an American/Canadian Stratigraphic reference card. Bed thicknesses use the following general designations: thin, <20 centimeters; medium, >20 centimeters; and thick, >50 centimeters. Total thickness of section measured is 538 meters for the Johnnie Formation, and 54 meters for the Stirling Quartzite (grand total of 592 meters).

## Locality 1 (section 4, d-d')

*Northeast part of Montgomery Mountains, measured about 3 kilometers west/southwest of Mt. Schader, starting at UTM zone 11S 0581729 m E 4035133 m N, and ending at UTM zone 11S 0581879 m E 4035004 m N.*

Stirling Quartzite (incomplete):

Zsa member (incomplete):

*Meters*

48. Breccia and conglomerate. Breccia and conglomerate are very pale orange (10YR 8/2); weather to dark yellowish orange (10YR 6/6) and grayish black (N2); grains are poorly sorted coarse sand, pebbles, gravel; massive bedding; irregular cliff-forming protrusions; slickenlines on slickensided surfaces. Samples 20BW15 (590 m breccia) and 21BW15 (591 m). Incomplete measurement of bed.

4

47. Massive orthoquartzite. Orthoquartzite is pinkish gray (5YR 8/1); weathers to moderate yellowish orange (10YR 7/6); medium-coarse well-sorted grains; massive bedding with conjugate fractures; some cliff-forming protrusions on mostly recessive slopes. Sample 19BW15 (583 m-orthoquartzite).

14

144

46. Dolomitic sandstone. Dolomitic sandstone is grayish orange pink (5YR 7/2); weathers to grayish brown (5YR 3/2); fine-grained; laminated medium beds; trough cross strata; resistant cliff-forming unit.

8

45. Orthoquartzite and carbonate cemented sandstone. Orthoquartzite is very pale orange (10YR 8/2); weathers to dark yellowish orange (10YR 6/6); fine- to medium-grained; thick bedded; some laminations with fractures both along laminations and sub-orthogonal to laminations; channel fill with normal grading near base. Carbonate cemented sandstone is pale reddish brown (10R 5/4); weathers to olive black (5Y 2/1); fine-grained; medium-thick bedded; sometimes laminated.

28

---

Total of incomplete Zs member 54

---

Total of incomplete Stirling Quartzite 54

Johnnie Formation (incomplete):

Zjr member:

44. Sandstone and siltstone in ball-and-pillow structure, and dolostone. Ball-and-pillow structure is 1-2 m thick; light brown (5YR 6.4); weathers to dusky yellowish brown (10YR 2/2); sandstone is fine- to medium-grained; siltstone casted around sandstone. Other sandstone is pale red (5R 6/2); weathers to dark yellowish orange (10YR 6/6); fine-grained; medium bedded. Siltstone is typical VSS with additional new hue of pale red (5R 6/2); weathers to light greenish gray (5GY 8/1); speckled by 1 mm hematite grains; laminated. Dolostone is medium light gray (N6); weathers to yellowish orange (10YR 6/6) and light brown (5YR 6/4). Base of dolomitic sandstone is moderate yellowish brown (10YR 5/4); weathers to dusky yellowish brown (10YR 2/2) medium grains; some south-dipping foresets.

4

43. VSS and calcite-cemented sandstone. VSS as previous. Sandy limestone is pale red (10R 6/2); weathers to pale reddish brown (10R 5/4); very fine-grained; thin lenses of flaser beds.

8

42. Limestone breccia and sucrosic limestone. Limestone breccia is light gray (N7); weathers to light olive gray (5Y 5/2). Sucrosic limestone is pale red (10R 6/2); weathers to pale reddish brown (10R 5/4). Sandy limestone and calcite cemented sandstone with

laminated thin interbeds of sucrosic limestone; recessive, slope-forming unit.

24

41. Mixed siltstone and carbonate-rich sandstone. Siltstone as VSS; finely laminated. Sandstone is pale red (10R 6/2); weathers to dark yellowish brown (10YR 4/2); fine-grained, thin- to medium-bedded. Siltstone and sandstone form recessive slope-forming unit.

18

40. Argillite and limestone. Argillite is medium dark gray (N4); weathers to medium gray (N5); very fine mica, phyllitic texture. Limestone is laminated, as in unit 38.

5

39. Folded limestone. Same as liver limestone (38): pale reddish brown (10R 5/4); weathers to grayish red (10R 4/2); varnish is very dusky red (10R 2/2); folded top to west, pitted dissolution surfaces.

1

38. Liver limestone. Limestone is pale reddish brown (10R 5/4); weathers to grayish red (10R 4/2). Fine-grained with interspersed quartz grains; thinly to medium bedded, massive to laminated beds; occasional brecciation near top.

11.5

37. Carbonate-rich sandstone. Sandstone is grayish red (10R 4/2); weathers to pale reddish brown (10R 5/4) and dark yellowish

orange (10YR 6/6) and various similar hues; fine-medium grains**;** thinly bedded and finely laminated with rare north-dipping foresets.

7.5

36. Dolomitic oolite; “Johnnie Oolite”. Oolite is pale yellowish brown (10YR 6/2); weathers to grayish orange (10YR 7/4); very coarse-grained.

2

35. VSS. VSS is finely laminated, occasionally phyllitic, with rare N-dipping foresets and occasional quartz veins.

17

---

Total of Zjr member 98

Zjl member (combine with Zjl from section 3):

34. Laminated dolostone. Dolostone is pale yellowish brown (10YR 6/2); weathers to moderate yellowish brown (10YR 6/4); thick, laminated beds.

2

33. VSS and dolomitic sandstone (incomplete). VSS as previous. Dolomitic sandstone is medium gray (N5); weathers to moderate yellowish orange (10YR 5/6); fine-grained. Beds are massive with varnish of dark gray (N3).

6

**Locality 1 (section 3, c-c')**

*Northeast part of Montgomery Mountains, measured about 3 kilometers west/southwest of Mt. Schader, starting at UTM zone 11S 0580829 m E 4033958 m N (approximate), and ending at UTM zone 11S 0580984 m E 4033808 m N.*

*Meters*

Johnnie Formation (incomplete):

Zjl member (combine with Zjl from section 4):

32. Orthoquartzite and siltstone (VSS) as in 31. Sample 18BW15 (430 m), medium-grained orthoquartzite (incomplete).

36

31. Orthoquartzite and minor siltstone. Light brownish gray (5YR 6/1); weathers to moderate brown (5YR 4/4) and grayish black (N2); siltstone is fine-medium grained; thin-thick parallel beds with some hummocky cross-strata.

12

30. Siltstone and fine sandstone with minor orthoquartzite. Siltstone and fine sandstone, as VSS, are variegated; bluish white (5B 4/1) weathers to blackish red (5R 2/2) and green (undocumented), thin

beds. Orthoquartzite is medium light gray (N6); weathers to moderate reddish brown (10R 4/6).

13

---

Total of Zjl member 69

Zjk member:

29. Dolostone with chert. Dolostone is medium gray (N5); weathers to light olive gray (5Y 5/2) and medium yellowish brown (10YR 6/4). Dolostone is medium bedded with chert in lower third of section. Chert is medium light gray (N6); weathers to grayish black (N2). Hummocky cross-stratified mounds with anastomosing laminations in middle of section. Samples J63 (371 m), J62 (370.5 m), J61 (370), J60 (369.5), J59 (369), J58 (368.5), J57 (368), J56 (367.5), and J55 (367).

4

28. Siltstone and orthoquartzite, mainly parallel bedded.

18

27. Dolostone. Medium gray (N5); weathers to moderate olive brown (5Y 4/4) and moderate yellowish brown (10YR 5/4). Medium bedded with basal sandy dolostone. Samples J54 (349 m), J53 (348.5 m), J52 (348 m), and J51 (347.5 m).

150

2

26. Siltstone and orthoquartzite. Siltstone is typical variegates sandstone and siltstone, bluish white (5B 4/1) and blackish red (5R 2/2) and green (undocumented color), thinly bedded with thin beds or orthoquartzite. Orthoquartzite is medium light gray (N6); weathers to moderate reddish brown (10R 4/6), ripple laminations.

15

---

Total of Zjk member 39

Zjj member (combine with Zjj from section 2):

25. Dolostone and sandy dolostone. Dolostone is medium-dark gray (N4); weathers to olive gray (5Y 4/1); medium-thick bedded; some hummocky cross-stratified structures. Sandy dolostone is medium gray (N6-N8); weathers medium yellowish brown (10 YR 5/4); medium-thick beds with pure dolostone blebs and no chert. Samples J50 (332 m), J49 (331.5 m), J48 (331 m), J47 (330.5 m), J46 (330 m), J45 (329.5 m), J44 (329 m), and J43 (328.5 m).

5

24. Orthoquartzite and Siltstone. 2-4 m thick orthoquartzite and siltstone beds in rhythmic sets every 5 m. Siltstone coarsens upward into top (final) orthoquartzite bed.

151

23

23. Siltstone and sandstone. Siltstone is variegated (variegated sandstone and siltstone=VSS); mainly bluish white (5B 4/1); weathers to blackish red (5R 2/2); also typically green (undocumented color); thinly bedded. Sandstone is orthoquartzite; medium light gray (N6); weathers to moderate reddish brown (10R 4/6); minor in abundance.

19

22. Dolomitic sandstone marker bed. Light olive gray (5Y 6/1); weathers to moderate brown (5YR 4/6); fine to medium sand; some hummocky cross stratification (HCS). Samples J42 (285 m), J41 (284.5 m), and J40 (284 m).

1

21. (combine with unit 21 in section 2) Orthoquartzite, sandstone and siltstone. Orthoquartzite is medium light gray (N6); weathers to moderate reddish brown (10R 4/6); fine sand; thickly bedded. Sandstone and siltstone are variegated (VSS); “both “green-brown” and “lt. blue-red” shades of variegation present in VSS”-green color undocumented; bluish white (5B 4/1); weathers to blackish red (5R 2/2); fine sand; thinly bedded; some hummocky cross stratification (HCS).

27

**Locality 1 (section 2, b-b')**

*Northeast part of Montgomery Mountains, measured about 3 kilometers west/southwest of Mt. Schader, starting at UTM zone 11S 0581155 m E 4034809 m N, and ending at UTM zone 11S 0581315 m E 4034785 m N.*

*Meters*

Johnnie Formation (incomplete):

Zjj member (combine with Zjj in section 3):

21. (combine with unit 21 in section 3) Orthoquartzite, sandstone and siltstone. Orthoquartzite is medium light gray (N6); weathers to moderate reddish brown (10R 4/6); fine sand; thickly bedded. Sandstone and siltstone are variegated (VSS); "typical green fine sand of VSS"-green color undocumented; thinly bedded. Samples 17-BW-15 (247 m-sandstone) and 16-BW-15 (246.5 m-siltstone). 13

---

Total of Zjj member 88

Zji member (also see Zji from section 1):

20. Dolomitic sandstone. Medium gray (N5); weathers to pale reddish-brown (10R 5/4) and moderate yellowish-brown (10YR 5/4); fine to medium sand; medium bedded. Hummocky cross stratification (HCS), with an east-west trend in one well-exposed hummock. Samples J39 (244 m), J38 (243.5 m), J37 (243.25 m), J36 (242.75), J35 (241.5 m), J34 (241 m), and 15-BW-15 (242 m-dolomitic sandstone).

3

19. Orthoquartzite and siltstone. Orthoquartzite is medium light gray (N6); weathers to moderate reddish brown (10R 4/6); fine sand; thickly bedded. Siltstone has some sandstone (~25%) and is variegated (VSS); mainly bluish white (5B 4/1); weathers to blackish red (5R 2/2); fine sand; medium bedded. Orthoquartzite and siltstone occur in relative abundances of 75%/25% (respectively) throughout this section. Hummocky cross stratification is very prominent at ~190 m (most sandstone beds involved) and good hummocks in cross section at ~184 m; sandstone is more commonly medium-grained and micaceous at ~210 m; conspicuous thickly bedded intervals in 5-10 m cycles begin at ~215 m and continue through ~240 m. Sample 14-BW-15 (210.5 m-orthoquartzite; light purplish gray (5P 8/1); weathers to dark yellowish brown (10YR 4/4) and dusky yellowish brown (10YR 2/2); medium sand; thickly bedded). Thickness is

154

approximate; contact is covered in talus; bed surfaces in the float contain asymmetric ripples.

63

18. Orthoquartzite and siltstone. Orthoquartzite is grayish red (5R 4/2); weathers to very dusky red (10R 2/2); fine to medium sand (borderline); bedding thickness unknown. Siltstone is variegated (VSS); mainly blush white (5B 4/1); weathers to blackish red (5R 2/2); thinly bedded. Siltstone occurs in decimeter partings on ~30-70 cm sandstone beds.

14

17. Sandstone (dolomitic at the base of this unit) and siltstone. Sandstone can be light bluish gray (Munsell code unknown), grayish red purple (5RP 4/2) where carbonate-poor, and light brown (5YR 5/6) where carbonate-rich; weathers to moderate yellowish brown (10YR 5/4) where carbonate-poor, and moderate/light brown (5YR 4/6) where carbonate-rich; fine to medium sand; medium to thickly bedded. Siltstone is variegated (VSS); mainly bluish white (5B 4/1); weathers to blackish red (5R 2/2); thinly bedded. Carbonate cement occurs in lowest 2-3 sand beds; some hummocks observed, mainly parallel laminations. Sample J33 (152 m).

20

**Locality 1 (section 1, a-a')**

*Northeast part of Montgomery Mountains, measured about 3 kilometers west/southwest of Mt. Schader, starting at UTM zone 11S 0581057 m E 4035219 m N, and ending at UTM zone 11S 0581293 m E 4035178 m N.*

*Meters*

Johnnie Formation (incomplete):

Zji member (also see Zji from section 2):

16. Orthoquartzite and siltstone. Orthoquartzite is light gray (N7); weathers to brownish black (5YR 2/1); fine to medium sand; thin to medium bedded, mainly low angle hummocky cross stratification and parallel lamination. Siltstone is variegated (VSS); mainly medium to light bluish gray (5B 6/1), moderate red (5R 4/3 or 5R 5/4?), grayish orange pink (5YR 7/2), and grayish orange (10YR 7/4); weathers to light greenish gray (5GY 8/1), and brownish gray (5YR 4/1); laminated to massive. At the bottom, mainly low angle hummock cross stratification and parallel lamination; at the top, unit forms uniform, fairly steep hillsides and is predominantly parallel bedded with some hummocky cross stratification. Sample 13-BW-15 (198 m-coarse orthoquartzite from highest thick bed).

156

Note: unit 16 is omitted because for section 2, we restart at the base of the Zji member and repeat the same stratigraphy.

(58)

---

Total of Zji member 100

Zjh member:

15. Dolostone; medium gray (N5) and dark gray (N3); weathers to moderate yellow brown (10YR 5/4) and medium gray (N5); fine-grained to sucrosic; thickly bedded. Some evidence of hummocky cross stratification, but not as pronounced as in lower carbonate. “Colors vary; reddish gray top and bottom from alteration; more conspicuous here than in most markers.” Samples J32 (144 m), J31 (143.66 m), J30 (143.33 m), J29 (143 m), J28 (142.5 m), J27 (142 m), J26 (141.5 m), J25 (141 m), J24 (140.5 m), and J23 (140 m).

5

14. Sandstone and siltstone. Sandstone is medium light gray (N6); weathers to brownish gray (5YR 4/1); fine sand; thin to medium bedded. Siltstone is variegated (VSS); mainly medium to light bluish gray (5B 6/1), moderate red (5R 4/3 or 5R 5/4?), grayish orange pink (5YR 7/2), and grayish orange (10YR 7/4); weathers to

light greenish gray (5GY 8/1), and brownish gray (5YR 4/1); laminated to massive. Mainly parallel bedding.

12.25

13. Sandy limestone; medium reddish brown (10R 4/6) and moderate yellowish brown (10YR 5/4); weathers to moderate brown (10YR 5/4); fine sand; medium bedded. No well-developed lamination or internal structure. Samples J22 (126.75 m), and J21 (125.75 m).

1

12. Very fine sandstone (vfs) and siltstone. Very fine sandstone is medium light gray (N6); weathers to dusky yellowish brown (10YR 2/2); thinly bedded. Siltstone has several "modes": brown and light green (Munsell codes unknown); pale red and light green (Munsell codes unknown). Photo of light green and red vfs at ~118 m.

14.75

11. Sandstone with minor carbonate (carbonate occurs in two separate decimeter-scale beds). Sandstone is light bluish gray (5B 7/1); weathers to grayish orange (10YR 7/4) or light brown (5YR 5/6); fine sand; thinly to medium bedded. Carbonate is grayish red (5R 4/2); weathers to grayish red (10R 4/2); fine sand; thinly to medium bedded. Overall, this unit forms a resistant interval; mostly parallel bedded with some cross stratification; intense hummocky cross stratification (HCS); hummocks are apparently cross-

stratified with decimeter-scale “mounds” similar to unit 9 carbonates. Samples J20 (109 m; moderate yellowish brown (10YR 5/4); weathers to moderate brown (5YR 5/4)), and J19 (107 m).

7

10. Very fine/fine sandstone and siltstone. Very fine/fine sandstone is pale yellowish brown (10YR 6/2); weathers to dark yellowish brown (10YR 4/2); thinly bedded. Siltstone is variegated (VSS); mainly light bluish gray (5B 6/1), moderate red (5R 4/3 or 5R 5/4?), grayish orange pink (5YR 7/2), and grayish orange (10YR 7/4); weathers to light greenish gray (5GY 8/1), and brownish gray (5YR 4/1); laminated to massive. Photo of “brown-light green VSS” at ~96 m.

10

9. Stromatolitic dolostone; light olive gray (N4 or 5Y 6/1) or grayish red (10R 4/2); weathers to light olive gray (N5) or moderate yellowish brown (10YR 5/4); “macroscopically, unit tends to whether brown, lesser olive gray”; fine-grained/very fine-grained to micritic; medium to thickly bedded. Dolostone is laminated with variably steep-sided mound structures ~0.5-1 m across (three photos at ~89 m and ~92 m). Truncations of mounds observed at bedding interfaces. Samples J18 (94 m), J17 (93.66 m), J16 (93.33 m), J15 (93 m), J14 (91.5 m), J13 (91 m), J12 (90.5 m), J11 (90 m),

J10 (89.5 m), J9 (89 m), J8 (88.5 m), J7 (88 m), J6 (87.5 m), and J5 (87 m).

7

8. Sandstone; thin to medium beds are medium light gray (N6), and weather to medium dark gray (N4) or moderate yellowish brown (10YR 6/4); basal bed is light greenish gray (5GY 6/1), and weathers to dark greenish gray (5GY 4/1); fine to medium sand. Inconspicuous orthoquartzites, sandstone, and variegated sandstones and siltstones (VSS) occur near the top of this unit; near the bottom, sands are thinly bedded with no/minor cross stratification (not orthoquartzite, somewhat friable and porous in places).

18.5

7. Very fine sandstone and siltstone. Very fine sandstone is light purplish blue (5PB 8/1), or "white"; weathers to dark reddish brown (10R 4/4); thinly to medium bedded. Siltstone is variegated (VSS); mainly light bluish gray (5B 6/1), moderate red (5R 4/3 or 5R 5/4?), grayish orange pink (5YR 7/2), and grayish orange (10YR 7/4); weathers to light greenish gray (5GY 8/1), and brownish gray (5YR 4/1); laminated.

4

6. Dolostone; dark gray (N3); weathers to moderate yellowish brown (10YR 5/4); fine-grained; medium bedded with laminations

and thin (~1-2 cm) siliceous stringers; some dispersed quartz grains; complex structures; disruptions in laminations. Samples J4 (64.5 m), J3 (64 m), J2 (63.5 m), and J1 (63 m).

1.5

5. Very fine sandstone and siltstone. Very fine sandstone is light purplish blue (5PB 8/1), or "white"; weathers to dark reddish brown (10R 4/4); thinly to medium bedded; interbeds are massively textured, with a fair degree of induration. Siltstone is variegated (VSS); mainly light bluish gray (5B 6/1), moderate red (5R 4/3 or 5R 5/4?), grayish orange pink (5YR 7/2), and grayish orange (10YR 7/4); weathers to light greenish gray (5GY 8/1), and brownish gray (5YR 4/1); laminated. Overall, this is a recessive, slope-forming unit.

17.5

4. Orthoquartzite and very fine sandstone/siltstone. Orthoquartzite is medium light gray (N6); weathers to medium gray (N5); fine to medium sand; thickly bedded at base, medium to thinly bedded higher in unit; heavy desert varnish and cross-stratified higher in unit; silty "caps" on sandstone beds have abundant grooves/tool-markings, and small current ripples. Very fine sandstone/siltstone can be moderate red/grayish red (5R 4/3), light brown (5YR 5/6), or medium light bluish gray (5B 6/1); weathers to moderate red/grayish red (5R 4/3), moderate brown (5YR 4/4), or light

161

greenish gray (5GY 8/1) and darker hues. Generally, orthoquartzite is resistant, while very fine sandstone is recessive.

6.5

---

Total of Zjh member 105

Zjg member (incomplete)

3. Interstratified variegated sandstone and siltstone (VSS), and orthoquartzite. Siltstone has various hues and is “patchy” or “pinstriped”; hues include medium light bluish gray (5B 6/1), grayish orange pink (5YR 7/2), and grayish orange (10YR 7/4); weathers to brownish gray (5YR 4/1), light greenish gray (5GY 8/1), and darker hues. Sandstone is moderate red to grayish red (5R 4/3); weathers to moderate red/grayish red (5R 4/3); fine-grained. VSS is interstratified on the cm-scale. Orthoquartzite is medium gray (N6); weathers to medium dark gray (N4); thinly to medium bedded; 0.5 m foresets with steeply truncated laminatiosn observed near base at ~16 m. VSS is generally recessive and slope-forming unit; orthoquartzite beds are resistant.

22

| | |
|---|---|
| 2. Orthoquartzite; medium light gray (N6); weathers to medium dark gray (N4); thinly bedded. Thickness of this unit is certainly >2 m because there is a minor break in section (due to poor exposure). | 162 |
| 1. Interstratified variegated sandstone and siltstone (VSS), and orthoquartzite. Sandstone is light brown (5YR 5/6); weathers to moderate brown (5YR 4/4); medium to fine sand; thinly to medium bedded. Siltstone is medium to light bluish gray (5B 6/1); weathers to light greenish gray (5GY 8/1) and darker hues; laminated to massive. Orthoquartzite is medium gray (N6); weathers to medium dark gray (N4); medium sand; thin to medium parallel bedding, with low-angle trough cross stratification observed at ~3 m. | 2 |
| | 15 |
| | --- |
| Total of incomplete Zjg member | 39 |
| | --- |
| Total of incomplete Johnnie Formation | 538 |